NAVAL POSTGRADUATE SCHOOL

MONTEREY, CALIFORNIA

THESIS

FREE-ELECTRON LASER (FEL) UTILIZATION IN SPACE APPLICATIONS (SHIP-BORNE POINTING ACCURACY, DEEP-SPACE COMMUNICATIONS, AND ORBITAL DEBRIS TRACKING)

by

Jason M. Wittrock

December 2011

Thesis Advisor:	Brij Agrawal
Thesis Co-Advisor:	William Colson

Approved for public release; distribution is unlimited

THIS PAGE INTENTIONALLY LEFT BLANK

REPORT DOCUMENTATION PAGE			Form Approved OMB No. 0704–0188
Public reporting burden for this collection of information is estimated to average 1 hour per response, including the time for reviewing instruction, searching existing data sources, gathering and maintaining the data needed, and completing and reviewing the collection of information. Send comments regarding this burden estimate or any other aspect of this collection of information, including suggestions for reducing this burden, to Washington headquarters Services, Directorate for Information Operations and Reports, 1215 Jefferson Davis Highway, Suite 1204, Arlington, VA 22202–4302, and to the Office of Management and Budget, Paperwork Reduction Project (0704–0188) Washington DC 20503.			
1. AGENCY USE ONLY *(Leave blank)*	**2. REPORT DATE** December 2011	**3. REPORT TYPE AND DATES COVERED** Master's Thesis	
4. TITLE AND SUBTITLE Free-Electron Laser (FEL) Utilization in Space Applications (Ship-Borne Pointing Accuracy, Deep-Space Communications, and Orbital Debris Tracking)		**5. FUNDING NUMBERS**	
6. AUTHOR(S) Wittrock, Jason M.			
7. PERFORMING ORGANIZATION NAME(S) AND ADDRESS(ES) Naval Postgraduate School Monterey, CA 93943–5000		**8. PERFORMING ORGANIZATION REPORT NUMBER**	
9. SPONSORING /MONITORING AGENCY NAME(S) AND ADDRESS(ES) N/A		**10. SPONSORING/MONITORING AGENCY REPORT NUMBER**	
11. SUPPLEMENTARY NOTES The views expressed in this thesis are those of the author and do not reflect the official policy or position of the Department of Defense or the U.S. Government. IRB Protocol number _____N/A_____.			
12a. DISTRIBUTION / AVAILABILITY STATEMENT Approved for public release; distribution is unlimited		**12b. DISTRIBUTION CODE** A	

13. ABSTRACT (maximum 200 words)

The U.S. Navy is currently conducting research which will support the production of a MW-class free-electron laser (FEL). The Navy's end-state goal is to design and implement a defense system capable of destroying a fast-flying, anti-ship cruise missile (ASCM) target. To this end, the necessity of ensuring accurate pointing control of the beam is required. The first part of this thesis focuses on the U.S. Navy's desired end-state and investigates the ability of feedback and feed-forward control methods to provide improved pointing accuracy to a beam director mounted on a naval vessel similar in size to that of a Ticonderoga-class cruiser while traversing through various sea-states. The second part of this thesis examines the feasibility of employing the FEL as a means of deep-space (Mars and beyond) communication and orbital debris removal and tracking of objects in low-earth orbit (LEO).

14. SUBJECT TERMS Free-Electron Laser, FEL, Pointing Accuracy, Space Communications, Orbital Debris Removal, Orbital Debris Tracking			**15. NUMBER OF PAGES** 137
			16. PRICE CODE
17. SECURITY CLASSIFICATION OF REPORT Unclassified	**18. SECURITY CLASSIFICATION OF THIS PAGE** Unclassified	**19. SECURITY CLASSIFICATION OF ABSTRACT** Unclassified	**20. LIMITATION OF ABSTRACT** UU

NSN 7540–01–280–5500 Standard Form 298 (Rev. 2–89)
Prescribed by ANSI Std. 239–18

THIS PAGE INTENTIONALLY LEFT BLANK

Approved for public release; distribution is unlimited

FREE-ELECTRON LASER (FEL) UTILIZATION IN SPACE APPLICATIONS (SHIP-BORNE POINTING ACCURACY, DEEP-SPACE COMMUNICATIONS, AND ORBITAL DEBRIS TRACKING)

Jason M. Wittrock
Lieutenant, United States Navy
B.S., University of Minnesota, 2006

Submitted in partial fulfillment of the
requirements for the degree of

MASTER OF SCIENCE IN ASTRONAUTICAL ENGINEERING

from the

NAVAL POSTGRADUATE SCHOOL
December 2011

Author: Jason M. Wittrock

Approved by: Brij N. Agrawal
Thesis Advisor

William B. Colson
Thesis Co-Advisor

Knox T. Millsaps
Chair, Department of Mechanical and Aerospace Engineering

THIS PAGE INTENTIONALLY LEFT BLANK

ABSTRACT

The U.S. Navy is currently conducting research that will support the production of a MW-class free-electron laser (FEL). The Navy's end-state goal is to design and implement a defense system capable of destroying a fast-flying, anti-ship cruise missile (ASCM) target. To this end, the necessity of ensuring accurate pointing control of the beam is required. The first part of this thesis focuses on the U.S. Navy's desired end-state and investigates the ability of feedback and feed-forward control methods to provide improved pointing accuracy to a beam director mounted on a naval vessel similar in size to that of a Ticonderoga-class cruiser while traversing through various sea-states. The second part of this thesis examines the feasibility of employing the FEL as a means of deep-space (Mars and beyond) communication and orbital debris removal and tracking of objects in low-earth orbit (LEO).

THIS PAGE INTENTIONALLY LEFT BLANK

TABLE OF CONTENTS

LIST OF FIGURES

LIST OF TABLES

THIS PAGE INTENTIONALLY LEFT BLANK

LIST OF ACRONYMS AND ABBREVIATIONS

ADR	Active Debris Removal
AGI	Analytical Graphics Inc.
AM	Amplitude Modulation
AMOS	Air Force Maui Optical and Supercomputing
APD	Avalanche Photo-diode
ASCM	Anti-Ship Cruise Missile
ASK	Amplitude Shift-Keying
BASK	Binary Amplitude Shift-Keying
BFSK	Binary Frequency Shift-Keying
BPSK	Binary Phase Shift-Keying
CEP	Circle Error Probable
FEL	Free-Electron Laser
FM	Frequency Modulation
FSK	Frequency Shift-Keying
GEO	Geosynchronous Orbit
GPS	Global Positioning Satellites
HEO	Highly Elliptical Orbit
ISS	International Space Station
LBNL	Lawrence Berkeley National Labs
LEO	Low-Earth Orbit
MDS	Minimum Detectable Signal
NASA	National Aeronautics and Space Administration
NFOV	Narrow-Field-of-View

ONR	Office of Naval Research
OOK	On/Off Shift-Keying
PCM	Pulse-Code Modulation
PSK	Phase Shift-Keying
QPSK	Quad Phase Shift-Keying
SETI	Search for Extra-Terrestrial Intelligence
SSN	Space Surveillance Network
STK	Satellite Tool Kit
WFOV	Wide-Field-of-View

ACKNOWLEDGMENTS

I would like to first and foremost thank the Lord, Jesus Christ, our Savior for providing me with the strength and perseverance to endure, especially during the times when the stress of this endeavor grew to over-whelming proportions, and to ultimately succeed in completing this thesis.

My heart-felt gratitude goes out to my parents, Michael and Debra Wittrock, who have always provided me with unfaltering support, regardless the challenges I was facing. To my mother, who tells me "all things happen for a reason," this experience has definitely pushed my abilities to their utmost and I have come out the other side a greater man for it. To my father, I only hope that I can continue to make you proud as I tackle each major obstacle in my life with the guidance and backing of my family. And, I must also give a great deal of appreciation to my younger brother, Jon. I have never had the shadow of a doubt as to whether or not you would be by my side, and because of that single fact I can stand confident through the worst of all my life's trials.

Finally, I am infinitely honored to have worked with each one of my advisors. Their patience in teaching me the finer details that I had over-looked or just did not have a total grasp on has helped me to make this thesis a body of work I can be proud of having completed. Also, for the multitude of extra hours they put in with me as we neared the dead-line that would mark the end of my time here at the Naval Postgraduate School, words alone can not convey my sincerest gratitude. I thank all of you, and know I will speak fondly of my time here at this school and my experiences working with you all.

THIS PAGE INTENTIONALLY LEFT BLANK

I. INTRODUCTION

The U.S. Navy's interest in the development of a MW-class free-electron laser (FEL) is primarily for the purpose of utilizing the technology as a supplement to the current close-in weapon system (CIWS). A significant amount of research is still required in order for a physical system to attain the power levels discussed within this thesis, but the theory and thought experiments herein will remain pertinent to the future applications of the FEL for when such a system is ultimately designed and built.

The universal problem which all directed-energy, laser weapons face, whether they are chemical, solid state or free-electron lasers is that of precision pointing accuracy. In order to ensure a target is being illuminated by the laser, automated control methods, such as feedback and feed-forward control, are absolutely necessary. For example, to illuminate a target beyond 5 km with a circular, laser beam, which has a 10 cm radius, requires a pointing accuracy on the order or microradians. Examination of this pointing accuracy problem has already begun with regard to employing the weapon system on ground-based platform. After reviewing the basics of the FEL physics and automated control systems, this thesis tackles the U.S. Navy's question of the effects of wave impacts upon a ship's hull and the resultant final pointing accuracy of a ship-mounted beam director. As this is only a first-order analysis, several assumptions were made to reduce coupling effects of the pitch, roll, and yaw motions as a result of the wave motion generated within the SIMULINK simulation model.

Potential space applications were then explored, following the examination of the FEL beam pointing error and the accuracies which were possible after introducing wave motion disturbances. The three space applications for which the FEL was considered viable were deep-space communications, orbital debris removal, and orbital debris tracking.

As for deep-space communications, a thorough comparison between the current RF communications links and a hypothesized FEL-based communications link was conducted. This comparison included an examination of required RF and optical receiver

sizes at distances beyond Mars, minimum and maximum feasible ranges for utilizing a FEL-based communications link, and the potential data rates which may be attainable using a FEL instead of RF communications links. Also provided, is an in-depth discussion of the analogy used to adjust RF modulation to provide potential modulation schemes which may be available to a FEL-based communications link.

Finally, the threat of orbital debris was approached from the stand-pointing of employing the FEL as a means of either removing the debris from Low-Earth Orbit (LEO) or significantly increasing the precision of the measured trajectory of a particular piece of debris.

II. FREE-ELECTRON LASER (FEL) BACKGROUND

A. A NEW CLOSE-IN WEAPON SYSTEM (CIWS)

The U.S. Navy is currently conducting research which will support the production of a MW-class free-electron laser (FEL). The Navy's end-state goal is to design and implement a defense system capable of destroying a fast-flying, anti-ship cruise missile (ASCM) target. The desired weapon system is meant to enhance the close-in defense capabilities of U.S. Navy ships by increasing the effective stand-off range for ASCM's from 2 to 4 km up to 5 km. It takes approximately 30 seconds for a missile traveling at the speed of sound (Mach 1, 330 m/s) to cover 10 km. The incoming missile must be tracked via radar for several seconds over a distance of several kilometers before a defensive system can even begin to fire projectiles in response. Taking into consideration the fact bullets and defensive missiles require time to reach the target, the incoming missile would be destroyed too close to the ship to prevent potential damage from the resultant debris.

With a defensive laser weapon system, it would be possible to engage the incoming missile beyond 5 km, and the kill would occur a few seconds after turning the laser on. This means the missile would be killed around 4 km, the initial engagement range of the current system. Also, because the energy is being transferred at the speed of light, the maneuverability of the missile is rendered irrelevant. Though, in order for any laser to accomplish the task of causing sufficient damage to an ASCM to either destroy or disable it, the laser must be capable of depositing several MJs of energy in the matter of a few seconds [1]. The energy required over this time dictates the necessity of a MW-class laser.

B. BASIC OVERVIEW OF A FREE-ELECTRON LASER

To achieve the desired increased stand-off range and response time, a laser is an attractive solution. We first examine the typical design of a free-electron laser and the inherent advantages. Figure 1.1 illustrates a typical block-diagram representation for a FEL oscillator.

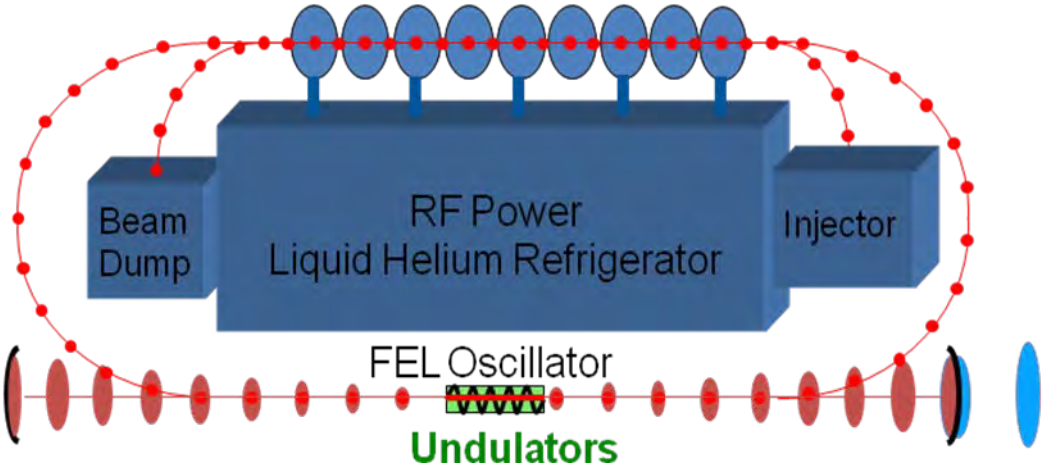

Figure 1.1 Typical FEL Oscillator Configuration. From [1]

A typical FEL will be comprised of five main components: injector; RF accelerator; undulators; resonator mirrors; and beam dump [2]. The injector serves as the point of entry for the electron beam generated by knocking electrons free from a cathode, similar, in principle, to those used in the old CRT televisions. The high power FEL requires that approximately 1 Amp of current leave the cathode. The free electrons are then passed through an RF accelerator in order to increase their energy to approximately 100 MeV. The accelerated electron beam then carries roughly 100 MW of power [1]. Following the accelerator, the electron beam will enter the optical cavity, which is comprised of the undulator and resonator mirrors [2]. Figure 1.2, is not to scale, but illustrates the typical component arrangement with respect to the electron beam.

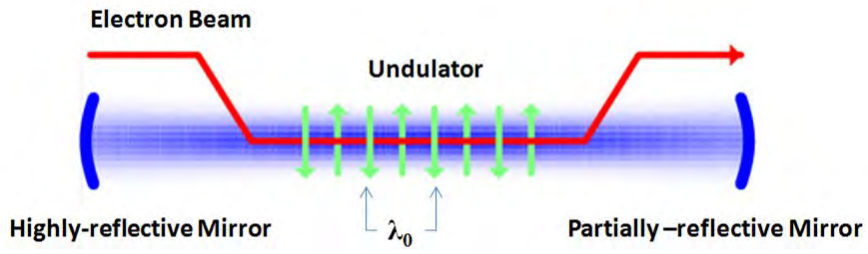

Figure 1.2 Illustration of the FEL Optical Cavity. From [1]

The undulator is comprised of a periodic series of magnets, which are placed such that the poles alternate throughout the length. For example, the first magnet in the undulator is oriented so that North is top and South is bottom, with the second magnet flipping the orientation 180 degrees, alternating until the end of the undulator on the undulator axis. The distance over one period is designated as the undulator period, λ_0. The flipping of the poles of the magnets results in magnetic field with sinusoidal periodicity. This variance in the magnetic field acts upon the electrons in the electron beam as they pass through the undulator, causing them to "wiggle." This electron acceleration causes the electrons to emit radiation. The light is then reflected between the resonator mirrors leading to stimulated emission wherein the light and the electrons in the electron beam interact and exchange energy. One of the mirrors is partially transparent, allowing on the order of 1% of the laser light to leave the optical cavity to be utilized by the system. Thus, to get around a MW of laser light from roughly 100 MeV electron beam carrying around 1 A of current, the cavity has to contain several megawatts of power [1], [2].

Another set of components are bending magnets, which are placed along the beam-line. These magnets serve to guide the electron beam from the accelerator into and out of the optical cavity and finally around to the beam dump. The beam dump provides a safe location to deposit the high-energy electrons after they have traveled through the beam-line. In some instances, the high-energy electrons may be directed back through the RF accelerator to be re-accelerated and sent through the beam-line repeatedly, prior to being deposited in the beam dump [2].

Finally, for any user of the optical beam, mirrors would be needed along the optical path in order to get the laser from the mirrors to the beam director and ultimately the target [2].

C. FEL ADVANTAGES

The greatest advantage the free-electron laser has over all other lasers is its unprecedented flexibility. All other lasers require passing through some physical lasing medium, (i.e., gas, liquid or solid-state) in order to produce coherent, electromagnetic radiation. The FEL uses the electron beam exclusively and can vary the desired operating wavelength without making significant changes to the overall design, something these other lasers are not capable of doing [1]. This is achieved through adjusting the electron beam energy or undulator magnetic field strength or both. Thus, a single FEL is continuously tunable over a wide range of wavelengths. The FEL can also be designed to operate in various wavelength ranges. It has already been successfully tested at microwave, infrared, visible, ultra-violet, and x-ray wavelengths [1]. This flexibility provides the system with the ability to adjust to the environment through which it is being fired, enabling the selection of the wavelength that will most efficiently transmit the energy to the target.

From the stand point of weapon system considerations, the amount of available ammunition and the cost of running the weapon system are important factors. For the purposes of determining the advantage of using a FEL weapon system in lieu of a conventional weapon system, it will be assumed that the FEL would be employed upon a naval vessel similar to the Ticonderoga-class cruiser. A Ticonderoga-class cruiser is powered by four General Electric LM2500 gas turbines, with an approximate fuel efficiency of 35%. From results provided via FELSIM (Advanced Energy Systems results), it is estimated that a FEL weapon system will have an electric efficiency of about 20% and that each shot lasts a few seconds [1]. Figure 1.3 shows that the FEL would require about one gallon of fuel oil per 5-second shot. At this rate of fuel consumption, the FEL could be fired repeatedly for a minimal total cost.

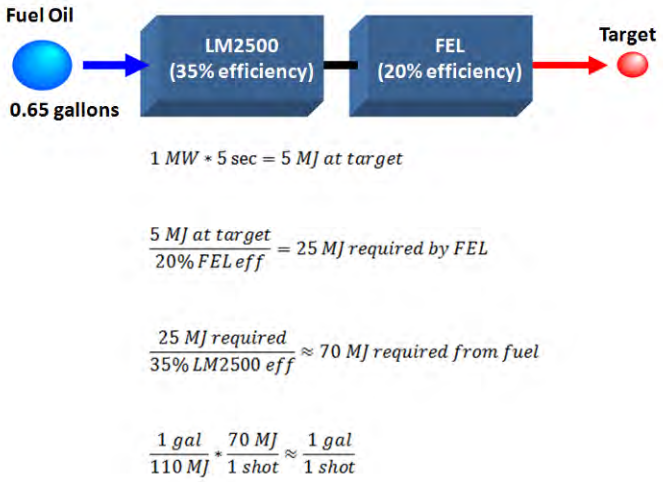

Figure 1.3 FEL Efficiency. From [1]

D. SHIP-BORNE EMPLOYMENT

There are currently two primary possible FEL configuration options that are capable of achieving the goal of having multiple available operating wavelengths: utilizing multiple beam-lines or varying the electron beam energy [2].

The first approach to solving the problem of multiple operating wavelengths is to have multiple, branching beam-lines. Designing to this solution requires in one branch from the main beam-line for each desired wavelength. Each branch is comprised of a single undulator and a pair of resonator mirrors. The undulators would need to be specifically engineered to provide the desired wavelength given the input electron beam energy. Lawrence Berkeley National Labs (LBNL) is currently designing an x-ray FEL in this sort of configuration [3].

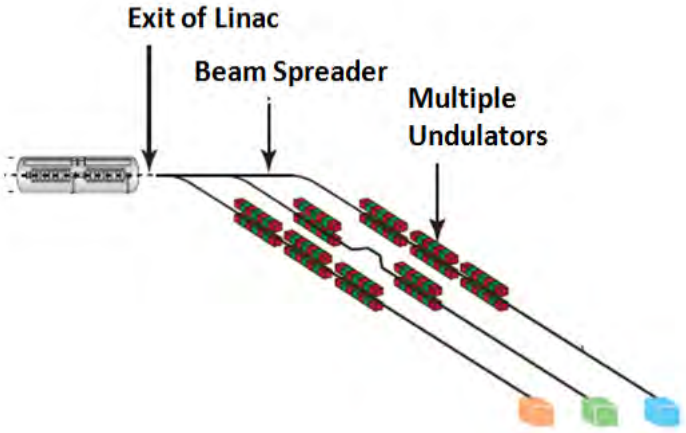

Figure 1.4 LBNL Next-Generation Light Source. From [3]

Figure 1.5 further illustrates the differences between the beam lines by highlighting the difference in the undulator periods for each desired wavelength.

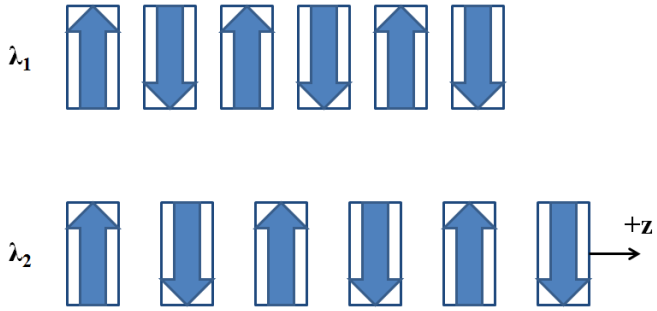

Figure 1.5 Qualitative Illustration of Multiple Magnetic Undulators

The second method involves varying the electron beam energy to obtain the different operating wavelengths. It will be shown in detail in the following section that the electron beam energy has a greater impact upon the resultant operating wavelength than the undulator characteristics. This configuration is probably the best approach for the Navy FEL design process. The multiple-undulator and multiple beam-line approaches are infeasible, due to ship size and spacing constraints. If the system is land-based, such as the facilities at White Sands or the Advanced Maui Optical and Space Surveillance facility, the multiple-undulator approach becomes more attractive.

Although, the added complexity can be avoided altogether by designing the system such that it varies the operating wavelength strictly through varying the input electron beam energy.

E. DESIGN PARAMTERS

As for the actual design of a free electron laser, the first parameter to be specified should be the desired operating wavelength [1]. Following the determination of the operating wavelength, the design method and configuration need to be decided upon. The subsequent equations will detail the second design approach for varying the operating wavelength as a function of various the electron beam energies. Equation 1.1 shows the dependence of the desired operating wavelength upon other FEL design parameters [2].

Eq. 1.1 $$\lambda = \frac{\lambda_0(1+K_{rms}^2)}{2\gamma^2}$$

where λ is the desired operating wavelength; λ_0 is the undulator period; and γ is the Lorentz factor. K_{rms} is the undulator parameter. K_{rms} is dependent upon the magnetic field strength present in the undulator and the undulator period as shown in Equation 1.2

Eq. 1.2 $$K_{rms} = \frac{eB_{rms}\lambda_0}{2\pi m_e c}$$

where e is the electron charge magnitude of 1.6 x 10^{-19} C and B_{rms} is the root-mean square of the magnetic field within the undulator given in Telsa [2].

For the typical undulator, B_{rms} is held at approximately 0.4 T. A typical undulator has a period λ_0 of approximately 3 cm and an undulator parameter K_{rms} of approximately 1. Defining the undulator using these typical parameters, gives Equation 1.3, which shows the operating wavelength, is primarily driven by the inverse square of the Lorentz factor γ [1].

Eq. 1.3 $$\lambda = \frac{0.03}{\gamma^2} meters$$

The Lorentz factor is defined by Equation 1.4

Eq. 1.4 $$\gamma = \frac{c}{\sqrt{c^2 - v_{elec}^2}} = \frac{1}{\sqrt{1-\beta^2}}$$

Eq. 1.5 $$\beta = \frac{v_{elec}}{c}$$

Finally, in determining the energy required by the electron beam, the Lorentz factor, which yields the desired operating wavelength can be calculated from Equation 1.3. The result of this calculation must then be substituted into Equation 1.6, which yields the relationship between the Lorentz factor and the energy in the electron beam [2].

Eq. 1.6 $$E_b = (\gamma - 1)m_e c^2$$

where γ is the Lorentz factor; m_e is the mass of the electron at 9.11 x 10^{-31} kg; and c is the speed of light at approximately 3 x 10^8 m/s. E_b can be converted from Joules to eV by dividing E_b by 1.6 x 10^{-19} J/eV. As the electron beam energy is usually provided in eV the product of $m_e c^2$ gives the rest energy of the electron at 0.511 MeV.

Thus the relationship between the electron beam energy and the operating wavelength is given by Equation 1.7 [1].

Eq. 1.7 $$\lambda = \frac{0.03}{\left(\frac{E_b}{m_e c^2} + 1\right)^2} = \frac{0.03(m_e c^2)^2}{(E_b + m_e c^2)^2} = \frac{0.03(0.511 MeV)^2}{(E_b + 0.511\ MeV)^2} meters$$

From these calculations, it is relatively easy to determine the required electron beam energy to obtain the desired operating wavelengths.

Table 1.1, on the following page, gives possible design values for these design methods. For the multiple-undulator configuration, the electron beam energy was held at a constant 65 MeV. In the first case with the multiple-undulator configuration, each of the undulators was presumed to be designed to have a K_{rms} of 1.0. As such, each of the undulators required a different B_{rms} to match the respective λ_0. In the second case, the magnetic field strength within the undulators was assumed to be held such that there was a constant B_{rms} of 0.36 T, while K_{rms} was varied as a result of the different λ_0. Finally, for the purpose of illustrating the flexibility of a single undulator, the electron beam was varied to yield the desired wavelength while maintaining K_{rms}, B_{rms}, and λ_0 constant.

INP Wavelength			
λ (nm)	900	1600	2100
Varying B_{rms} due to variance in λ_0			
E_{beam} (MeV)	65.00	65.00	65.00
K_{rms}	1.00	1.00	1.00
B_{rms} (T)	0.73	0.41	0.31
λ_0 (cm)	1.48	2.63	3.45
Varying K_{rms} due to variance in λ_0			
E_{beam} (MeV)	65.00	65.00	65.00
K_{rms}	0.68	0.94	1.07
B_{rms} (T)	0.36	0.36	0.36
λ_0 (cm)	2.03	2.81	3.21
Varying E_{beam}			
E_{beam} (MeV)	92.78	69.46	60.56
K_{rms}	1.00	1.00	1.00
B_{rms} (T)	0.36	0.36	0.36
λ_0 (cm)	3.00	3.00	3.00

Table 1.1 FEL Design Parameters for Different Configurations

THIS PAGE INTENTIONALLY LEFT BLANK

III. ATMOSPHERIC EFFECTS ON THE FEL

The infrared free-electron laser is subjected to the same atmospheric effects and diffraction as it propagates through the atmosphere. In order to mitigate these effects, the Office of Naval Research (ONR) determined a set of operating wavelengths between 1 and 2 μm, which would be ideal for the Navy's applications and are determined by the predicted effects of the atmosphere on the free-electron laser light [1]. The following sections discuss the primary atmospheric effects and diffraction, which contribute to beam degradation and the considerations that were made to minimize the beam degradation of the free-electron laser. These effects are spreading due to diffraction, scattering, and power loss due to atmospheric absorption, and thermal blooming.

A. DIFFRACTION

In the case of transmitting electro-magnetic waves, diffraction describes the spreading of the wave-front as it propagates further from the source. This spreading causes the beam to be less intense at a receiver some distance away. As a result of this spreading and to achieve the desired intensity at the receiver, the optics of the beam director must be specifically tailored to yield a spot-beam with the desired average intensity and/or the power of the laser must be increased [1].

Figure 2.1 gives the graphical representation of the spreading due to diffraction of a Gaussian beam, transmitted by a non-focusing mirror, as it propagates through the atmosphere or vacuum. In Figure 2.1, w(z) is the beam width as dependent upon the distance along the z-axis, wherein w_0 is the beam waist, or the smallest radius from of the beam from center axis to outer edge. In Figure 2.1, z = 0 also represents the location of the beam director.

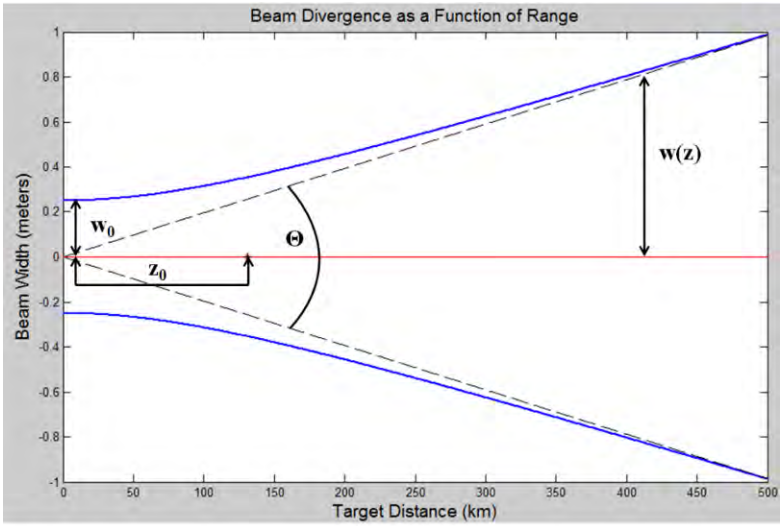

Figure 2.1 Divergence of a Gaussian Beam from a Beam Director

Equation 2.1 provides the method for determining the radial beam width at any range along the laser beam [1].

Eq. 2.1 $$w(z) = w_0\sqrt{1 + \left(\frac{z}{z_0}\right)^2}$$

where z_0 signifies the Rayleigh length for the particular wavelength and beam waist, as shown in Equation 2.2 [1].

Eq. 2.2 $$z_0 = \frac{\pi w_0^2}{\lambda}$$

The Rayleigh length varies with the operating wavelength and is calculated such that it delineates the distance from the beam director at which the cross-sectional area of the beam is doubled with relation to the beam waist [1]. Finally, Θ is the full angular spread of the beam and given by Equation 2.3. The beam divergence is represented by the variable θ. This angle is measured from the central axis to the asymptote created as the distance from the beam director z becomes much larger than the Rayleigh length and can be estimated by Equation 2.4 [1].

Eq. 2.3 $$\Theta = 2\theta$$

Eq. 2.4 $$\theta = \frac{\lambda}{\pi w_0}$$

Equations 2.1 to 2.4 describe Figure 2.1 and assume that the mirror in the beam director is non-focusing and so the laser beam diverges from the central axis to some larger beam width at the receiver. If the symmetry about the beam waist is maintained, but the location of the beam waist is shifted such that the beam waist is located at the receiver, we get the scenario illustrated in Figure 2.2. This provides a solution to the beam spread problem; using focusing mirrors in the beam director.

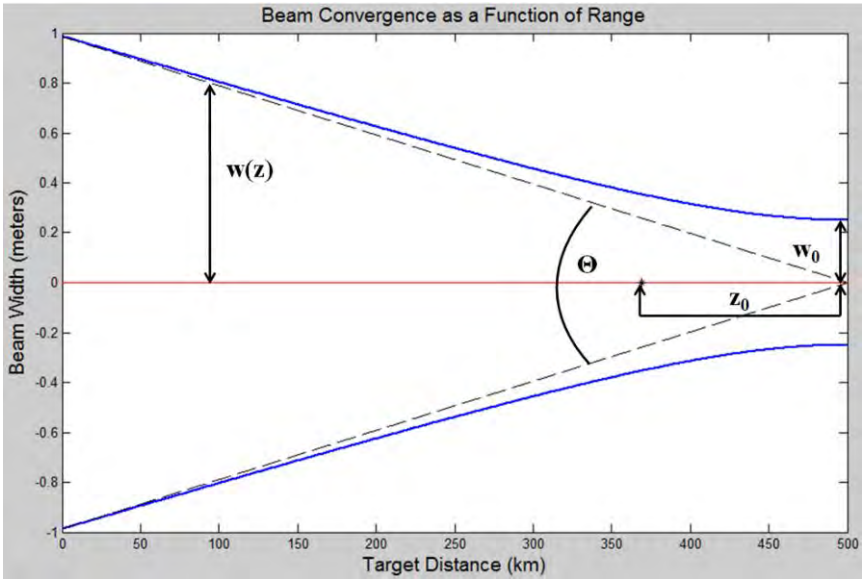

Figure 2.2 Convergence Resulting from a Focusing Mirror

For the purposes of a focusing mirror, Equations 2.2 to 2.4 are still applicable. Equation 2.5 shows the one modification required to make Equation 2.1 hold true while taking into consideration the new beam waist location.

Eq. 2.5 $$w(z) = w_0\sqrt{1 + \left(\frac{z - z_{receiver}}{z_0}\right)^2}$$

In Equation 2.5, z is still representative of the distance along the beam line from the beam director. The additional term, $z_{receiver}$, indicates the location of the target along the z-axis with respect to the beam director. For example, if the receiver engagement range were desired to be located 5 km from the ship, $z_{receiver}$ would be set to 5 km and the beam width could be determined at any point along the beam path between the beam director and the

receiver. With the determination of the beam width at some distance from the beam director, the corresponding intensity of the beam at that point along the beam path can be calculated. This allows for the determination of the minimum range at which the spot-beam intensity is no longer greater than the desired intensity threshold.

Another technology that is on the rise is adaptive optics. These optical control systems are designed to enable the bending or focusing of the beam director's mirror to provide the necessary radius of curvature to adjust the focal point of the beam for a given wavelength. It is through these adaptive optical systems that the Navy FEL will be able to vary the engagement range to match the mission needs regardless of the operating wavelength and the limitations imposed by the Rayleigh length [1].

B. RAYLEIGH AND MIE SCATTERING

Another phenomenon that influences the intensity of the spot beam arriving at the receiver is scattering. Scattering is the spreading of the transmitted beam due to photon-particle collisions. There are many forms of particle scattering, but the two that are dominant in atmospheric scattering are Rayleigh and Mie scattering [4].

Rayleigh scattering occurs when a photon collides with particles that have a diameter less than 10% of the wavelength of the photon. The impact angle of the collision is statistically random giving a random scattering angle. As the photons have no preference in their scattering direction, the resultant intensity at the receiver can be orders of magnitude less than desired. The resultant intensity of the beam is inversely proportional to the fourth power of wavelength. This wavelength dependence is important, as shorter wavelengths scatter significantly more than longer wavelengths [4]. In order to ensure the FEL experiences minimal dispersion effects and loss of beam intensity from Rayleigh scattering, longer wavelengths (on the order of microns) should be employed.

Mie scattering occurs when the photon collides with particulate matter in the atmosphere such as water droplets or dust particles [4]. Mie scattering takes place on the macroscopic level, and is similar to the interaction of waves bending around an obstruction. The photon's wave-like response to the obstructions causes two things to

occur at the receiver: the first is the diffusion of the beam, and thus the reduction in beam intensity at the target; and the second result is more photons scattering along the original beam path. The second result helps to slightly off-set the diffusion of the beam by ensuring more photons arrive at the target [4]. Thus, it is easier to achieve the desired intensity at the target if the wavelength is selected such that the primary scattering effect to mitigate is Mie scattering.

C. ATMOSPHERIC ABSORPTION

Another major detractor from the quality of the beam that arrives at the target is atmospheric absorption. Figure 2.3 is a depiction of the various atmospheric absorption bands and the wavelengths at which they occur. In this figure, the amount of the solar radiation that reaches the Earth's surface has been measured (red shading) and is compared to the known blackbody spectrum of the Sun (black line) and the sunlight as measured at the top of the atmosphere (yellow shading).

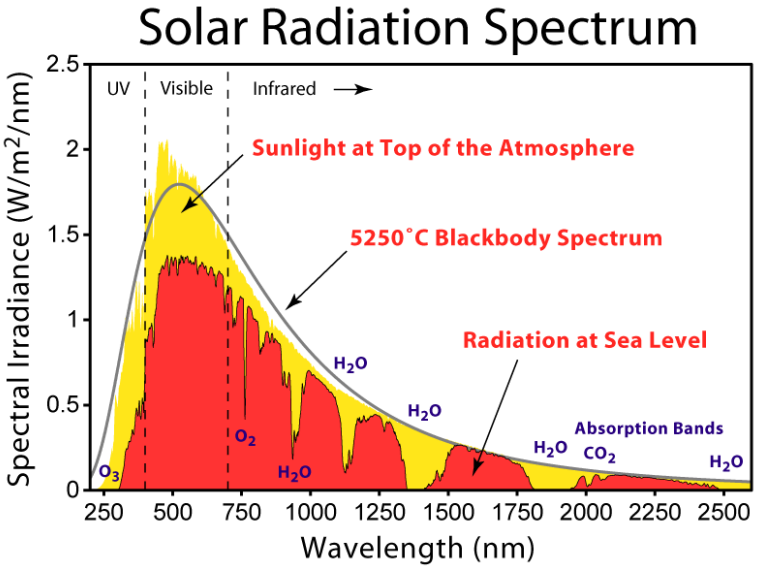

Figure 2.3 Atmospheric Absorption Bands (from Rohde 2007) [5]

As can be seen from Figure 2.3, the greatest impedance to transmitting a laser is the absorption resulting from water vapor in the atmosphere. The major water absorption bands occur at 850, 1150, 1300, and 1850 nm. The spectral bands with the lowest

amount of atmospheric absorption occur between 1500 and 1750 nm and 2100 to 2300 nm, making 1600 and 2100 nm attractive options for the operation of a high-power free-electron laser.

There are other absorption minimums in the figure as well and they are located around 1000 and 1250 nm. Before considering these wavelengths as options, a comparison of the Rayleigh scattering criteria needs to be examined. In comparing the significance of Rayleigh scattering on the different wavelengths, the case for using 1600 and 2100 nm is further solidified as the 1000 nm wavelength is affected by Rayleigh scattering 6.5 times more than the 1600 nm option and 19.4 times more than the 2100 nm option. These results come from comparison of the Rayleigh scattering dependence upon the inverse of the fourth power of the operating wavelength.

D. THERMAL BLOOMING

Finally, it should be briefly re-iterated that an alternative method of ensuring the laser arrives at the receiver with the desired intensity is to increase the power of the laser. Though, increasing the power of the laser may also result in the realization of a secondary, problematic phenomenon known as "thermal blooming [1]." Thermal blooming causes the beam to spread from the central beam path and is a power-dependent effect. The interaction between the laser and the atmosphere can result in the atmosphere heating along the laser's path. The increase in the temperature of the atmosphere causes a local change to the index of refraction, essentially causing the heated portion of the atmosphere to act as a distorting lens [6]. Many studies have been conducted in this area and there exist many computer algorithms for estimating the thermal blooming produced by a laser at a particular output power.

This is mentioned strictly for the purposes of informing the reader that a potential complication can arise at higher laser power levels and for beams that are intended to maintain a fairly narrow beam waist (near 10 cm). For many of the space applications explored in later chapters, thermal blooming is not an issue because the beam waist is several times larger than 10 cm.

E. OPERATING WAVELENGTH SELECTION

Evaluating all the background information included to this point, the ideal operating wavelengths for the Navy's purposes seem to be around 1600 and 2100 nm. This judgment takes into consideration the electron beam energy required to achieve these wavelengths (E_{beam} = 60–70 MeV); the typical undulator (λ_0 = 3 cm, $K_{rms} \approx 1.0$); and the predicted atmospheric effects that can effectively degrade the beam quality at the target. For the purposes of this thesis, the remaining calculations involving the FEL operating wavelength will be carried out using 1600 nm, as over long distances, shorter wavelengths provide the best results for minimizing beam spreading.

THIS PAGE INTENTIONALLY LEFT BLANK

IV. FUNDAMENTALS OF POINTING CONTROL

One of the most important operational difficulties the engineers who construct the U.S. Navy's FEL will face is that of ensuring the laser actually hits the intended target, which for the Navy's purposes will be an anti-ship cruise missile (ASCM) of one sort or another. When the base supporting the laser is stationary and the target is stationary, the targeting solution is the fairly basic point-and-shoot methodology. A more complicated case has the target moving in an unpredictable fashion while the FEL facility is stationary.

In contrast to a stationary FEL facility, a naval vessel is in a dynamic and continuously evolving environment [7]. The ocean's wave motion has a direct impact upon the stability of all structures fixed to the hull and the overall orientation of the ship. In order for the Navy to successfully integrate a laser-based ship-defense system in this environment, these wave motions must be taken into consideration. Attempts to predict the wave motion, and the ship's response to that motion, may prove futile due to the convolution of many different, and sometimes coupled, variables. Instead of attempting to predict and preemptively compensate for the wave motion, a viable alternative is to develop a reaction-based system capable of responding to variations as a result of the external base (hull) excitation. To further convolute the targeting problem, in the Navy's scenario, the target is still moving as well. Without some form of automated control system, the likelihood of actually hitting the target with the laser borders on impossibility. This realization leads to the necessity of designing an automated, reaction-based control system.

A. OPEN-LOOP CONTROLLER

Ultimately, most automated control systems can be reduced to combinations of three primary control types: open-loop, feedback, and feed-forward control [8]. In the instance of an open-loop controller a desired pointing angle is input into the control system and the actuator, motor, or other motion control mechanism translates that input into a control torque, which then causes the beam director, in this case, to move to the

commanded position [8]. Throughout these next two chapters SIMULINK will be used to simulate the hardware being controlled in a software environment. Figure 3.1 is a SIMULINK model of a basic open-loop controller.

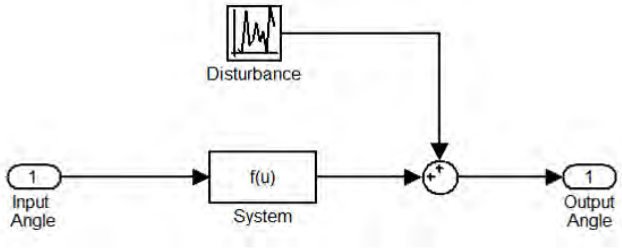

Figure 3.1 Open-Loop Controller

Figure 3.1 also includes the introduction of a random disturbance that will have a direct impact upon the output angle [8]. If the disturbance is known to be sufficiently small relative to the required accuracy of the final pointing angle, then the open-loop control system can solve the problem. For example, if a laser experiences a disturbance on the order of a few millirad, then the bore-sight pointing accuracy will only be off of the target mark by a few millimeters over the distance of a few meters. Depending upon the application, an error of a few millimeters may be totally acceptable. Unfortunately, for the ship-defense applications the Navy has in mind, with an engagement range of a few kilometers, the error grows to be on the order of meters at the target. The open-loop method of control has no means of checking for or correcting the error induced by the disturbance [8]. As such, open-loop controllers will most likely not be used in the controller designed for the ship-borne FEL.

It is important to understand that a disturbance can occur at any point within the system and that when conducting a simulation using modeling software such as SIMULINK the designer is required to decide upon the location that best simulates where the disturbance will be introduced in the actual, physical system. In Figure 3.1, the disturbance was introduced after the actuators and the control torque of the system, thus having a direct affect on the output pointing angle. The disturbance could also be added within the system block of the model to simulate disturbances experienced within the actuator or the rotational rate sensors. The fact disturbances can be added at various

locations of the model is necessary to remember when determining which disturbances will have the greatest impact on the simulation model that is eventually designed to simulate the Navy's targeting problem.

B. CLOSED-LOOP FEEDBACK CONTROLLER

The second control system mentioned was the closed-loop feedback controller. This particular controller is shown in Figure 3.2.

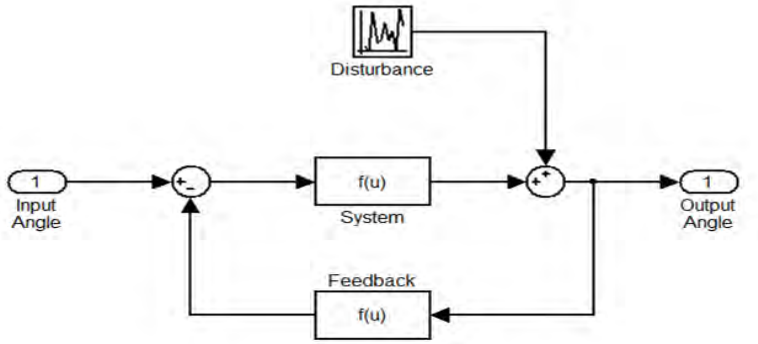

Figure 3.2 Closed-Loop, Feedback Controller

The typical feedback controller is comprised of the following components: desired angle input; the actuator, or control plant; a rate sensor; a position sensor; and proportional and derivative gains, which comprise the PD-controller [8]. Just as with the open-loop controller, the desired input angle represents the point at which the data from the ship's target tracking system is injected into the control loop. The system plant is configured to account for the moments of inertia of the pointing mechanism and to convert the differences between the current pointing angle and the desired pointing angle into an actionable torque [8]. The determined output torque, without disturbances, would be sufficient for adjusting the output pointing angle to match the input desired angle. With the disturbances included, the feedback portion of the loop is compared to the desired angle and that difference, combined with the proportional and derivative gains, is used in determining the necessary output torque [8]. This goal of this process is to achieve a difference between the output and input angles on the order of 10^{-6} radians measured error.

The feedback loop is necessary due to the fact that the open-loop system cannot handle unknown disturbances [8]. There is a delay to the feedback system that is unavoidable because each step checks the desired angle against the previously measured angular position. This is not to say the target position is never achieved, it just does not occur immediately, as illustrated in Figure 3.3, depicting the overshoot beyond the desired pointing angle at 1.3 seconds, and then the overshoot during the correction at 1.5, before settling at the desired pointing angle at 1.7 seconds.

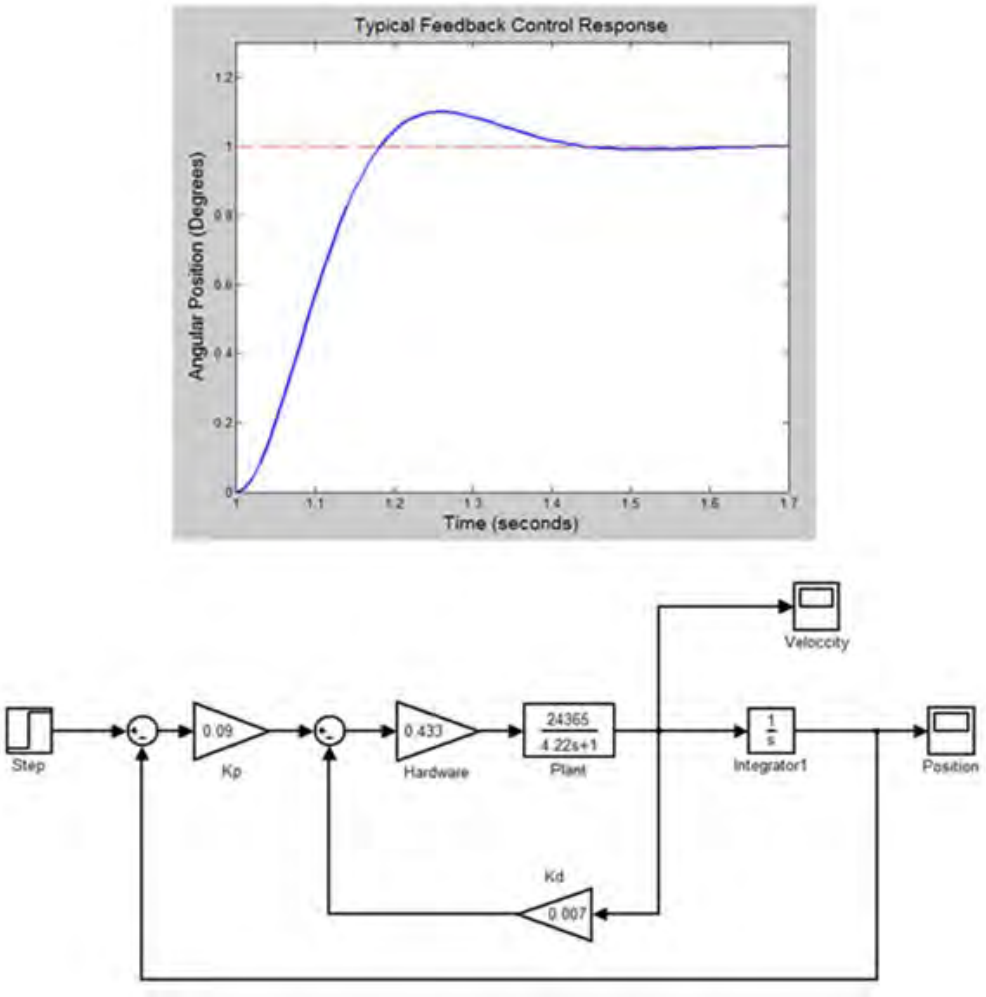

Figure 3.3 Closed-Loop Feedback Control Response to a Step Input

The controller used to generate the plot in Figure 3.3 is an example of a typical PD-controller. The two, nested feedback loops, the inner loop for rate feedback and the outer loop for position feedback, provide the comparison control for determining the necessary torque from the plant output [8]. The K_p gain is the proportional gain and scales the error between the desired pointing angle and the current actual pointing angle and the K_d gain scales the information from the rate sensor and feeds that back into the control process after the proportional gain and just prior to the system plant. The block diagram in Figure 3.3 can also be represented mathematically as Equation 3.1

Eq. 3.1
$$u = K_p(\theta_{desired} - \theta_{actual}) + K_d(\omega_{desired} - \omega_{actual})$$
$$e = \theta_{desired} - \theta_{actual}$$
$$u = K_p e + K_d \dot{e}$$

where u is the resultant control torque; $\theta_{desired}$ is the commanded angle, in this case a constant 1 degree input; θ_{actual} is the measured pointing angle; $\omega_{desired}$ is the angular rate that is required to meet the end-state conditions; ω_{actual} is the measured angular rate detected by the rate sensors; and e is the difference between the desired and the actual angles [8].

Figure 3.3 helps to highlight the one of the two advantages the feedback controller has over an open-loop control system, its ability to react to a changing environment with unknown disturbances. The second advantage a feedback controller has is its ability to be tuned to give the desired type of response that is necessary for a given mechanical process. In some cases an overshoot is desired as all that is required is that the beam director be rotated quickly; in other instances precise pointing accuracy, with no overshoot, may be required and so the motion is slower and more exact. Dependent upon the magnitudes of the K_p and K_d gains, the system response can be adjusted. The response shown above in Figure 3.1 is for an under-damped system, which explains the slight overshoot. For a critically damped system, there would be no overshoot, but the controlling actuator would move much slower than the under-damped system. The one remaining damping possibility is that of an over-damped system, in which case the beam director may never reach the desired angle, but there will be absolutely no chance of an overshoot either.

C. FEED-FORWARD CONTROLLER

Now, because of these two benefits, the ideal solution for many control problems is to employ a feedback control system, but if it is possible to accurately model and predict incoming disturbances, then another control option becomes available, feed-forward controllers [9]. Feed-forward controllers require that the incoming disturbance can be predicted such that it can be summed with the desired input angle prior to the desired input angle being passed to the system controller. In this manner, the system controller is commanding a torque that takes into account the expected disturbance to be experienced by the system as well as the desired pointing angle [9]. This essentially has the effect of nullifying the disturbance prior to it having a significant effect upon the final output pointing angle. The measurable result of using a feed-forward system can yield a great improvement in the error reduction of the system. Figure 3.4 shows how this controller would be modeled in SIMULINK.

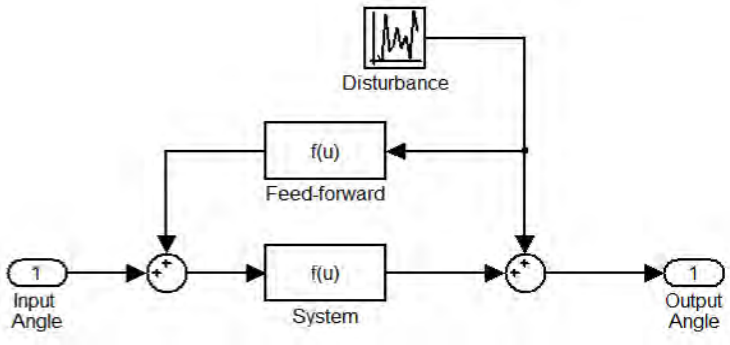

Figure 3.4 Feed-Forward Controller

As wonderful as it would be to reduce the few millirad error assumed to be present in the final pointing angle earlier in this chapter to a few microrad, utilizing only a feed-forward control system will not provide the successful results desired. This type of controller is not ideal for the large movements that are resultant from pitch, roll, and yaw of a naval vessel and the direct impact this motion has on the final pointing angle of the beam director. One can attribute this to the notion that predicting the exact wave motion in real-time is an exercise in futility. Certainly, computer models have been

developed for simulating the ocean's surface behavior, but these models will not provide the fidelity necessary to successfully implement an exclusively feed-forward control system. I state the problem with the feed-forward control system in this manner because it is within the realm of possibility to couple a feed-forward controller with a feedback controller to provide the exceptional results, which can otherwise only be attained through use of automated error prediction and correction.

THIS PAGE INTENTIONALLY LEFT BLANK

V. FEL POINTING SIMULATION

A. FEL POINTING SIMULATION MODEL DESCRIPTION

Equipped with an understanding of the available control systems that can be potentially implemented to solve the targeting problem posed by the Navy's ship-borne FEL, a software simulation model could now be designed. The key factors taken into consideration when designing this model were the necessity of continuous tracking of an incoming projectile; fine pointing accuracy with an acceptable error of roughly 10^{-6} radians; and the overall impact of the surface wave motion on the final pointing angle.

A previous Naval Postgraduate School technical report (NPS-MAE-09–001) had discussed the feasibility of utilizing a high-energy laser testbed to refine algorithms and controls for assessing the viability of mounting a laser on a U.S. Army ground fighting vehicle [10]. The model designed for simulating that testbed and the approach to modeling the disturbances experienced by the ground fighting vehicle served as the skeletal framework for the solution proposed to the Navy's targeting problem. Figures 4.1 and 4.2 show the picture of the laboratory beam control testbed and a line-drawing schematic of this testbed.

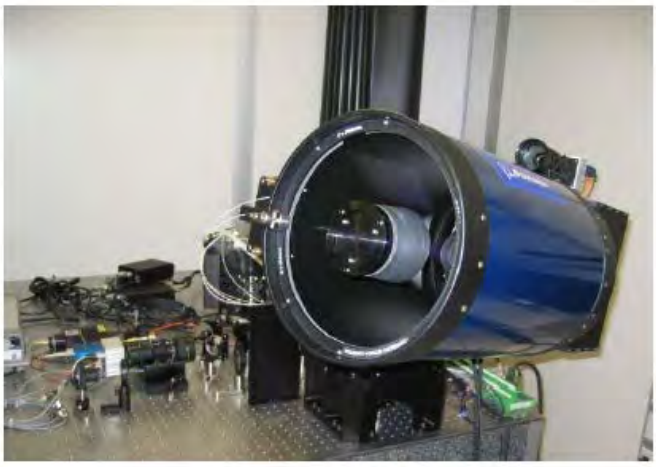

Figure 4.1 Beam Control Testbed. From [10]

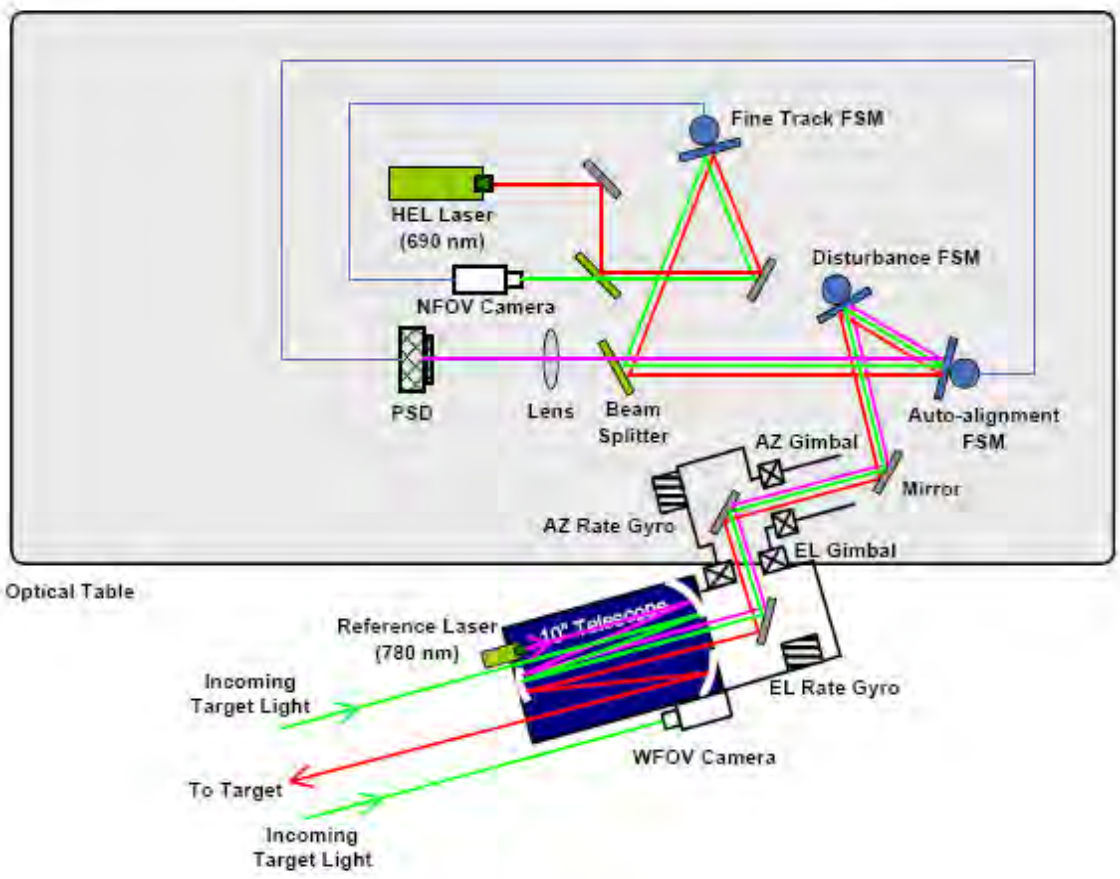

Figure 4.2 Line-Drawing Schematic of Beam Control Testbed. From [10]

The Wide-Field-of-View (WFOV) Tracking Loop computes the error between the beam director's measured line-of-sight and the center of the target being tracked using a WFOV tracking camera. The desired pointing angle is driven by the target's angular location with respect to the ship, and used to command azimuth and elevation gimbals of a beam director. The WFOV Track Loop is comprised of two feedback control loops, one for the angular rate sensor and one for the angular position sensor.

As for the Narrow-Field-of-View (NFOV) Tracking Loop, this is comprised of a camera and a fast-steering mirror (FSM). The purpose of the NFOV Tracking Loop is to apply final corrections to the pointing control. In other words, the NFOV Tracking Loop detects and corrects the errors for which the WFOV Tracking Loop could not compensate, or remove. This further minimizes the error between the line-of-sight and the target.

Figure 4.3 shows the SIMULINK model for the ship-borne WFOV and NFOV elevation tracking control in its finalized state.

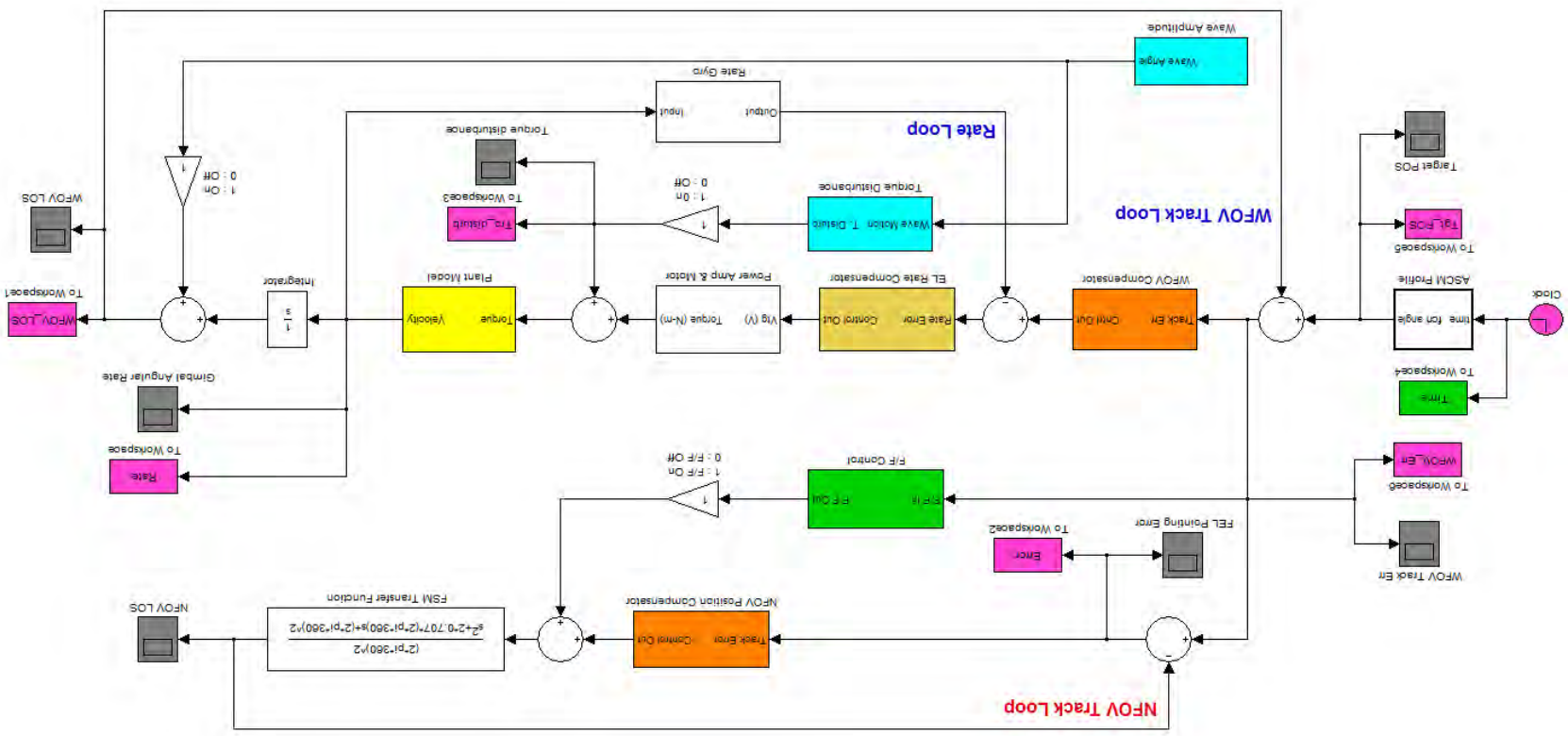

Figure 4.3 Ship-borne WFOV/NFOV Tracking SIMULINK Model

The specifics of each of the loops and disturbances will be discussed in more detail in the following sections.

As this model was to serve as the preliminary estimation of the controllability of the beam to within the acceptable limit of 10^{-6} radians, some pretty significant assumptions were made. First, it was assumed that the housing structure for the beam director would have enough rigidity that rotations through angles in the azimuth and elevation directions could be completely de-coupled from one another. With this assumption, no corrections would be required for the elevation pointing angle as the beam director were moved through an azimuth rotation, and vice versa, no compensations would be necessary for the azimuth pointing angle as the beam direct were moved through an elevation rotation.

The second critical assumption was that the Navy vessel would only experience pure motion. The implication of this is that if the ship is caused to pitch, then only the elevation pointing angle is affected as the pitch will not result in any roll or yaw motion. In reality, this is in an over-simplification of the environment, as an impact from a wave upon the hull is likely to cause the ship to respond in a manner that is some combination of pitch, roll, and yaw. Though, for a first approximation, this was deemed an acceptable constraint in order to keep the tracking problem from becoming too complex without having any prior data points.

Third, the primary disturbances are the result of the wave motion and the ship's reaction to the wave impacts upon the hull. This implies the motion of the waves at various times and locations needs to simulated and treated as an input into the system. Also, with some consideration, it was determined the wave disturbances needed to be introduced into the system at two locations within the system. This was because the wave motion was of a very low frequency when compared to the frequencies experienced by the ground fighting vehicle traversing terrain [7], [10]. The first place the disturbance needed to be implemented was in addition to the desired torque, just prior to being input into the system plant. This is an inertial disturbance torque to the gimbal due to the base

motion. The second location was in direct addition to the final position angle, as the entire hull will pitch, roll, or yaw, in response to the waves.

The final assumption was inferred from the knowledge that this ship-defense system was being designed to be first employed on a ship of a size similar to a Ticonderoga-class guided-missile cruiser. With this knowledge, the assumption as to the length of the vessel was made to be 180 meters, with a bow height of 20 meters. Also, the primary pitch axis was assumed to be one-third the length from the location the beam director was to be mounted, at 60 meters aft from the bow.

Having established constraints to the problem, the model that was originally designed to determine the reliability of a high-energy laser system employed on a ground fighting vehicle [10], was modified and adjusted to suit the purposes of providing the U.S. Navy with an initial analysis of the feasibility of utilizing a similar type of system, powered by a free-electron laser, on its proposed all-electric ships [1].

B. DISTURBANCES – WAVE MOTION AND INERTIAL TORQUE

In this set of simulations, the wave motion was treated as the sole cause of various disturbances within the system. As for the magnitude of the waves that were examined, in these simulations, the maximum mean wave height was set to be approximately 4 meters. According to the World Meteorological Organization, a wave height of 4 meters is right on the border between being classified as rough or very rough seas [11]. This was considered the ideal test condition because any ship-defense system is going to be required to function in the best possible weather as well as in the worst possible weather. The driving belief being if the controller is able to correct the pointing angle and maintain a successful track on the target while pitching in rough seas, it will have absolutely no problem tracking the same target during calmer seas.

Figures 4.4 and 4.5 go somewhat hand-in-hand. Figure 4.4 is the wave spectrum that was used throughout the simulations and calls to attention the fact that the majority of the wave motion occurs at frequencies less than 1 rad/sec. This power spectrum was generated from Equation 4.1 to Equation 4.3 [7].

Eq. 4.1 $$\xi(x,y,t) = \sum_{i=0}^{N} \bar{\xi}_i \cos(k_i x \cos\chi + k_i y \sin\chi + \omega_i t + \theta_i)$$

where ξ is the wave height; ξ_{bar} is the mean wave height as determined by the frequency spectrum provided in Equation 4.2; k is the wave number, which is 2π over the wavelength; χ is the incident angle of the wave against the hull, with aft being 0 degrees and the bow being 180 degrees; ω is the wave frequency of the particular component; and θ representative of the phase magnitude of the wave. [7]

Eq. 4.2 $$\bar{\xi}_i = \sqrt{2\int_{\omega_i-\frac{\Delta\omega}{2}}^{\omega_i+\frac{\Delta\omega}{2}} S(\omega)d\omega}$$

In Equation 4.2, each of the frequencies are divided by an equivalent interval, $\Delta\omega$; the limits for the integral are what could be considered the separation buffers, and extend half-way to the next interval, and half-way down to the previous interval; and S(w) is the spectrum magnitude at the input frequency [7]. Equation 4.3 is the Modified Pierson-Moskowits (MPM) spectrum , and was used in creating the wave spectrum in Figure 4.4, which was then propagated forward through time to predict or simulate the motion of the ocean at various times and locations [7]. The only two variables not yet introduced by Equation 4.3 are the mean wave height, h and the mean wave period T. For purposes of these simulations, h was varied between 0 to 4 meters and T was varied between 5 and 10 seconds.

Eq. 4.3 $$S(\omega) = \frac{4\pi^3 h^2}{\omega^5 T^4} e^{\left(\frac{-16\pi^3}{\omega^4 T^4}\right)}$$

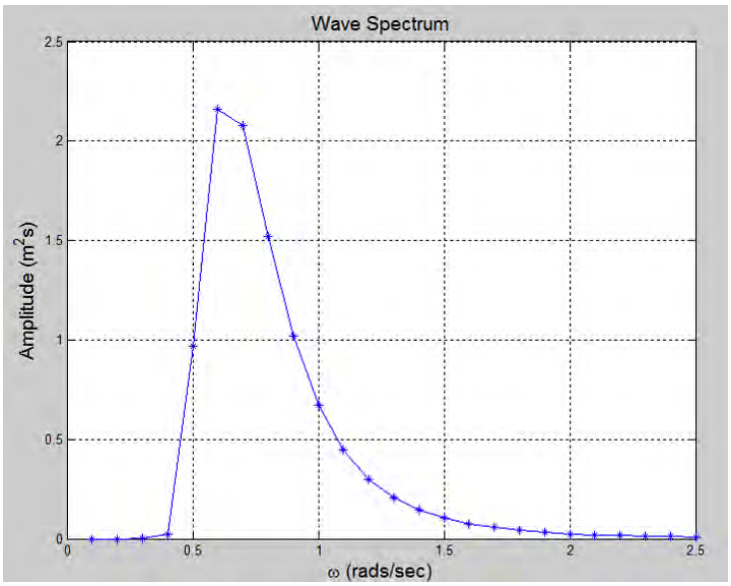

Figure 4.4 Simulated Wave Spectrum

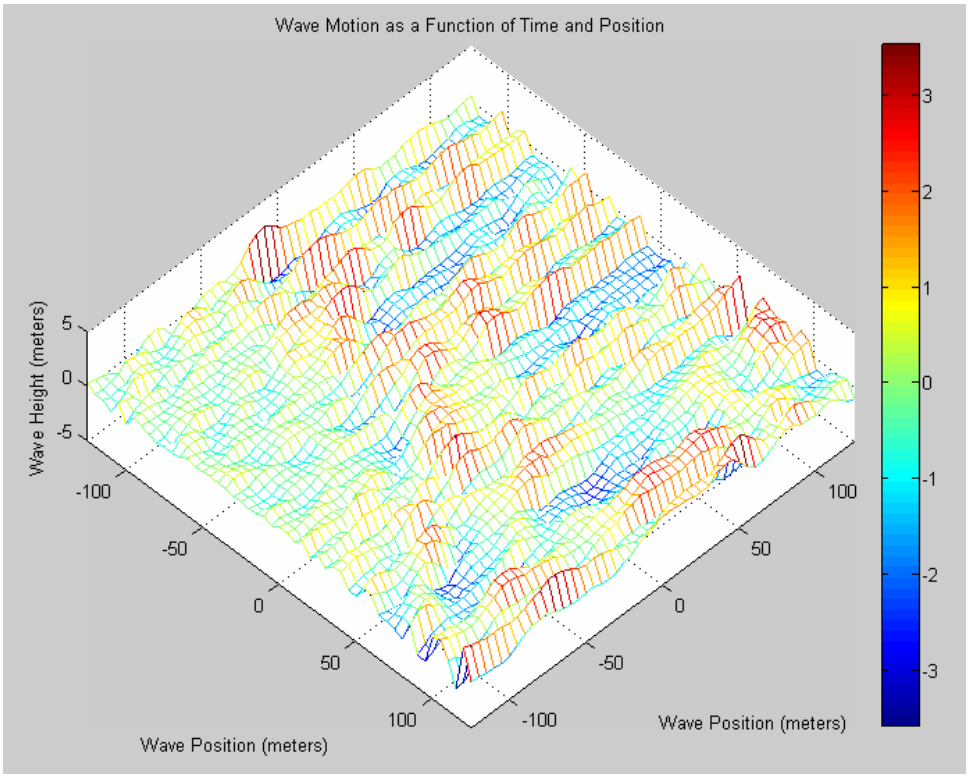

Figure 4.5 Simulated Wave Motion

Figure 4.5 depicts the random wave motion created from the spectrum generated by Equation 4.1 through Equation 4.3 and shown in Figure 4.2. The wave motion seen in Figure 4.5 was the motion that was input into the SIMULINK model for the purpose of simulating the total movement at the bow of the ship, where the beam director was located. The wave motion and the response of the ship are related by the Response Amplitude Operator (RAO).

This motion was also used to determine the acceleration of the bow as it passed over the incoming waves, which was then translated into the system's disturbance torque and experienced by the gimbal within the beam director housing. The disturbance torque was incorporated into the model as a result of the relationship expanded in Equation 4.4 [8].

Eq. 4.4 $$J_g\ddot{\theta}_g = \tau_{control} + \tau_{dist} = \tau_{control} - (J_g\ddot{\theta}_{ship})$$

C. FEL BEAM POINTING

1. Wide-Field-of-View (WFOV)

If pointing control is considered from the stand-point of taking a series of steps until eventually arriving at some desired end-point, wide-field-of-view (WFOV) tracking control would be the first step in the path to solving this target tracking problem. WFOV tracking functions as the coarse, large-angle adjustments for the tracking system [10]. These large-angle adjustments require the entire structure of the beam director to re-orient. The gimbals used for this segment of the tracking system generally have a large range of angular motion available to them, and the relatively high saturation limits with respect to their angular rates. This permits very rapid movements through large angles to track the target's motion. The inherent downside is the amount of over-shoot incurred due to the high angular rate of rotation and the necessity of constantly correcting the final pointing angle. Even with this limitation, the WFOV tracking loop provides an acceptable first approximation to the angular position of the target.

For the design of the WFOV controller, a single feedback control loop was initially tested, wherein the current pointing angle position was measured and compared

with the desired pointing angle position and iterated until the desired angle was achieved. In order to provide inertial stabilization of the gimbal, the angular rate loop is also added into the control system.

Figure 4.6 shows this configuration for the WFOV tracking loop. Also, as mentioned in the previous section, the wave motion disturbance is incorporated into the system at two different points. The first disturbance is input at the summation of the torque applied to the gimbals while the second input is located at the summation of the actual pointing angle.

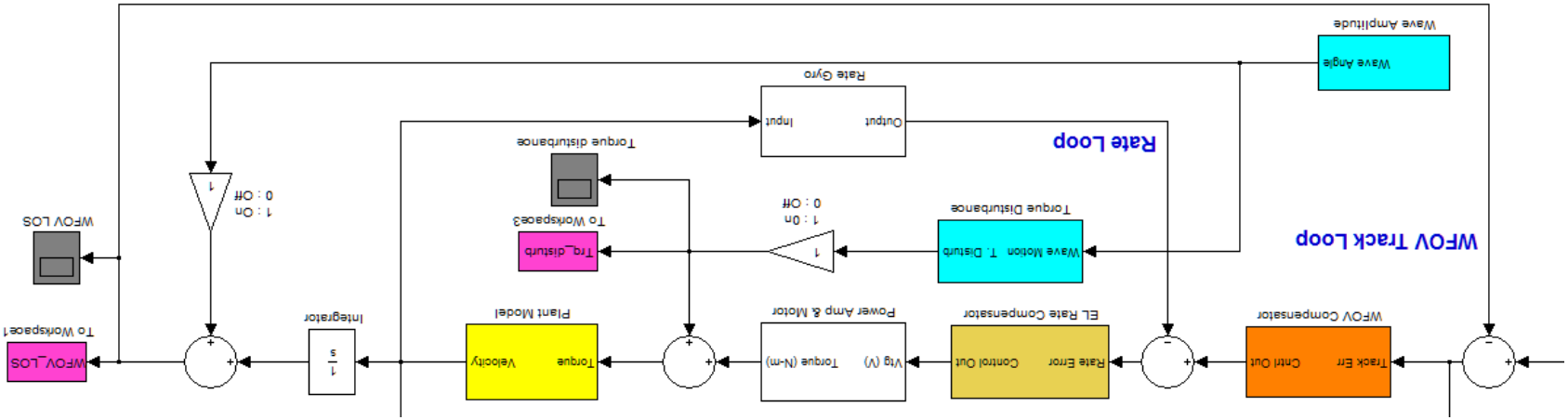

Figure 4.6 WFOV Track Loop

Even with the two feedback control loops being used in Figure 4.4, when the target is highly maneuverable, all of the tracking error can not be completely removed with the feedback control design shown in Figure 4.6. Figure 4.7 shows the error that remains as the wave motion is combined with the target motion.

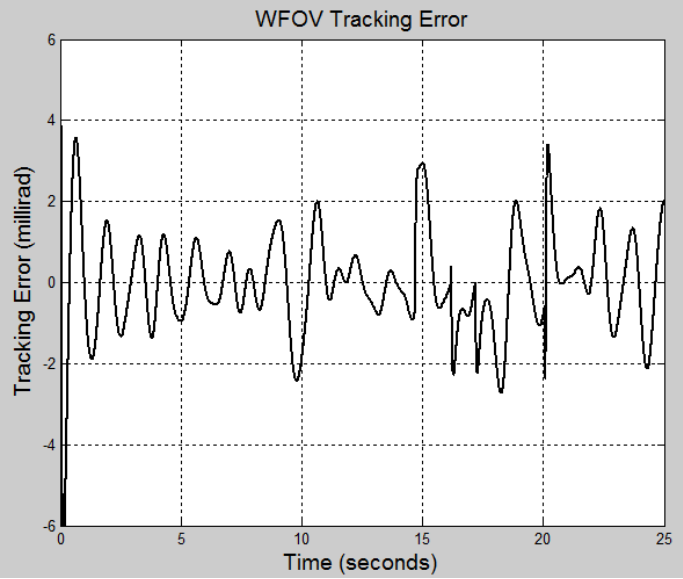

Figure 4.7 WFOV Tracking Error

At first glance, these are not bad results, maintaining an error of between +/- 4 millirads. This accuracy is still not sufficient as over the large distances across which this ship-defense system is intended to be used (5 to 10 km), these minor errors have a large impact. At 5 km with a 4 millirad pointing error, the bore sight of the laser is moved over a range of +/- 20 meters from the center point on the target. When trying to shoot down a target that is just less than 1 meter in diameter, an envelope of +/- 20 meters does not have a high probability of accomplishing the mission goals of disabling the incoming ASCM.

2. Narrow-Field-of-View (NFOV)

If the WFOV controller affects the coarse adjustments for the beam director, additional cleaning up of the pointing error and fine tune adjustments are made with the

narrow-field-of-view (NFOV) controller. The NFOV track loop receives the measured error between the desired angle and the measured angle from the WFOV track loop and treats the received error as the desired pointing angle for its feedback loop. Also present in the NFOV controller is a coupled, feed-forward control input. This takes the measured error and handles it as a required correction. The disturbance is then coupled with the error between the WFOV pointing error and the NFOV pointing angle prior to the plant correcting the errors. In this way, the NFOV controller is correcting the WFOV track error in "real-time" by negating the sampling delay that is inherent in feedback-only loops. Figure 4.8 depicts the SIMULINK model as it was used in creating the NFOV controller. The fast-steering mirror (FSM) transfer function is straight from the ground vehicle model as that transfer function describes the FSMs that are to be used on the testbed [10].

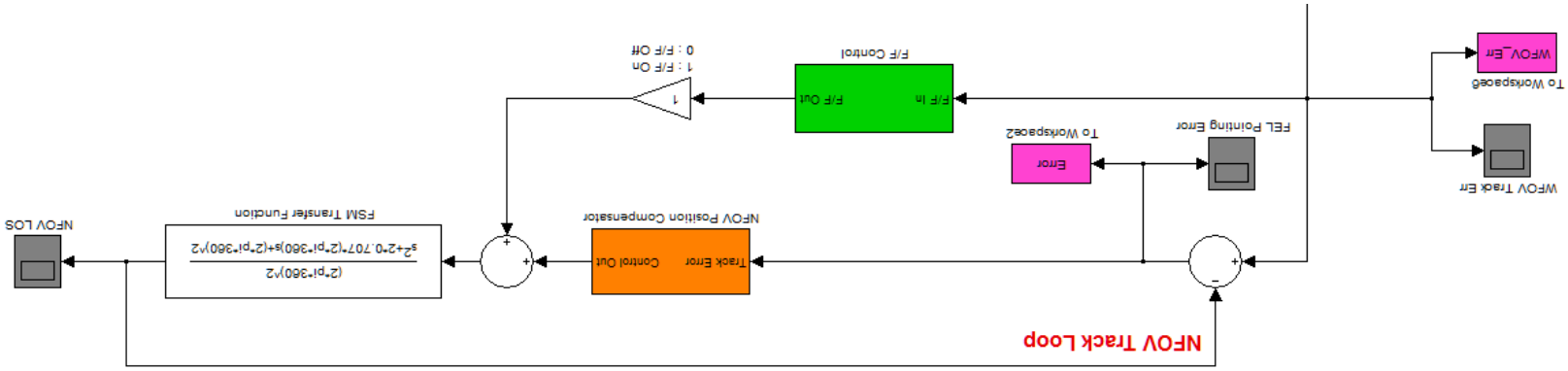

Figure 4.8 NFOV Track Loop

D. SIMULINK SIMULATION RESULTS

The following sections detail the results of the simulations. Three different cases were examined: a target that maintained a constant elevation and distance from the ship; a target that moved up and down with a constant period and maintained a constant distance from the ship; and a typical anti-ship cruise missile (ASCM) flight profile. For each of the simulations the maximum mean wave height was set to 4 meters with a frequency of less than a rad/sec, as shown earlier in Figure 4.4.

1. Target – Stationary

The input parameter for the target that maintained constant elevation and distance with respect to the ship was simply a constant value. This ensured no angular variation in the elevation due to the target moving towards the ship and thus having an apparent increase in elevation. Figure 4.9 shows the WFOV tracking error compared to total tracking error from incorporating the NFOV tracking loop.

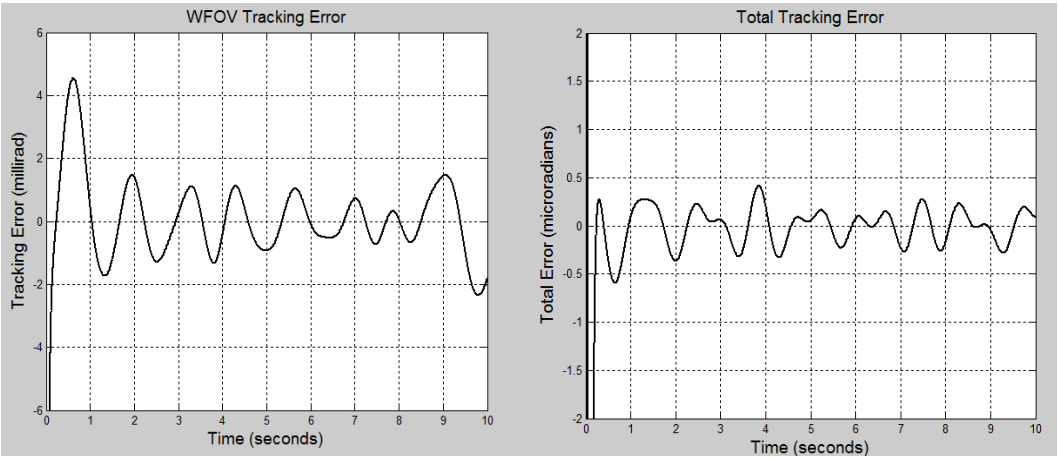

Figure 4.9 "Stationary" Target Tracking Errors

As can be seen the WFOV does not get the job done alone, but incorporating the NFOV tracking loop gives the total error of less than one microrad. This means that even out as far as 10 km from the ship, the bore sight of the laser will have shifted no more than one centimeter.

2. Target – Sinusoidal Motion

The motion for a target that is varying only its elevation, not its distance, with respect to the ship was modeled using a simple sinusoidal input, with the results shown in Figure 4.10. The maximum angular amplitude for the sine wave was 2 degrees and the period was 0.5 Hz.

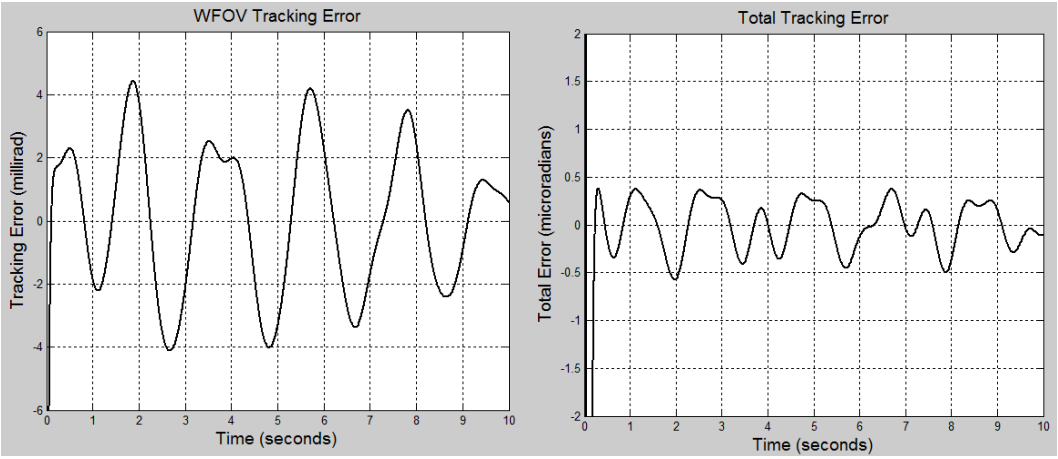

Figure 4.10 Sinusoidal Target Tracking Errors

With the sinusoidal input yielding results to the same order of magnitude as the "stationary" target, it was concluded that the model was functioning correctly and it was providing very promising results. The final test case involved re-creating the flight profile for a typical ASCM that may be encountered by the ship-defense system once it is deployed and certified operational.

3. Target – Anti-ship Cruise Missile (ASCM)

The ASCM target flight profile was designed with three primary phases: a set mid-level cruising altitude of 1500 m prior to target acquisition; between 10 to 15 km from the intended target, pop-up to 3000 m and perform a target acquisition maneuver; upon locating the intended target drop to a sea-skimming altitude of around 30 to 50 meters and begin "side-winding" maneuvers to evade ship-defense tracking and

neutralization attempts. The velocity of the ASCM is presumed to vary between Mach 2 and Mach 3 at different point in the flight profile. Figure 4.11 illustrates the three phases of the ASCM flight profile.

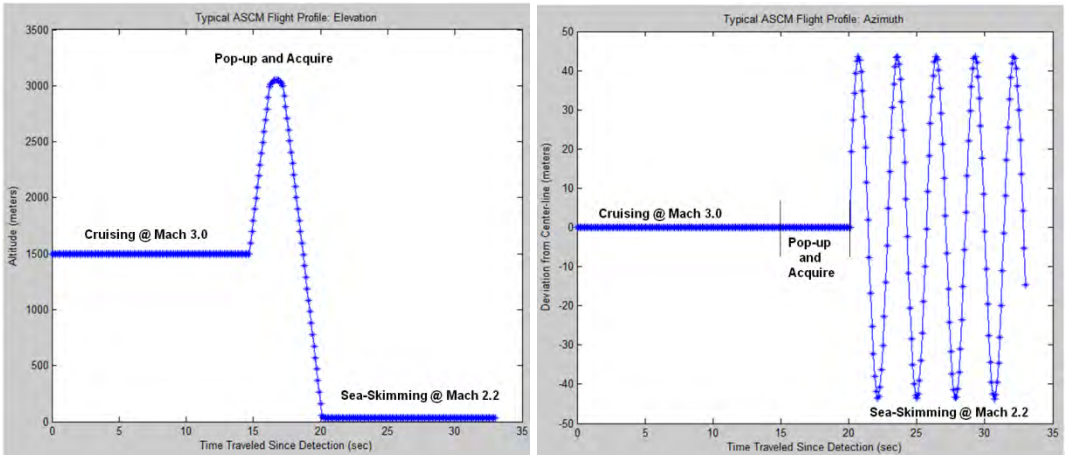

Figure 4.11 ASCM Flight Profile, Elevation and Azimuth

The left inset is the flight profile as seen from the side (elevation profile) and the right inset is the flight profile as seen from the top (azimuth profile). The time listed along the x-axis is the time since detection. This simulation assumed the ship-borne sensors did not detect the ASCM until it was within 25 km of the ship.

As the pointing system had already proven its ability to successfully track the sinusoidal motion in the previous test, the elevation profile became the profile of interest. The particularly difficult portion for the tracking system would be to maintain the track through the aggressive maneuvers in changing altitude. Figure 4.12 gives the full 3D perspective of the ASCM profile and its approach to the ship.

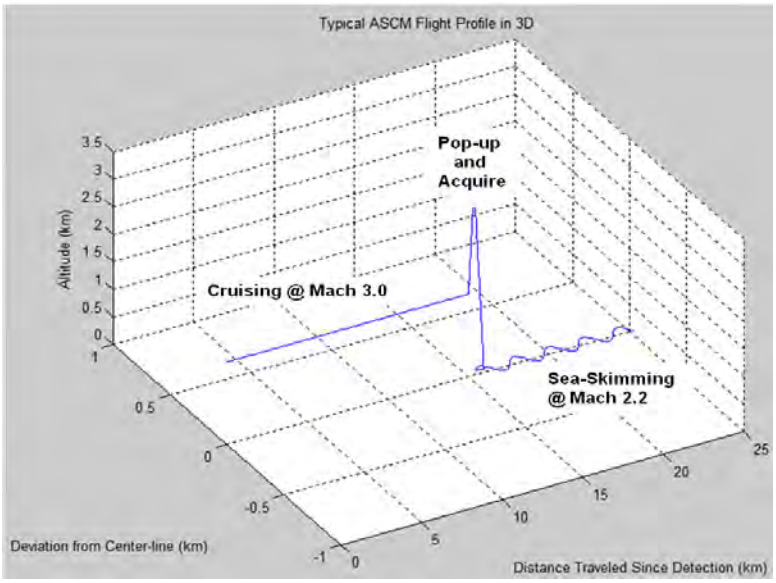

Figure 4.12 ASCM Flight Profile, 3D Representation

The WFOV and NFOV tracking errors for the duration of the flight profile are provided in Figure 4.13.

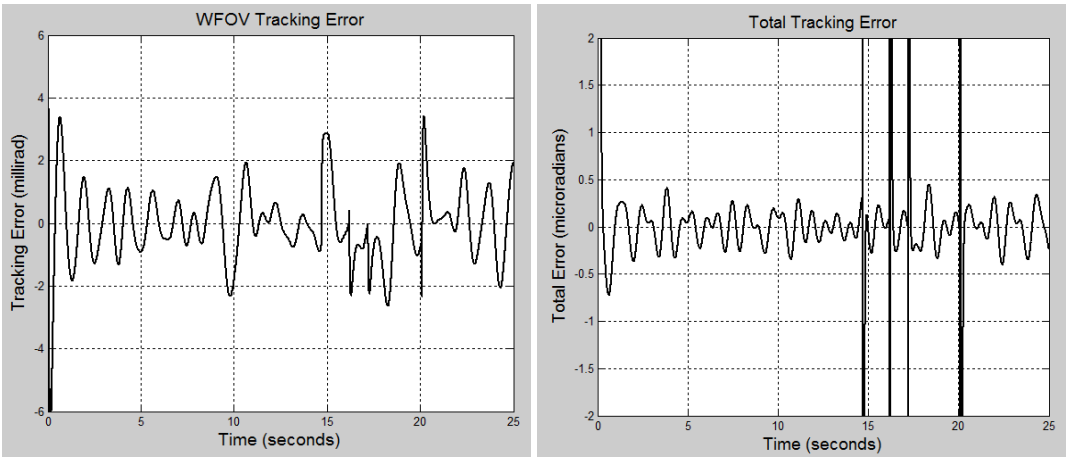

Figure 4.13 ASCM Target Tracking Errors

Of importance in Figure 4.13, on the Total Tracking Error plot, are the four black, vertical lines between 14 and 21 seconds. These occur at the four points of aggressive altitude change. Two hypotheses were developed as to why these occurred. The first hypothesis is the pointing control was just unable to move at a fast enough rate in order to keep the bore sight tracking with the ASCM through such sharp changes in its velocity

vector. The second hypothesis is that these lines may be highlighting some unrealized discontinuities in the designed flight profile. These may be explored at a later time, by another individual, but due to time constraints, the focus was placed upon how the target was tracked within the defense system's proposed engagement range. Figure 4.14 zooms in and isolates the last 5 seconds of elevation tracking prior to what would be the impact with the ship to show that the pointing accuracy was still exceptionally good.

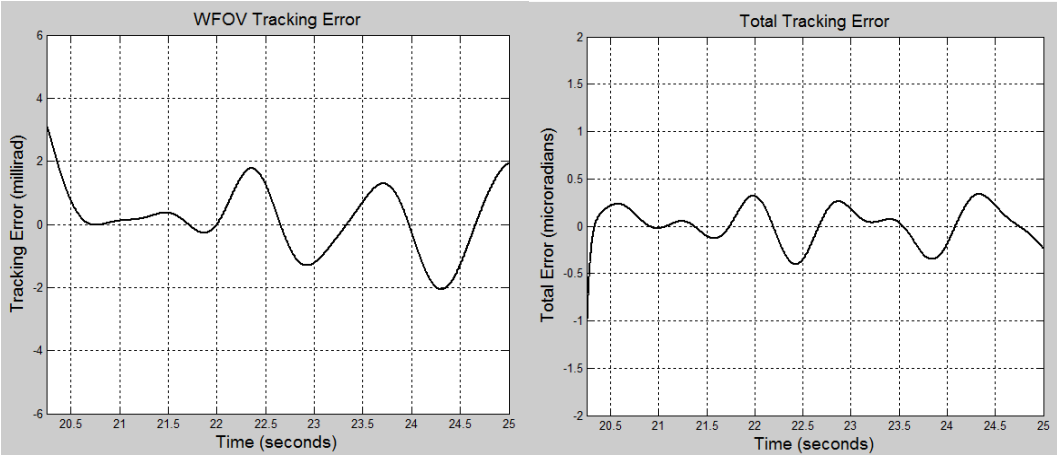

Figure 4.14 ASCM Target Tracking Errors, Effective Range

From the simulations conducted, it was decided that using these methods of automated controllers provides a feasible starting point to integrating a FEL-based ship-defense weapon system onto a cruiser class naval vessel. Future work can still be done on line-of-sight stabilization. Jitter control due to platform jitter is not explicitly addressed in this thesis, and will need to be examined by another student to ensure it can be corrected to a point that it does not affect the end-state pointing angle of the NFOV tracking loop.

THIS PAGE INTENTIONALLY LEFT BLANK

VI. INFORMATION SYSTEMS AND RF COMMUNICATIONS

Information systems are designed for the purpose of being able to transmit and receive information either through free-space transmission or via some form of wired connection. The most simplistic communications system is comprised of the following components: input signal generator; modulator; transmitter; receiver; de-modulator; output signal generator [12].

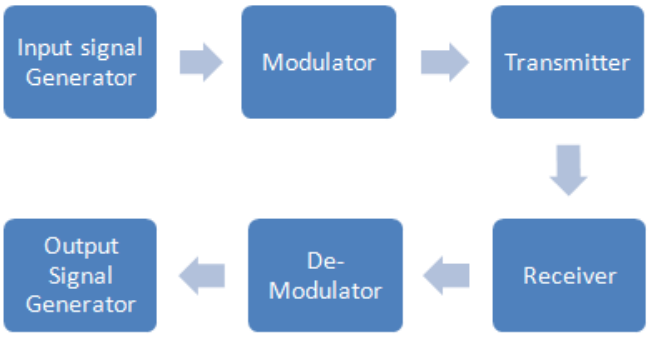

Figure 5.1 Block Diagram of Simplified Comms System

The input signal generator passes the information to be transmitted to the modulator, which then formats the information for transmission. After the signal is transmitted and arrives at the receiver, the signal is de-modulated. This de-modulated signal is then passed to the output signal generator resulting in the re-construction of the input signal.

In an ideal scenario, there are no losses and no interference from noise sources. The signal processed at the receiving antenna would be identical to the original broadcast. However, in a real-world scenario, there are a number of factors that directly impact the quality of the signal that arrives at the receiving antenna [12].

A. ANTENNA GAIN

Starting at the transmitter, the geometry of the antenna being used for the transmission (as well as reception) is directly proportional to how much energy is

detected by the receiver. The antenna geometry is used to determine the directional "gain" of a particular antenna. This directional "gain" is taken to be a ratio between the power put into a particular section of a sphere (P_{in}) with respect to the power that would be put out by an isotropic antenna. An isotropic antenna radiates equal amounts of energy in all directions of the sphere. The isotropic antenna is taken to have a gain of 1, which is equivalent to 0 decibels (dB). Figure 5.2, illustrates the increase in antenna gain as the beam becomes more directed to a particular section of the sphere.

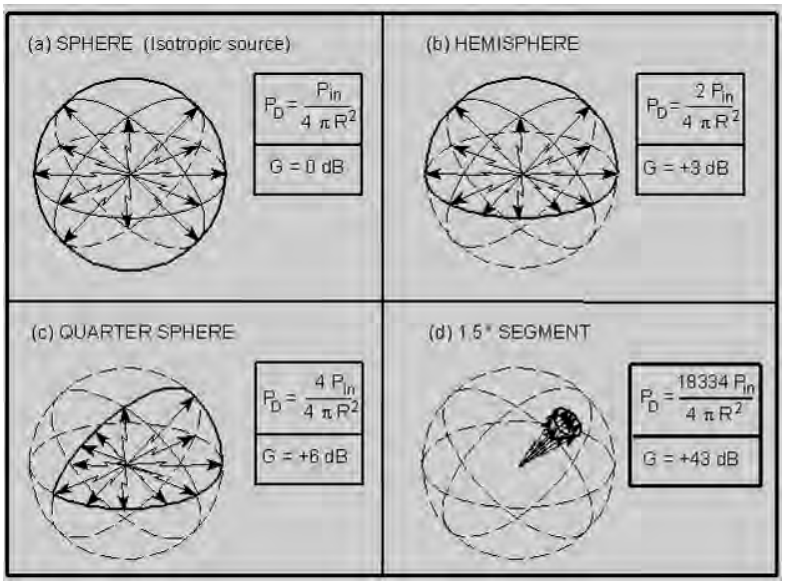

Figure 5.2 Examples of Various Directional Gains. From [13]

Another method of determining the directional gain of a parabolic antenna takes into consideration the diameter of the antenna as well as the wavelength being transmitted or received. If the projection of the beam is illustrated in Block (d) of Figure 5.2, then the area of that projection can be determined by multiplying the azimuth and elevation beam width arc lengths together. The gain of the antenna can then be calculated as Equation 5.1.

Eq. 5.1 $$G_d = \frac{\textit{Solid Angle of a Unit Sphere}}{\textit{Solid Angle Beam Projection}} = \frac{4\pi}{\Delta\varphi * \Delta\theta}$$

wherein, $\Delta\varphi$ and $\Delta\theta$ represent the azimuth and elevation beam widths respectively, with both given in radians [14]. These beam widths are measured from the half-power point, or -3 dB point, of the main lobe of the radiation. The half-power beam width for an antenna can be approximated as the wavelength (λ) divided by the horizontal (L_H) and vertical (L_V) aperture lengths of the transmitting, or receiving, antenna. The product of these two aperture lengths gives the antenna's effective area (A_{eff}). Thus, the directive gain equation can be manipulated into the following intermediate form,

Eq. 5.2 $$G_d = \frac{4\pi}{\Delta\varphi * \Delta\theta} = 4\pi\left(\frac{L_H * L_V}{\lambda^2}\right) = \frac{4\pi A_{eff}}{\lambda^2}$$

In the case of a circular, or parabolic, antenna, the effective area becomes Equation 5.3 [12].

Eq. 5.3 $$A_{eff} = \frac{\pi d^2}{4}$$

Replacing the circular antenna efficiency into the directional gain equation gives the final result, Equation 5.4, which ultimately relates the directional gain of an antenna to the diameter of the antenna and the wavelength that is being either transmitted or received [12].

Eq. 5.4 $$G_d = \left(\frac{4\pi A_{eff}}{\lambda^2}\right) = \left(\frac{\pi^2 d^2}{\lambda^2}\right)$$

B. DIFFRACTION (FREE-SPACE LOSSES)

Another factor in determining the amount of energy that will be detected at the receiver is the distance the transmission has to travel. The "free-space loss" describes the loss in signal strength of an electromagnetic wave in the instance the signal does not experience any scattering or absorption. In other words, it is the loss resultant from spreading due to diffraction of a transmitted signal through air, or space, without the hindrance of obstacles.

The determination of free-space loss takes into consideration two physical effects of transmitting RF through free-space. The first is the spreading of the energy by diffraction as the wave travels further away from the point of origin. The intensity, as a

function of distance from the transmitter, is found via the same equation as used to illustrate the incident energy on a sphere from an isotropic antenna, Equation 5.5 [14].

Eq. 5.5 $$S = \frac{P_t}{4\pi R^2}$$

where S, the intensity on a spherical surface in the units of Watts/m^2 (power/unit area); P_t is the power being transmitted; and R is the distance between the transmitting source and the receiver.

The second effect is dependent upon the receiving antenna's aperture. The size of the receiving antenna not only determines the directive gain of the antenna, but its ability to detect a particular frequency. This is also known as the relative response of an antenna. Combining Equation 5.5 and Equation 5.6, the two equations that describe these effects, gives the equation for determining free-space loss of transmitted energy, Equation 5.7 [14].

Eq. 5.6 $$P_r = S\left(\frac{\lambda^2}{4\pi}\right)$$

Equation 5.7 gives the free-space loss as a ratio between transmitted and received power.

Eq. 5.7 $$L_{fs} = \frac{P_t}{P_r} = \frac{4\pi R^2 S}{S\left(\frac{\lambda^2}{4\pi}\right)} = \left(\frac{4\pi R}{\lambda}\right)^2$$

Recalling the fact the speed of light (c) can be obtained from the product of the frequency (f) and wavelength (λ) of the electromagnetic wave, the above equation can be further simplified to Equation 5.8.

Eq. 5.8 $$\lambda = \frac{c}{f} \rightarrow L_{fs} = \left(\frac{4\pi R f}{c}\right)^2$$

As Equation 5.8 was developed with regard to an isotropic transmitter, analyzing the case of a directed gain antenna at both the transmitter and the receiver sites gives the modifications in Equation. 5.9. This is due to the fact antenna gains are multiplicative.

Eq. 5.9 $$L_{fs} = \frac{P_t G_t G_r}{P_r}$$

Re-arranging the terms from the free-space loss equation yields the generic form of the formula, which can be used in determining the power received by an antenna as a function of transmit power; transmitter gain; receiver gain; and free-space loss.

Eq. 5.10 $$P_r = \frac{P_t G_t G_r}{L_{fs}}$$

This equation serves as the primary factor in the development of RF communications link budgets.

C. MODULATION TECHNIQUES

Signals encoded to send information typically require two parts, a carrier wave signal and a message wave signal. The carrier wave is the signal, which will be transmitted and detected throughout the communications link. The message signal contains the information (the voice, image, video, or other data) to be transmitted embedded upon the carrier wave [12].

This requirement arises from the fact that transmitting energy at a single frequency alone can not result in the transmission of any useful information or data. In order to transmit usable information between a transmitting station and a receiving antenna, the information must be encoded onto a carrier signal. This encoding is accomplished via one of the various forms of modulation that will be described in subsequent sections.

The two of the most commonly used methods for modulating analog RF communications are amplitude modulation (AM) and frequency modulation (FM). As far as digital modulation schemes are concerned, the most commonly used techniques are amplitude shift-keying; frequency shift-keying; and phase shift-keying. Regardless of which modulation method is chosen, all of the modulation methods use the same mathematical definition for the carrier wave signal. This equation is listed below and is derived from the equation for general electro-magnetic waves [15].

Eq. 5.11 $$y(t) = A\sin(\omega t + \varphi)$$

In Equation 5.11, A is the amplitude of the transmitted signal in volts; ω denotes the angular frequency of the signal in radians per second, and yields the frequency in Hertz after dividing by 2π; and φ represents the phase of the transmitted signal, with the carrier assumed to have a phase of zero.

In the following sections, the various methods of imparting either analog or digital modulation upon a carrier signal will be discussed. After discussing the various modulation methods, the manner in which information can be encoded onto a carrier signal will be illustrated.

D. ANALOG MODULATION TECHNIQUES

This section describes the two methods of analog modulation that are typically used for transmitting information that is continuous in nature. The human voice and music are prime examples of information that can be transmitted in this manner, and is most readily observable via AM/FM radios.

1. Amplitude Modulation (AM)

Amplitude modulation occurs when a high-frequency, carrier wave is modulated to correspond to a source signal. The source signal, or message signal, is of lower frequency than the carrier, by at least an order of magnitude [12]. For the example in Figure 5.3, the carrier wave is at a frequency of 10 kHz, while the modulating signal is at 1 kHz.

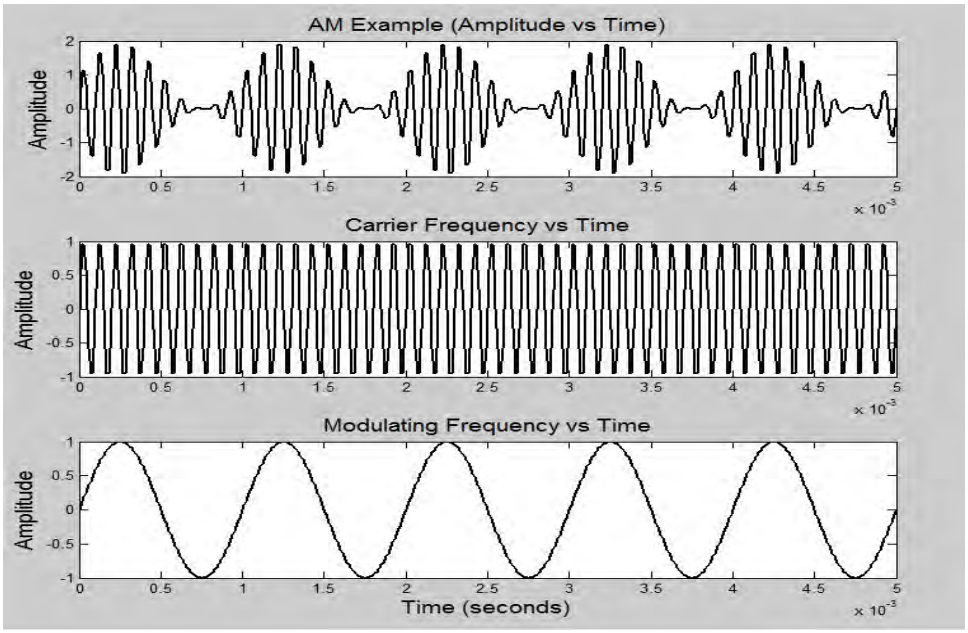

Figure 5.3 Periodic Representation of AM

In this scenario, each individual component of the signal has the general form given by Equation 5.11.

Eq. 5.11 $$y(t) = A\sin(\omega t + \varphi)$$

As the amplitude is the parameter being modulated, the phase of the carrier is of no importance, thus φ is treated as equal to zero for convenience. As the phase is irrelevant in amplitude modulation, Eq 5.11 reduces to Equation 5.12 and Equation 5.13.

Eq. 5.12 $$y_c(t) = A_c\sin(\omega_c t)$$

Eq. 5.13 $$y_m(t) = A_m\sin(\omega_m t)$$

where y_c and y_m are the carrier and message signals respectively. The carrier signal amplitude is periodic in time, without the presence of the message signal. When both the carrier and message signals are present, the amplitude of the final, transmitted signal has a magnitude equivalent to the sum of the maximum amplitude of the carrier wave and the instantaneous amplitude of the message signal [12].

Eq. 5.14 $$A_f(t) = A_c + y_m = A_c + A_m\sin(\omega_m t)$$

This only describes the amplitude of the transmitted signal and how it varies as a function of the message frequency, it does not take into consideration the effects of the carrier frequency. In order to account for the carrier frequency, the carrier wave amplitude from Eq 5.14 is replaced with the final amplitude given in Equation 5.12. Substituting and using product of sums for sines results in Equation 5.15, which defines amplitude modulation.

Eq. 5.15 $$y_f(t) = (A_c + A_m\sin(\omega_m t))\sin(\omega_c t)$$

$$y_f(t) = A_c\sin(\omega_c t) + A_m\sin(\omega_m t) * \sin(\omega_c t)$$

$$y_f(t) = A_c\sin(\omega_c t) + \frac{1}{2}A_m\cos\big((\omega_c - \omega_m)t\big) \ldots$$

$$-\frac{1}{2}A_m\cos\big((\omega_c + \omega_m)t\big)$$

Eq. 5.15 describes the variations in amplitude of the transmitted signal as a function of time. The three parts of the equation give information of the carrier wave, the upper side frequency ($\omega_c - \omega_m$), and the lower side frequency ($\omega_c - \omega_m$). Figure

5.4illustrates the relative locations of these three peaks, wherein the time-variant equation has been transformed to the frequency domain. The amplitude is given typically in Volts.

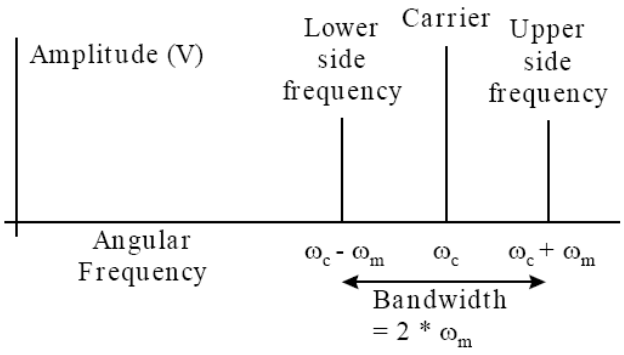

Figure 5.4 Bandwidth in the Frequency Domain. From [12]

The difference between the upper and lower side frequencies determines the signal's bandwidth, which correlates directly to the power required to transmit the signal. Calculations of the power required for transmission of a modulated signal will be discussed in a later section. The bandwidth of an AM signal is calculated using Equation 5.16.

Eq. 5.16 $$AM\ Bandwidth = (\omega_c + \omega_m) - (\omega_c - \omega_m) = 2\omega_m$$

2. Frequency Modulation (FM)

Frequency modulation occurs when the frequency of a carrier wave is modulated to correspond to a source signal. As in amplitude modulation, the source signal is of lower frequency than the carrier.

In order to modulate the frequency of the carrier wave, the maximum deviation above and below the carrier frequency must be specified. In Figure 5.5, the carrier frequency (ω_c) was 10 kHz and the message frequency (ω_c) was 1 kHz.

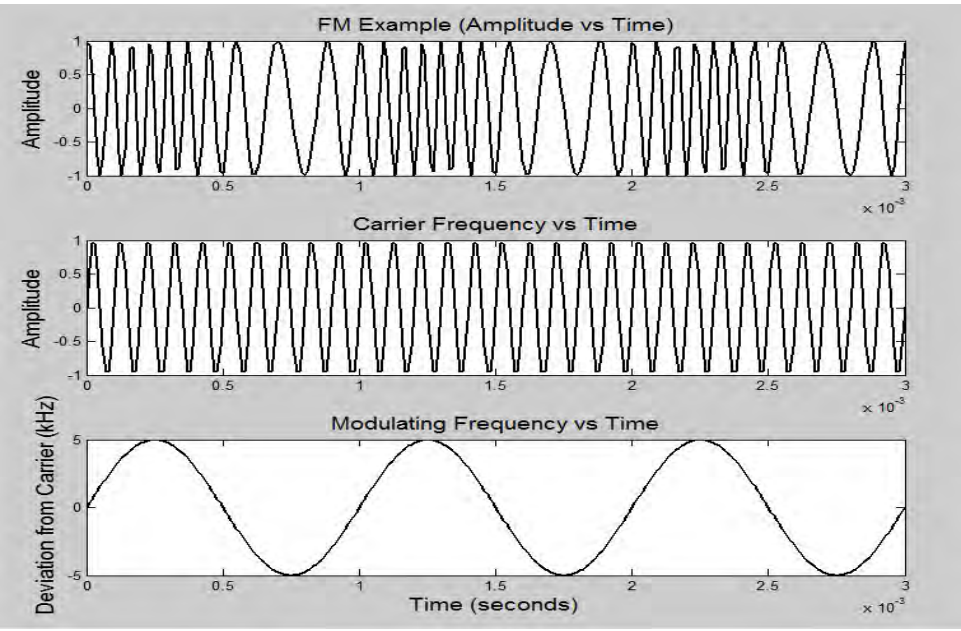

Figure 5.5 Periodic Representation of FM

The maximum deviation (Δω) above and below the carrier frequency was specified as 5 kHz. This means that the frequency of the transmitted signal will vary between 5 kHz and 15 kHz. Thus, Equation 5.17 gives the instantaneous frequency (ω_{inst}) [12].

Eq. 5.17 $$\omega_{inst} = \omega_c + \Delta\omega \sin(\omega_m t)$$

The integral for the change in ω_{inst} defines the signal's instantaneous phase angle (ωt).

Eq. 5.18 $$\theta_{inst} = \int \omega_{inst} dt = \omega_c - \frac{\Delta\omega}{\omega_m} cos(\omega_m t)$$

Placing the results of the instantaneous angle as a function of time into the general equation of a wave gives the equation for frequency modulation of a carrier wave.

Eq. 5.19 $$y_f(t) = A_c \sin\left(\omega_c - \frac{\Delta\omega}{\omega_m} cos(\omega_m t)\right)$$

The determination of the bandwidth required to transmit this signal is not as easy to discern as it was for the amplitude modulated case. This is caused by the fact that there are an infinite number of upper and lower sidebands created as harmonics (integer multiples of the message signal frequency) [12]. As a result, converting the time domain representation to the frequency domain requires the use of a table of Bessel's Functions

as a function of the modulation index. The modulation index is defined as the ratio between the maximum deviation from the carrier wave and the frequency of the message signal.

Eq. 5.20 $$h = \frac{\Delta\omega}{\omega_m}$$

The modulation index is then utilized in Carson's Bandwidth Rule (CBR) to determine the required bandwidth of the FM signal.

Eq. 5.21 $$FM\ Bandwidth = 2(h+1)f_m$$

E. DIGITAL MODULATION TECHNIQUES

An alternative method of encoding information on the carrier wave uses digital techniques. Digital information is stored, transmitted, and processed as a series of discreet voltages. These voltages are then translated by the signal generator into the bit stream, a series of ones and zeros containing the message. This process of generating a bit stream results in a binary waveform called a "pulse-code modulation" (PCM) waveform [12].

The number of states a particular bit stream is capable of representing is determined by how many bits are allocated per symbol. Equation 5.22 gives a general rule for determining the number of states that can be supported by a particular system [12].

Eq. 5.22 $$States = 2^M$$

where M is the number of bits each symbol represents. In the most basic case of binary representation, M is equal to 1 bit per symbol. Thus, there exist only two states, which are then allocated to two possible symbols within the modulation scheme. As the complexity and length of the bit stream is increased, the number of bits per symbol can be increased. Allocating more bits per symbol ensures the transmission time does not have to increase proportionally to the increased length of the bit stream. The true significance of the number of bits per symbol will be further explored in the following chapter, during the discussion of encoding information using the free-electron laser.

1. Pulse-Code Modulation (PCM) Waveforms

All PCM waveforms fall into one of four categories: nonreturn-to-zero (NRZ); return-to-zero (RZ); phase encoded; and multilevel binary [12]. Some of the more common PCM waveforms of these types can be seen in Figure 5.6.

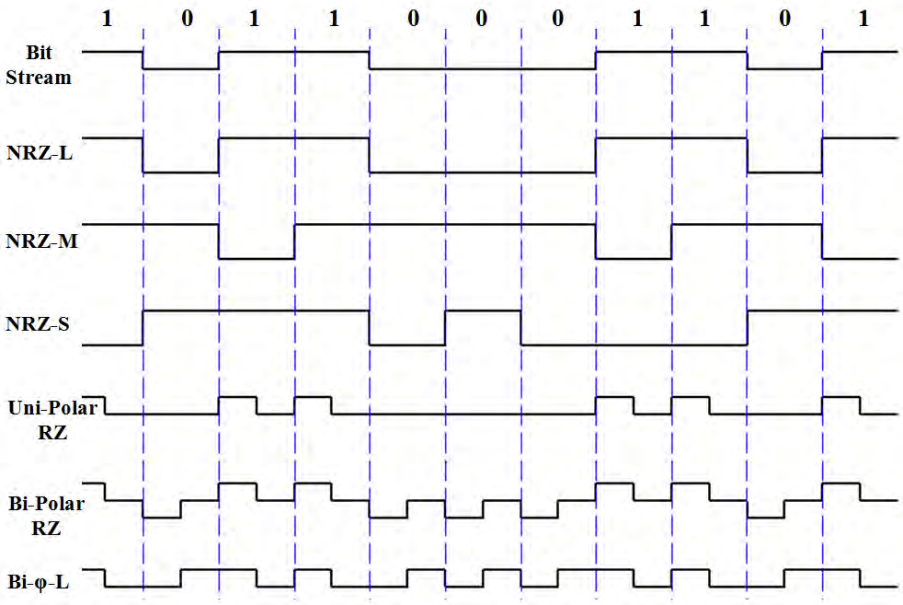

Figure 5.6 PCM Waveforms. From [12]

Along the top of Figure 5.6 is the binary bit stream that was to be encoded and communicated using the various modulation waveforms. Each of the waveforms treats the "mark," or the 1, in a different manner. For the three NRZ waveforms, the differences are in the transition points. On the NRZ-L (nonreturn-to-zero, level) waveform, the mark is a positive voltage while the zero is a negative voltage. For the NRZ-M (nonreturn-to-zero, mark) waveform, the voltage switches sign at the mark and remains constant for a zero. The NRZ-S (nonreturn-to-zero, switch) waveform is the compliment of the NRZ-M waveform maintaining a constant voltage for the mark and switching at the zeros. The RZ waveforms are configured such that only half of the interval has a pulse present. In the case of Uni-Polar RZ, the pulse is present in the first half of the interval whenever the mark is present and the pulse is absent when the bit is a

zero. The Bi-Polar RZ waveform has a pulse present in the first half of each interval with the mark being a positive voltage and the zero being a negative voltage. The Bi-φ-L waveform has a pulse present in the first half of the interval when the mark is present and in the second half of the interval for zeroes. This waveform is also known as Manchester coding [12].

Any of the waveforms in Figure 5.6 can be used to encode information for transmission via the FEL. The next sections describe the various modulation techniques that can be applied to these encoded PCM waveforms for the purpose of transmitting the data. In order to highlight the differences between the modulation techniques, the simple NRZ-L PCM waveform is used in all three illustrations, with a "one" being represented by a positive voltage, and a "zero" being represented by a negative voltage.

2. Amplitude Shift-Keying (ASK)

One of the simplest methods of modulating a signal with a digital bit stream is to use On/Off-Shift Keying (OOK). When using On/Off-Shift Keying to modulate the message, the presence or the absence of the carrier signal characterizes the state of the bit stream at a particular time. Thus, in systems that utilize OOK to modulate and transmit messages, the presence of the carrier signal over a cycle indicates a bit stream state of 1, while the absence of the carrier signal indicates a state of 0.

With this understanding, On/Off-Shift Keying (OOK) is the simplest form of Amplitude-Shift Keying (ASK). In ASK modulation, multiple voltage amplitude levels are used to indicate the state of the bit stream. In OOK modulation, only two voltage levels are used to represent the state of the bit stream: the presence of a voltage is a 1; and the absence of a voltage is a 0. For example, Figure 5.7 illustrates Binary ASK using OOK as the primary method for representing the variance between the two voltage levels.

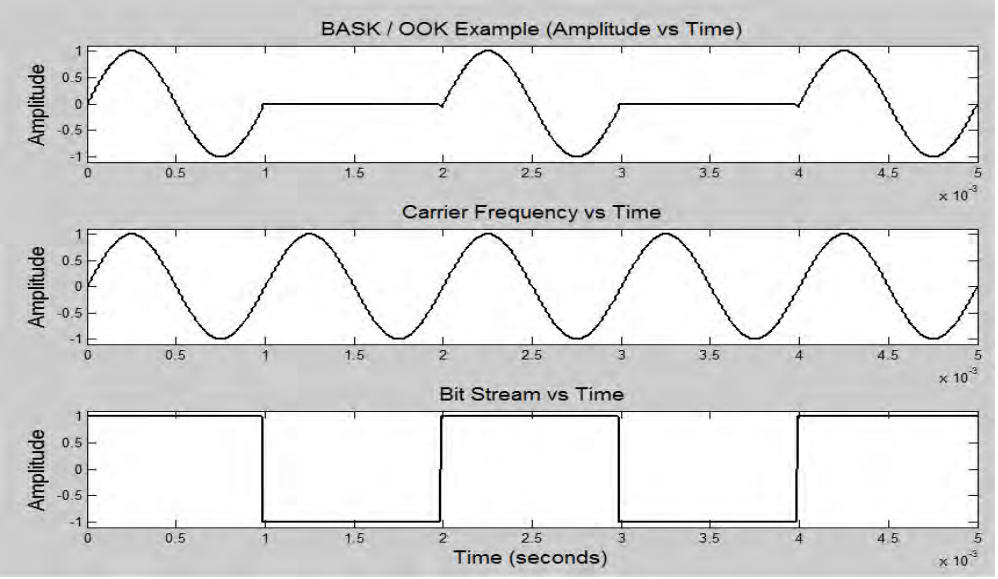

Figure 5.7 Periodic Representation of ASK

It is possible to increase the number of represented states by increasing the number of amplitudes. This also increases the number of bits that can be represented by individual amplitudes. However, using this modulation technique and this PCM waveform requires one amplitude to represent each of the possible states of the elements comprising the initial bit stream. To further this point, the Binary ASK example in Figure 5.7 has only two states, 1 or 0; on or off. Increasing the BASK to a Quad ASK system would require the addition of two more amplitudes to handle increased number of states from 2 to 4. Following this progression, it can be seen that systems that use exclusively ASK rapidly grow as more amplitudes are necessary to handle greater variety in states.

3. Frequency Shift-Keying (FSK)

Another digital modulation scheme is Frequency-Shift Keying (FSK). For a system that utilizes FSK to modulate a message, each state of the bit stream is assigned to a particular frequency. Just as with the ASK modulation scheme, the number of states

the bit stream can have can be increased by incorporating additional frequencies into the system. Binary Frequency Shift-Keying (BFSK) is the easiest to illustrate and is shown in Figure 5.8.

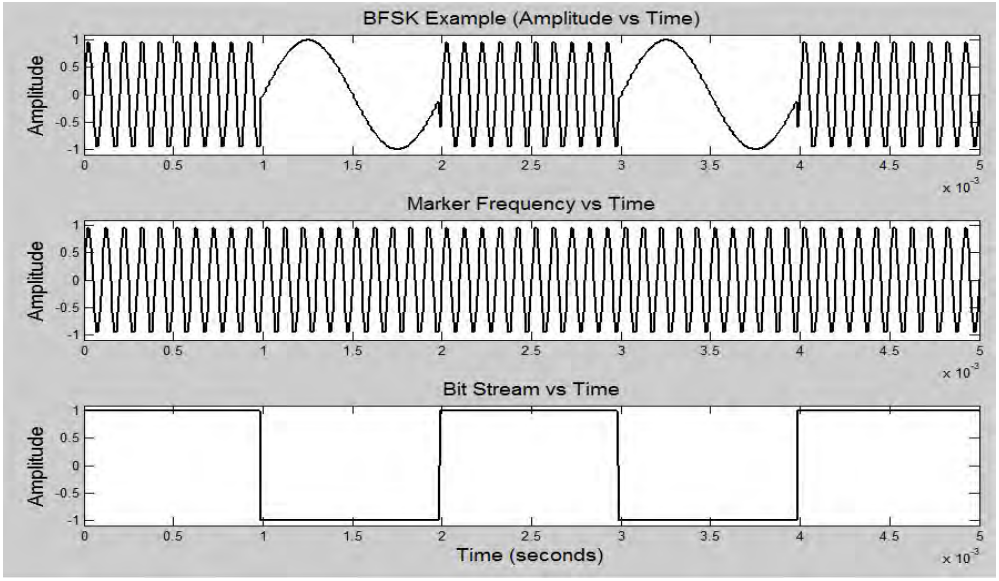

Figure 5.8 Periodic Representation of FSK

In Figure 5.8, the differences between the two frequencies have been exaggerated to ensure the reader can easily differentiate between the two represented states. Since the FEL is continuously tunable in timescales on the order of a microsecond, this may actually be one of the best options for communication applications utilizing the FEL.

4. Phase Shift-Keying (PSK)

A system that utilizes Phase-Shift Keying (PSK) to modulate the bit stream maintains a constant carrier frequency, but switches the transmitted phase of the carrier signal to signify changes in the state of the bit stream.

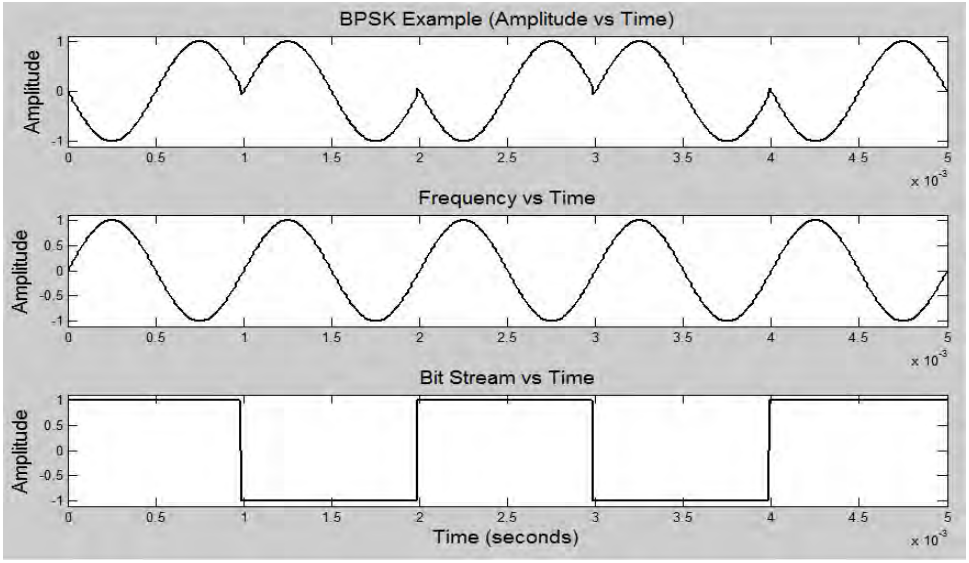

Figure 5.9 Periodic Representation of PSK

Though Figure 5.9 depicts an example of binary PSK, PSK is usually used in quad PSK systems or those systems requiring a greater number of bits per symbol. As with the two previous modulation schemes, adding more representable states requires the addition of more keying elements, phases in this case.

The addition of multiple amplitude levels in ASK and the addition of multiple frequencies in FSK is easily visualized. Table 5.1 details the phase difference between each state as the number of represented states is increased from 2 to 16.

Modulation	Bits / Symbol	Max # of States	Phase Difference
BPSK	1	2	180º
QPSK	2	4	90º
8-PSK	3	8	45º
16-PSK	4	16	22.5º

Table 5.1 Properties of Individual States in PSK

The significant aspect of Table 5.1, as far as PSK is concerned, is the phase difference. It should be noted that as the bits per symbol are incrementally increased, the phase difference between individual states is decreased by half. This reduction in the

phase difference continues as additional bits need to be represented. Serving as a companion figure to Table 5.1, Figure 5.10 is provided to assist in visualizing the phase separation when adding additional phases to the system. Each of the rows from Table 5.1 is displayed in Figure 5.10.

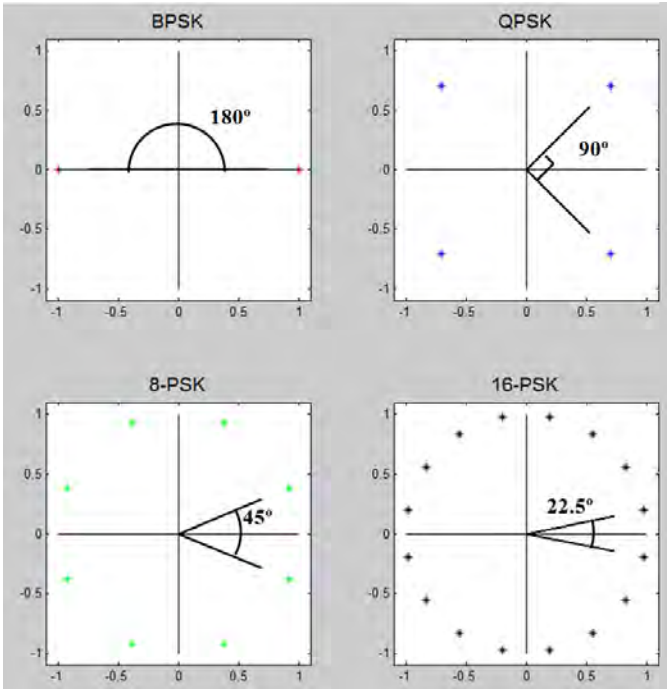

Figure 5.10 PSK State Allocation

F. LIMITATIONS

Each of the three digital modulation schemes discussed has its own unique limitation preventing the number of states that can be represented from sky-rocketing to infinity. Amplitude-Shift Keying, for example, is limited by the sensitivity of the receiver and the relative range from the noise floor of each of the transmitted amplitudes. If the receiver is unable to discern the difference between two amplitudes with relatively close magnitudes due to the background noise floor, then the demodulated message will have gaps or errors. Also, if a signal amplifier is incorporated into the receiver, there is the risk of increasing the received amplitudes beyond the saturation limits of the receiver.

Saturating the receiver would cause multiple amplitudes to appear to be the same symbol, thus introducing additional errors to the demodulated message.

When using FSK to modulate the signal, the saturation of the receiver is usually of minimal concern. However, since the frequencies are shifted through some range, the receiver's sensitivity remains the limiting factor of the system. There needs to be enough of a gap, roughly a few percent, between each of the frequencies being used to ensure the receiver can discern one symbol from another. This limitation in the receiver is expressed in the rate at which the filter falls off at its edges. From the transmit side of the communications link, the FEL provides the advantage of being able to adjust the frequency, roughly 10%, without requiring any significant modifications to the major hardware components of the beam line, though a variation of around 2–3% is probably all that will be necessary for this application [16]. This frequency shift range is determined by the frequency bandwidth of the multi-layer dielectric mirrors within the resonator cavity. As a conservative estimate, 2–4 frequencies could be used to ensure the FEL remains within the bandwidth limitations. Also, these changes in the frequency would occur on a microsecond timescale, which would enable the FEL to maintain approximately a MHz symbol transmission rate.

Finally, the PSK system begins to experience problems as more states are added due to the reduction in the phase difference between neighboring states. The receiver will eventually reach some limit where it is no longer able to identify the separation between two closely spaced states. As with the other two modulation schemes, when this occurs the demodulated signal has gaps or errors in it.

THIS PAGE INTENTIONALLY LEFT BLANK

VII. DEEP-SPACE COMMUNICATIONS USING THE FEL

The purpose of Chapter V was to provide a spring-board from traditional RF communications into the analogy of laser communications. Inherently, the end-state goal of RF communications and communication using lasers is the same: move information from one location to another at a reasonable rate. This information must be transmitted in such a way that the receiving end can re-construct the original transmitted signal and extract the information that was encoded upon the transmitted signal with minimal errors or gaps in the received information.

In order to mitigate the occurrence of discrepancies between the transmitted and received messages, an understanding of the limiting factors that exist for both the RF and laser communications approaches is necessary. Regardless of whether the transmitted message is in the traditional RF bands or sent via a laser, similar limitations are present. The factors that have an effect upon the power received at the receiving station are: the beam width of the transmitted signal; the distance and medium between the receiving station and the transmitting station; the transmitting power of the transmitting station; and the data and bit error rates. The following sections detail many of the limitations that exist when transmitting information and the differences between those limitations when comparing traditional RF to laser communications systems.

A. BEAM WIDTH DEPENDENCE

The beam width has a direct impact on how much of the energy contained within the transmitted signal is lost over the distance traveled to the receiver. The degradation of the transmitted signal due to beam spreading is dependent upon a number of parameters. Those parameters with the greatest effect are the distance to the receiving station and the beam divergence. The sizing of the receiving antenna, for RF, or optic, for the FEL, can help to mitigate some of the loss due to beam spread, and will be discussed in the following section, but there is a limit to how large a diameter a receiver can have before it becomes infeasible.

As discussed in previous chapters, all electromagnetic transmissions spread due to diffraction. The divergence of the beam from the center line is combined with the distance to the receiving station in determining the overall beam spread at the receiving station. The RF beam divergence is calculated using a combination of Equation 5.1 and Equation 5.4. Equations 5.1 and 5.4 are provided for reference.

Eq. 5.1 $$G_d = \frac{Solid\ Angle\ of\ a\ Unit\ Sphere}{Solid\ Angle\ Beam\ Projection} = \frac{4\pi}{\Delta\varphi * \Delta\theta}$$

Eq. 5.4 $$G_d = \left(\frac{4\pi A_{eff}}{\lambda^2}\right) = \left(\frac{\pi^2 d^2}{\lambda^2}\right)$$

Recall that G_d is the directive gain of the RF antenna; $\Delta\varphi$ and $\Delta\theta$ represent the azimuth and elevation beam widths respectively, both given in radians; A_{eff} is the effective area of the antenna, which for circular or parabolic antennas is the same as the circular area of the antenna; d is the diameter of the antenna; and λ is the transmitting wavelength. Setting the results of Equation 5.1 equal to the results from Equation 5.4 and solving for the azimuth ($\Delta\varphi$) and elevation ($\Delta\theta$) beam widths yields Equation 6.1.

Eq. 6.1 $$\Delta\varphi * \Delta\theta = 4\pi * \left(\frac{\lambda}{\pi d}\right)^2$$

If it is assumed that the transmitting antenna is nearly circular and that the spread is isometric from the center of the antenna then the beam widths far from the transmitter can be considered square giving the beam spread along the azimuth as Equation 6.2

Eq. 6.2 $$\Delta\varphi = \sqrt{4\pi * \left(\frac{\lambda}{\pi d}\right)^2} = \left(\frac{2\lambda}{\pi d}\right)\sqrt{\pi}$$

For comparison, recall Equation 2.1, which describes the beam spread of the FEL.

Eq. 2.1 $$w(z) = w_0\sqrt{1 + \left(\frac{z}{z_0}\right)^2}$$

Table 6.1 gives numerical values for the total beam spread at various ranges, assuming a transmitting antenna, or optic, radius of 0.25 meters. Larger transmitting antennas do exist, however, using the Air Force's Starfire Optical Range in Albuquerque, New Mexico as an approximate model for the upper limit on typical beam director sizes limits the laser beam director to a size of 1.0 m in diameter [17]. As such, 0.5 m seemed a reasonable assumption for the laser beam director used in this comparative scenario.

	RF = 10 GHz	RF = 14 GHz	RF = 95 GHz	Laser (λ = 1.6 μm)
1 km	135.4 m	96.7 m	14.3 m	0.50 m
10 km	1.35 km	0.97 km	0.14 km	0.50 m
25 km	3.38 km	2.42 km	0.36 km	0.51 m
125 km	16.93 km	12.09 km	1.78 km	0.71 m
500 km	67.70 km	48.36 km	7.13 km	2.10 m
35786 km	4.85×10^3 km	3.46×10^3 km	510.26 km	0.15 km
3.84×10^5 km	5.20×10^4 km	3.71×10^4 km	5.47×10^3 km	1.56 km
1.00×10^8 km	1.35×10^7 km	9.67×10^6 km	1.43×10^6 km	407.44 km

Table 6.1 Calculated Beam Spread at Various Ranges

The 10 GHz and 14 GHz transmitting frequencies in the transmitter column of Figure 6.1 are mid-range X-Band and Ku-Band transmitting frequencies, respectively. The 95 GHz frequency is included primarily to show the continued progression to lesser and lesser beam spread with the increase of transmit frequency. By comparison, the laser wavelength of 1.6 μm results in a transmit frequency provided by the laser of 187.5 THz. The first three distances in Table 6.1 (1 km, 10 km, and 25 km) were calculated to determine the beam spread in a terrestrial, line-of-sight (LOS) application. The laser only spreads by 10 cm over 25 km, while the traditional RF transmissions have spread by a few kilometers at the same range from the transmitting station. The 125 km range is included because it is beyond the Rayleigh length of the laser and illustrates a measurable increase in the laser's beam spread. Though, even at this range, the laser's beam spread is still many orders of magnitude less than the spread experienced by the RF transmissions. The last four entries of Table 6.1 are included to further the case for deep-space communications using high-energy lasers: 500 km represents a mid-Low-Earth Orbit (LEO) satellite; 35768 km represents a satellite in geosynchronous orbit (GEO); 3.84×10^5 km is the mean distance to the Moon; and 1.00×10^8 km is the next closest

approach to Mars on March 3, 2012 [18]. Referring again to Equation 6.2, the divergence of the beam from the centerline can be calculated for circular antennas. Figure 6.1 presents the variance in beam divergence as a result of a change in the transmit frequency.

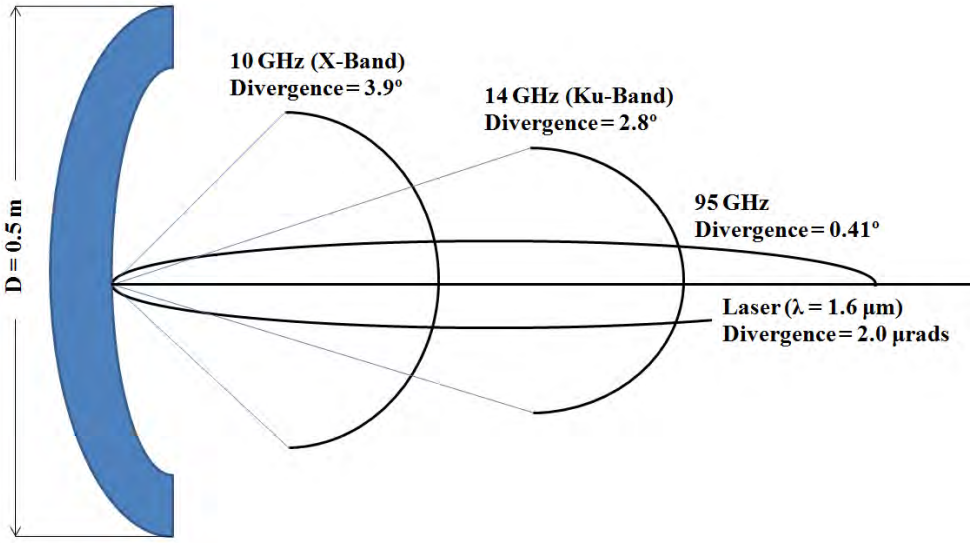

Figure 6.1 Beam Divergence

B. EFFECTS OF POWER AND RANGE VARIATION

As mentioned in the previous section, the size of the receiving antenna can help in mitigating some of the signal loss from diffraction. Traditional RF communications methods usually require fairly large antennas in order to have sufficient gain built into the receiving station. In order to determine the necessary size of a receiving RF antenna, Equation 5.10 must be solved for the receive antenna gain (G_r), giving Equation 6.3.

Eq. 5.10 $$P_r = \frac{P_t G_t G_r}{L_{fs}}$$

Eq. 6.3 $$G_r = \frac{P_r L_{fs}}{P_t G_t} = \left(\frac{\pi^2 d^2}{\lambda^2}\right)$$

Eq. 6.4 $$d = \left(\frac{\lambda}{\pi}\right)\sqrt{\frac{P_r L_{fs}}{P_t G_t}}$$

where P_r is the received power at the antenna; L_{fs} is the power loss due to diffraction; P_t is the transmit power; G_t is the transmit antenna gain; d is the diameter of the receive antenna; and λ is the wavelength of the carrier wave.

Completing an analogous calculation for FEL-based transmissions allows one to determine the aperture of the avalanche photo-diode (APD) to be used at the receive station of the laser. The aperture size of a laser receiver is directly dependent upon the intensity of the beam arriving at the receive station. The range to the receive station is used in determining the beam spread and then the area of the circular beam at the APD is calculated from Equation 6.5.

Eq. 6.5 $$A_{beam} = \pi W^2$$

The power received is then calculated as shown in Equation 6.6, with A_{APD} being the area of the APD's aperture and G_{APD} being the gain of the APD. Typical silicon avalanche photo-diodes have gains that are nominally between 50 and 200, while APDs made of InGaAs generally have gains of 50 or less [19]. An InGaAs APD was assumed due to the fact operating laser wavelength is greater than 1.0 μm, and the silicon APDs tend to be reliable only up to 1.0 μm [19].

Eq. 6.6 $$P_r = \frac{P_t A_{APD} G_{APD}}{A_{beam}} = \frac{P_t \pi R_{APD}^2 G_{APD}}{A_{beam}}$$

Solving Equation 6.6 for the radius of the APD (R_{APD}) gives Equation 6.7.

Eq. 6.7 $$d_{APD} = 2R_{APD} = 2\sqrt{\frac{P_r A_{beam}}{\pi P_t G_{APD}}}$$

Table 6.2 illustrates the disparity between the required size of RF receiving antennas and the necessary APD apertures used for FEL transmission when transmitting from an Earth station either to satellites in LEO or GEO and to probes or landers beyond our Moon. Notice the laser column in Table 6.2 has three rows that are dashed out. This is because the calculated APD sizes were so small that it led to the conclusion that a FEL-based communications system would not be feasible at those ranges. Table 6.2 also brings to light the fact the FEL transmissions do not become an appealing option until transmitting beyond the Moon.

	RF = 10 GHz	RF = 14 GHz	Laser (λ = 1.6 μm)
500 km	5.26 mm	3.76 mm	-
35786 km	0.38 m	0.27 m	-
3.84×10^5 km	4.04 m	2.89 m	-
1.00×10^8 km	1.05 km	0.75 km	0.64 mm

Table 6.2 Calculated Receive Antenna Size Dependent Upon Range

The results provided in Table 6.2 were calculated using the following parameters: P_t was equal to 1 W; P_r was 1 x 10–^{16} W (-160 dBW); G_{APD} was set to 50; and the transmitting antennas had a 0.5 m diameter. The transmit power was chosen arbitrarily. Though, considering the required receive power was set to -160 dBW it seemed setting the transmit power to be equivalent to 1 W, which is equivalent to a decibel level of 0 dBW, would be best for comparison. As for the required received power, this was chosen based upon existing GPS receivers. The minimum signal strength required by a GPS receiver to close a link between a satellite and a ground terminal is -160 dBW, which is equivalent to 1 x 10–^{16} W [20].

Two additional factors were taken into consideration: the first was the typical efficiencies of RF antennas and APDs; the second was RF transmission fade losses. Fade losses are those losses that are experienced in an RF link budget that account for the losses in the cabling between the signal generator and the transmitter, as well as attenuation losses due to moisture in the atmosphere. Given examples provided by [12], rain attenuation appears to be between 5 and 15 dB and typically assumed line losses are 2 dB on each side of the transmission. An additional loss value of 15 dB was used in these calculations. As for the efficiency of the RF receive antennas, the nominal efficiency for parabolic antennas, which were assumed for the receive antenna, is 55% [12]. Comparatively, the quantum efficiency of the APD was treated as 80%[19].

The results calculated for Table 6.2 represented RF antenna sizes that were much smaller than had been expected, especially when considering the antennas that one is

accustomed to seeing throughout day-to-day activities. These are the calculated lower limit to the antenna size. Anything smaller would not be able to provide the necessary gain to the signal to overcome the noise floor during signal processing. Thus, receiving antennas that are designed with larger diameters will obviously provide more than enough gain to support the necessary received-power requirement imposed by the sensitivity of the receiver's signal processors. Also, upon analyzing other communications link budgets, it was found that many of them had a higher required received power to close the link than the GPS link requirements [12]. This led to an exploration of the criteria in determining the minimum detectable signal (MDS) level of a receiver.

The minimum detectable signal is utilized as a measure of the sensitivity of the receiver. It is generally taken to be the minimum power that the receiver can process, and stated to be at a level which is 3 dB greater than P_{min}. Where P_{min} is the minimum power the receiver can detect but cannot differentiate from the noise floor [21]. Thus, in order to determine the MDS of a particular receiver, the noise inherent to the receiver must be determined. The noise inherent to a receiver is calculated using Equation 6.8 [12].

Eq. 6.8 $$Noise\ Floor = k_B T_0 BW$$

where k_B is the Boltzmann's constant 1.38 x 10^{-23} J/K; T_0 is the system temperature, assumed to be 290 K; and BW is the bandwidth of the signal, which is assumed to be approximately 20 MHz for signals with carrier frequencies in the GHz range. This gives a noise floor roughly -130 dBW (10^{-13} W). The MDS is then -127 dBW. If it is assumed that a 10 dBW signal-to-noise ratio (SNR) is required to process the signal at the receiver, the resultant minimum received power that can be processed is -117 dBW. Re-calculating Table 6.2 with the new required received power of -117 dBW yielded Table 6.3. Just as in Table 6.2, the rows of the FEL column, which are dashed out, were calculated to be too small to be feasible for implementation.

	RF = 10 GHz	RF = 14 GHz	Laser (λ = 1.6 μm)
500 km	0.67 m	0.48 m	-
35786 km	47.68 m	34.05 m	-
3.84×10^5 km	0.51 km	0.37 km	0.31 mm
1.00×10^8 km	133.22 km	95.16 km	81.49 mm

Table 6.3 Calculated Receive Antenna Size Dependent Upon Range, Adjusted

Using Table 6.3 as a realistic baseline having considered system noise, line losses, atmospheric losses and antenna, or optic, design, it can be easily seen that at ranges beyond geosynchronous orbits the required minimum antenna sizes become entirely infeasible. Granted, due to the manner in which RF link budgets are designed, the antenna sizes can be reduced through clever encoding techniques, the reduction of the data rate, and/or the implementation of low-noise amplifiers on the receiver's signal path. And while these design processes can attain longer ranges with smaller antennas, ultimately, RF communications can not compete when compared to a FEL communications link over astronomical ranges. Additionally, further comparison of the FEL portion of Tables 6.2 and 6.3 show that incorporating the APD efficiencies into the calculations makes FEL communications appear feasible as close to Earth as our own Moon.

This raises the question of the ideal minimum and maximum ranges for laser communications using avalanche photo diodes as the receivers. Based upon the fact that the majority of APDs are built between 0.3 and 0.5 mm in diameter [19], a good approximation for the minimum range can be determined by assuming an APD of 0.3 mm in diameter receiving power from a transmitter at 1 W. A good approximation for the maximum feasible range might be generated using the following assumptions: the desired megawatt level FEL serves as the transmitter; the transmitting beam director is 1.0 m in diameter like the one located at the Starfire Optical Range; the receiver aperture is a cluster of APDs such that the group has a receiving diameter of 0.5 m; and an

increase in the sensitivity of the photon counters within the receiver to be able to increase the MDS to -160 dBW. Using these lower and upper boundaries and the middle desired operating wavelength for the FEL of 1.6 μm, it was found that the minimal receiving range may be just beyond the orbit of the Earth's Moon, at 4.12 x 10^5 km and the maximum feasible receiving range may be as far out as 18 light-years, where one light-year is equivalent to 9,460,730,472,580.8 km [15].

A drawback of transmitting to stars that are farther and farther away from the Earth is that the attainable data rate will be negatively impacted. Currently, there is no really significant competition for technology that can reach these ranges, so this is not a major concern, but rather a minor inconvenience. In order to ensure a measurable number of detectable photons reach the receiving end of the transmission, the pulse duration will have to be gradually increased from microseconds to milliseconds. By increasing the pulse duration, more photons will be packed into each pulse, which will help to minimize the loss of total photons per pulse due to the effects of diffraction on the beam as it propagates deeper through space.

C. ENCODING INFORMATION

Just as with RF communications, transmitting energy is the easy part of the process. Transmitting energy that contains information complicates the process. The first aspect of the information system to be addressed is the point of information injection. In RF communications, this occurs at the signal generator, which then feeds the signal to be transmitted into the modulator to encode the information upon a carrier frequency. A direct analogy for the FEL would be to have the information encoded via adjustments to the electron beam either prior to the injector or throughout the RF accelerator. An alternative location to modulate the laser beam and encode the desired information is at some point along the laser beam path, after the laser energy has passed through the partially-reflective mirror and out of the resonator cavity. If this location is chosen, the transition chamber would have to be able to withstand the high-power of the laser.

The modulation techniques that can be used for a FEL-based communications system are largely dependent upon the chosen injection point. Another factor to be

considered is the specifically designed pulse structure of the FEL. Due to this pulse structure, digital modulation techniques become the optimal choices for encoding information upon a FEL beam. This is regardless of the location of the chosen injection point. All three of the information injection points shown in Figure 6.2 will be discussed to highlight a few of the possible modulation schemes that could be used in the FEL transmission of information. These modulation schemes are initial proposals as methods of encoding information and are based upon digital techniques that are currently in existence and utilized in both RF communications and low-energy satellite laser cross-links.

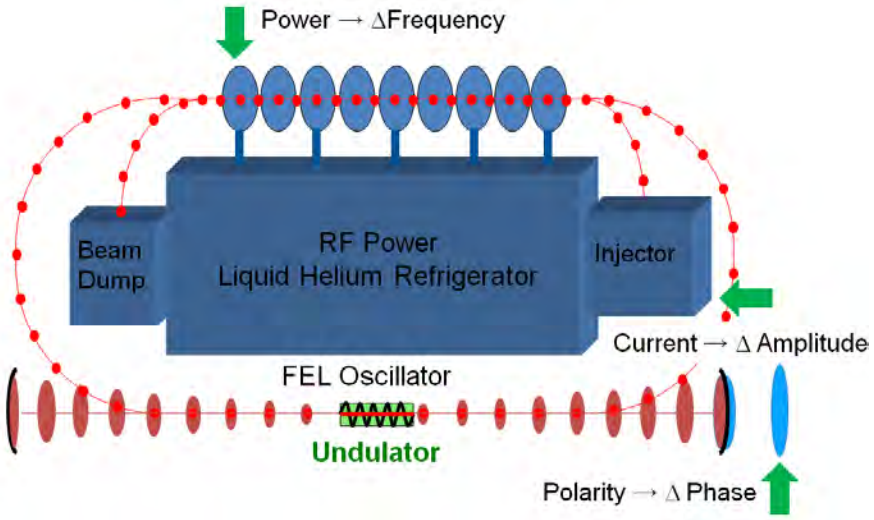

Figure 6.2 Information Injection Points on a Typical FEL

1. Amplitude Shift-Keying (ASK) Using the FEL

The FEL is modulated through variations in the electron beam current or pulse separation interval at the injector. In this configuration, the information signal generator would provide one of the digital PCM waveforms containing the information to be transmitted to the modulator. The modulator would be positioned as a controller for the drive laser. The intensity of the drive laser has a direct impact upon the number of electrons released from the cathode within the electron beam injector [15]. The increase in the number of electrons is proportional to the increase in the total current and

ultimately proportional to the total power within the resultant electron beam. Using On/Off Shift-Keying (OOK) as a modulation technique requires only two different current levels, and so the modulator need only adjust the drive laser between two different intensities.

In the simplest configuration, the modulator would provide an information signal to the drive laser so that for bits determined to be 1's the FEL would be "on" for a microsecond and for bits determined to be 0's the FEL would be "off." Each "1" and "0" would contain approximately 10^3 micro-pulses at a rate of GHz, internal to the single MHz macro-pulse. Using this set-up, the modulator could pass the PCM waveform directly to the electron beam injector. For example, using any of the PCM waveforms from Figure 5.6, the modulator could be designed such that it makes the drive laser be "on" for all positive voltages of the PCM and "off" all zero and negative voltages of the PCM. The only PCM that would not be perfectly re-created in this manner is the Bi-Polar RZ, as there is no way for an On/Off Shift-Keying system to signify a negative valued pulse for half a cycle. Given the provided modulator design, the receiving station would not be able to differentiate between a Bi-Polar RZ and a Uni-Polar RZ. This is because both PCM waveforms would be transmitted in the Uni-Polar RZ format after passing through the modulator.

To further increase the flexibility of a system configured in this manner, the drive laser could be set to fire at multiple intensities, rather than only two. In order to make the detection and differentiation of these multiple intensities at the receiving aperture possible, there would have to be a significant separation between any two intensity levels. This would ensure there is enough of an energy differential over a transmission cycle at the receiving aperture to determine which intensity level was transmitted. This is probably possible with a FEL, but the details would require more research.

2. Frequency Shift-Keying (FSK) Using the FEL

Using the information injection point, indicated in Figure 6.2, at the RF accelerator allows the users to modulate the signal frequency analogous to those used in RF systems. In RF communications, a Binary Frequency Shift-Keying (BFSK)

transmitter is programmed to send one frequency for 1's and a different frequency for 0's. The same effect can be recreated by changing the RF accelerator power in one cavity. As an example the final RF accelerator cavity would nominally be the cavity, which would finish accelerating the electron beam to the desired power level, over a +/- 1 MW range. For a transmit frequency of 1.6 μm, the final energy of the electron beam can be around 69.5 MeV. In order to attain a 2–3% up- or down-shift in the frequency, the final RF accelerator could be used to increase the electron beam power to either 70.5 MeV or 68.5 MeV. This limit is imposed as a result of the typical reflectivity bandwidth of the mirrors used in the resonator cavity [16].

As for actually encoding the information to be transmitted, frequency modulation has some advantages and disadvantages, when compared with amplitude modulation. For example, the tremendous advantage that FSK has over ASK is the flexibility to vary over a great many wavelengths within the boundaries of the upper and lower 2–3% frequency limits. Given that the receiving aperture, at very large distances, would be designed to count photons, minimal separation between the transmitted frequencies is required. This becomes more important as additional states are desired and each frequency is required to represent more bits. To illustrate this point: 2 states, at 1 bit per symbol, require 2 frequencies; 4 states, at 2 bits per symbol, require 8 frequencies; 8 states, at 3 bits per symbol, require 8 frequencies; and so on.

The power of the FEL may vary with the changing of the transmit frequency. As such, the photon counters and detectors that comprise the receiving aperture must be designed with very specific minimum and maximum limits. The lower limit will require a sensitivity that provides the desired minimum detectable signal at the lowest transmit power of the laser. The upper limit will require a saturation cut-off point that is high enough so as to not exclude the power received from the highest transmitted laser power.

3. Phase Shift-Keying (PSK) Using the FEL

The final suggested information injection point is just after the laser light has passed through the partially-reflective mirror. An additional medium would be positioned such that the laser beam line passes directly through the medium's center.

This medium would be designed to be capable of exploiting the Faraday effect, using a controlled magnetic field to rotate the polarization of the laser light. The magnetic medium must be designed to maintain a constant magnetic field at varying orientations. In the ideal scenario, the magnetic field would be variable through the range of angles between 0º to 180º. The change in polarity would have the same effect as changing the phase of a transmitted carrier signal in an RF communications system. The medium selected could be as easy to manufacture as a glass rod wrapped in a current-carrying solenoid, but the diameter of such a rod would have to be have to relatively large. This is because the material selected as the medium would be required to transmitting a few MW of power and the only way to avoid damaging the material chosen would be to spread the beam prior to passing it through the medium [16].

Figure 6.3 illustrates the polarity shifts as a result of the presence of various magnetic fields. In Figure 6.3, the dashed vertical line represents the initial direction of the electric field component of the laser light; the solid line denotes the final direction of the electric field component, after passing through the magnetic cavity; and the angle β is equal to the total rotation between the initial and final electric fields orientations. It is assumed that the laser is traveling into the page and so the magnetic field component of the laser light is initially parallel to the bottom edge of the page.

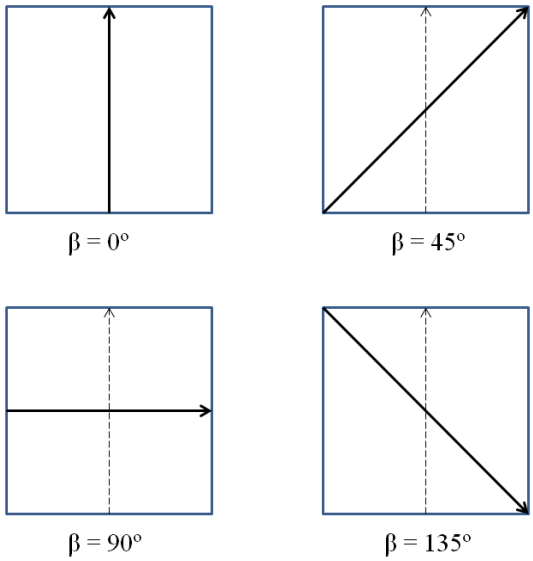

Figure 6.3 Faraday Effect and Change of Polarization Angle β

The main detractor from this particular modulation technique is in the lag time between the phase changes. For the ASK and FSK modulation techniques with the FEL, the lag time has been measured as being on the order of μsec between transitions [16]. In contrast, the change to the polarization angle is hypothesized at being on the order of msec [16]. This plays an important role in the determination of the overall data rate of any communications system designed around this modulation technique. The fact that polarity modulation is a thousand times slower than ASK or FSK immediately makes it the least attractive option for implementation in a FEL-based communications system.

D. DATA RATE ESTIMATION

1. Single Modulation Techniques

The feasible range of the FEL places any communications system employing an FEL as the transmitter outside of any real competition. At the ranges over which the FEL will be best suited, very low data rates are required. Using BASK or BFSK modulation schemes; approximately 1 μsec cycle times; and 1 cycle per transition between the FEL's operating states; and an ideal transition with no lag time, the transmit data rate is roughly 1 Mbit/sec. If the lag time between transitions were assumed to be 1 μsec, the total cycle time would then be 2 μsec: 1 μsec for the state and 1 μsec for the transition lag. In this case, the data rate is still around 500 kbits/sec. An additional reduction in data rate would be incurred by the BASK modulation if one of the PCM waveforms that required a transition every half-cycle was used (i.e., Bi-φ-L, also known as Manchester encoding). For a transmission of this type, the total cycle time would be around 4 μsec as 1 μsec would be required to represent the first half-cycle of the waveform; 1 μsec for the transition; 1 μsec for the second-half cycle of the waveform; and finally 1 μsec for the transition between consecutive cycles. This gives a data rate of 250 kbits/sec. By comparison, the spacecrafts Pioneer 6–9 had five selectable data rates: 512, 256, 64, 16, and 8 bits/sec [22]. Also, the Galileo spacecraft had been designed to have a maximum data rate with its high-gain antenna deployed of 134 kbits/sec [23]. Both of these examples are nearly 10 times less than what is possible with the FEL in a minimal binary ASK or FSK transmission configuration. Even the polarization modulation technique,

which is the slowest technique by a factor of 1000, could surpass the Pioneer spacecraft and maintain data rates of a minimum of 500 bits/sec.

The approximation of possible data rates was completed based upon the assumption that there was only 1 bit allocated per symbol. However, as described in the previous section, it is possible to configure each of the systems using these individual techniques in order to allocate more bits per symbol, thus increasing the overall data rate. If the megawatt-level FEL system being designed by the Navy is completed, then the nominal electron beam pulse-repetition frequency is approximately 1 GHz, or 10^3 electron pulses per second [1]. In the BASK case, the current can be reduced to as low as $10–^8$ the nominal value to ensure a significant difference between the "on" state and the "off" state [16]. To further improve upon the BASK modulation scheme, multiple power levels can be generated through varying either the intensity of the drive laser, which causes the charge in the electron beam to vary; varying the pulse-repetition frequency between a band of 0.1 to 1.0 GHz; or combinations that involve varying both parameters. If it is assumed that the avalanche photo diode (APD) receiver bunch is capable of detecting a difference between received power levels of approximately 3 dBW, then for transmit power levels below roughly a MW, this can be used as the criteria for the amount of separation required between each power level. Recall that a change of +3 dBW is equivalent to an increase by a factor of 2 between power levels. For power levels which are approximately 1 MW or greater, perhaps 1 to 3 MW, a required variation between power levels of roughly 20% might be assumed. Table 6.4 was developed using these constraints in order to present potential ASK current and pulse-repetition frequency (PRF) pairs, which may be used to provide more flexibility to a FEL-based communications system.

State	Bits	Charge (nC)	PRF (MHz)	Current (mA)	Transmit Power (MW)
0	000	0.80	50	40.0	0.12
1	001	0.80	100	80.0	0.24
2	010	0.80	200	160.0	0.48
3	011	0.80	400	320.0	0.96
4	100	0.80	500	400.0	1.20
5	101	0.80	600	480.0	1.44
6	110	0.80	700	560.0	1.68
7	111	0.80	800	640.0	1.92

Table 6.4 ASK Power Level Division

This initial estimate for varying the transmit power levels via varying the pulse-repetition frequency does not take into consideration the possible limitations imposed upon the laser's flexibility by the materials used in designing the components of the FEL beam line. For example, the first concern that was mentioned deals explicitly with the resonator cavity and beam steering mirrors and the effects on their reflectivity, absorption, and transmission as a function of the power imparted upon them.

If the eight PRF divisions in Table 6.4 are achievable at the transmit station and the receive station can indeed discern between the different states, this would allow the user to quadruple the data rate of the standard BASK when using the FEL.

Applying a similar method of quantified states to the BFSK modulation permits the creation of multiple frequency states. This would be achieved by adjusting the power in one RF accelerator cavity and thus altering the total beam energy which, in turn, changes the frequency of transmission of the laser beam. These additional states would be inserted between the upper (70.5 MeV, $\gamma = 139$) and lower (68.5 MeV, $\gamma = 135$) frequency bounds established for the BFSK case with a difference in frequency between each subsequent state of between 0.5% and 1.5%. Table 6.5 provides suggested FSK frequency divisions as determined by incremental Lorentz factor values. This separation

provides eight states, where three bits are represented by each frequency. Also, using these frequency divisions increases the data rate of the transmission by a factor of four over the BFSK transmission.

State	Bits	γ	E_{beam} (MeV)	Frequency (THz)
0	000	139.0	70.52	193
1	001	138.5	70.26	192
2	010	138.0	70.01	190
3	011	137.5	69.75	189
4	100	137.0	69.50	188
5	101	136.5	69.24	186
6	110	136.0	68.99	185
7	111	135.0	68.47	182

Table 6.5 FSK Frequency Division (Central Wavelength = 1.6 μm)

While it is apparently possible to configure the FEL in a way to obtain eight or more states using either amplitude or frequency shift-keying, when modulating the signal via the polarity of the laser light, it seems that the FEL may be limited to using only four states. This recommendation ensures there is enough angular separation between the adjacent polarities to allow for some margin of polarity shifting over the transmission range. In this way, it would be possible to design the detector such that a state would be actually represented by any signal received within a 40º bandwidth centered at the initial β angle. The result would be four bands of 40º separated by buffers of 5º on either side.

For example, if the rotation of the laser light's polarity were 45º at the transmitter, then the receiver would treat received laser light with a polarity between 25º and 65º as corresponding the to the state represented by a β angle of 45º. This modulation scheme still provides an increase to the overall data rate of its binary counter-part, but the data rate is only double vice quadrupled as it is with the amplitude and frequency modulations. Table 6.6 lists the four polarization states that may be implemented into use with the FEL communications system.

State	Bits	β angle (°)
0	00	0
1	01	45
2	10	90
3	11	135

Table 6.6 PSK Polarity Phase Separation

2. Combined Modulation Techniques

Similar to RF modulation and encoding techniques, the different modulation schemes can be combined in order gain more bits per symbol. Equation 6.9 illustrates the relationship between bits per symbol, symbol rate, and bit rate [14].

Eq. 6.9 $$Data\,Rate = \frac{Bits}{Second} = \frac{Bits}{Symbol} * \frac{Symbols}{Second}$$

Continuing with the RF communication analogy, if one were to modify a system that had been designed to transmit QPSK (2 bits per symbol) such that it was now capable of varying the amplitude of the signal as well, the data rate would be doubled. In the new configuration, 3 bits would be allocated to each symbol, giving a total of 8 representable states, shown in Figure 6.4.

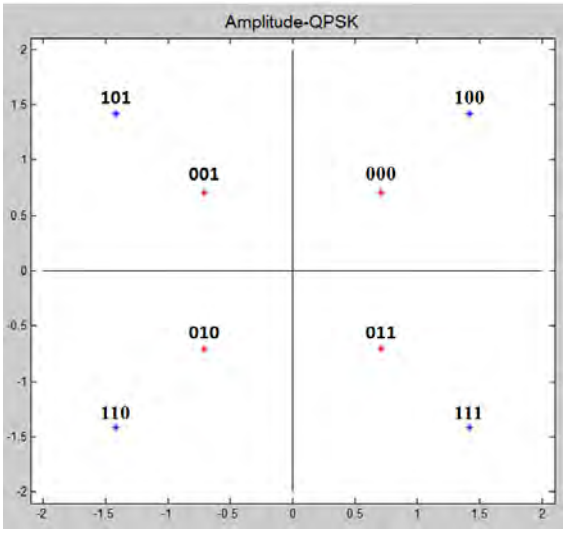

Figure 6.4 Example of Combined Modulation and Symbol Allocation

This same idea can be applied to working with signal modulation with the FEL. It is most ideal to use a combination of amplitude and frequency modulation, as they change on roughly the same time scale of a μsec. The primary complication that this method has that a RF communications system does not have is that the amplitude and frequency are not de-coupled [1], [16]. When changing the frequency, the electron beam's energy is also changed, which results in a change in the overall transmit power. To mitigate this coupled effect, the current or pulse-repetition frequency of the electron beam can be adjusted to maintain between a 1 dBW to 3 dBW separation between adjacent transmit power levels. In Table 6.7, I have used 4 different frequencies between the upper and lower frequency limits and 4 different electron pulse-repetition frequencies.

State	Bits	γ	E_{beam} (MeV)	Frequency (THz)	Charge (nC)	PRF (MHz)	Transmit Power (MW)
0	0000	139	70.52	193	0.80	75	0.13
1	0001	139	70.52	193	0.80	150	0.25
2	0010	139	70.52	193	0.80	300	0.51
3	0011	139	70.52	193	0.80	600	1.02
4	0100	138	70.01	190	0.80	75	0.13
5	0101	138	70.01	190	0.80	150	0.25
6	0110	138	70.01	190	0.80	300	0.50
7	0111	138	70.01	190	0.80	600	1.01
8	1000	136	68.99	186	0.80	75	0.12
9	1001	136	68.99	186	0.80	150	0.25
10	1010	136	68.99	186	0.80	300	0.50
11	1011	136	68.99	186	0.80	600	0.99
12	1100	135	68.47	182	0.80	75	0.12
13	1101	135	68.47	182	0.80	150	0.25
14	1110	135	68.47	182	0.80	300	0.49
15	1111	135	68.47	182	0.80	600	0.99

Table 6.7 Combined Amplitude and Frequency Shift-Keying

Having this many variable parameters allows the user to represent 4 bits per symbol and provides an improvement over the binary modulation techniques of a factor of 8. With a μsec transition between states, the data rate easily reaches 16 Mbits/sec. And even if 2 μsec are used as the transition to allow 1 μsec buffer between states to establish stability, the overall data rate is still up around 8 Mbits/sec, which is nearly 60 times greater than the highest designed data rate for the Galileo spacecraft. Furthermore,

in order for Galileo to achieve its designed max data rate of 134 kbits/sec, the Earth-side receiver required an antenna with a diameter of 70 meters [23]. By contrast, with the FEL there is a 1 meter diameter transmitter and a 0.5 meter diameter receiver and when considering space applications a savings in size equal a savings in money.

Taking the results of Table 6.7 into consideration, it is then reasonable to assume the remaining 4 suggested frequencies from Table 6.5 (at γ = 136.5, 137, 137.5, and 138.5) could be coupled with these same 4 PRFs (75, 150, 300, and 600 MHz) to double the data rate again, raising the total number of states to 32 and the number of bits per symbol to 5. Also, in the example shown in Table 6.7, the electron beam charge was held constant. This could also be varied to allow even more improvement to the number of bits represented per symbol.

E. POTENTIAL FEL MESSAGES

Up to this point, the discussion has been about how to encode information onto a laser beam generated by a free-electron laser. In the previous sections, the implicit assumption had been made that the receiver was man-made and so the ability to decode the encoded information would reside within the signal processor at the receiver station. This section covers exactly what information to send with a free-electron laser and to whom. The over-arching vision for using a FEL for deep-space communications is that the FEL could supplement or replace the current methods of Active SETI (Search for Extra-Terrestrial Intelligence). The major advantage provided by the FEL has been re-iterated throughout this thesis: the FEL suffers from much less diffraction than any of the RF systems. Ultimately, this means the FEL would provide a much more directed beam of energy towards a star suspected of supporting life on its surrounding planets.

From the perspective of space exploration, future probes could be configured such that they are capable of receiving their command data from a ground station powered by a free-electron laser. These probes would be able to go to greater distances from the Earth and still be sent significant amounts of commands, perhaps in a queue to be

executed in sequence. This would allow the transmit station to only have to contact the probe on a weekly or even monthly basis dependent upon the scientific research being conducted by the probe.

Conceptually the next Martian Rover could even be configured to receive its commands in this manner. As highlighted in Table 6.3, the final listed distance of 1×10^8 km is the next closest approach to Mars. Using this range, the APD cluster that would be required on a Martian Rover designed to receive commands from a FEL would need to be just over 8 cm in diameter, assuming the same 0.5 diameter transmitting mirror. When considering the data rates that can be achieved with the FEL, this makes the current method of using Earth-based RF transmitters of 70 meters in diameter and receivers on the Rover that are approximately 0.25 meters in diameter obsolete [24].

Finally, we look at using the FEL in assisting with the SETI program. To this end, a few questions must be addressed: 1) What might a message from an intelligent race look like?; 2) How is it formatted?; and more importantly 3) What information should the message contain? In addressing the first question, in order for a message transmitted by an intelligent race to be identified as a man-made transmission and not a naturally occurring event, there must be an identifiable structure to the message. Any receiver designed to detect laser light that may be present at deep-space ranges from the transmitting FEL on Earth, will determine the presence of a signal based upon received photon counts, but packets of photons alone is not evidence of design or structure.

Now, recall that the free-electron laser transmits energy on two time structures: the micro-pulse and the macro-pulse. Generally, the macro-pulse has a duration of a μsec, which gives the FEL a MHz repetition frequency. These μsec long macro-pulses contain approximately 10^7 photons. At deep-space ranges, the number of photons per square meter is reduced significantly. In order to ensure a detectable concentration of photons is received, larger durations of macro-pulses are required in order to pack more photons into each separate pulse. This means at deep-space ranges the largest unit of detectable transmitted energy would potentially be a macro-pulse generated on a kHz time-scale. With this in mind, the ASK and FSK modulation techniques and

combinations, which have been discussed previously, would now make use of kHz macro-pulse while the inherent micro-pulse structure can provide further proof the transmission is of intelligent design.

With respect to how the message should be formatted, the first series of messages need to be very simplistic in the modulation technique utilizing only two states. This allows for the message being transmitted to be sent as a black and white pictograph: the 1 state would represent the white pixels, and the 0 state would represent the black pixels. A single string of greater than 16 bits could be used to designate the end of a pictographic line. The receiver would be able to recreate the image by arranging the received bits so that the ending string is aligned for each separate line, as shown in Figure 6.5.

0	0	0	1	1	1	0	0	1	1	1	0	0	0	1	0
1	0	0	0	1	0	0	0	1	1	1	0	0	0	1	0
0	1	1	1	1	1	1	0	1	1	1	0	0	0	1	0
1	1	1	1	1	1	1	0	1	1	1	0	0	0	1	0
0	1	1	1	1	1	1	0	1	1	1	0	0	0	1	0
1	0	0	0	1	0	0	0	1	1	1	0	0	0	1	0
0	0	0	1	1	1	0	0	1	1	1	0	0	0	1	0

Figure 6.5 Illustration of Pictograph End-line Alignment

In this way, the first messages transmitted using the FEL would be similar to those transmitted using the RF station at the Arecibo facility. Figure 6.6 is the Arecibo message as it was transmitted. In Figure 6.6, the color-coded pixels were transmitted as 1's and the black were transmitted as 0's [25].

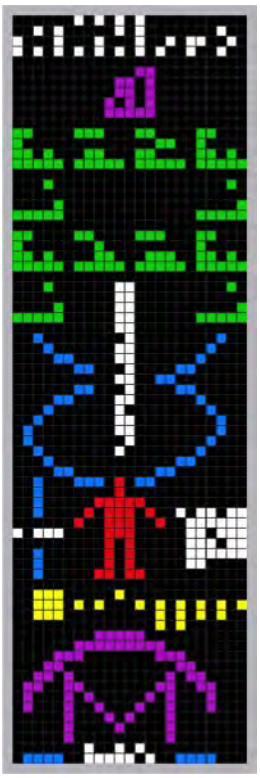

Figure 6.6 Arecibo Message

The image in Figure 6.6 is color-coded for the ease of the reader. The color-coding is provided to answer the third of SETI's questions: what information should the message contain? For example, the Arecibo Message was created by Carl Sagan and his associates to demonstrate the capabilities of the Arecibo facility and contains the first 10 numbers in binary; the chemical formulations for the nucleotides that comprise human DNA; basic information on the size of a human and the world's population; as well as Earth's location in our solar system [26] . While the Arecibo message contains a large amount of information, the Pioneer plaques, shown in Figure 6.7, accomplish a similar goal, and could easily be recreated in this same pictographic fashion [27].

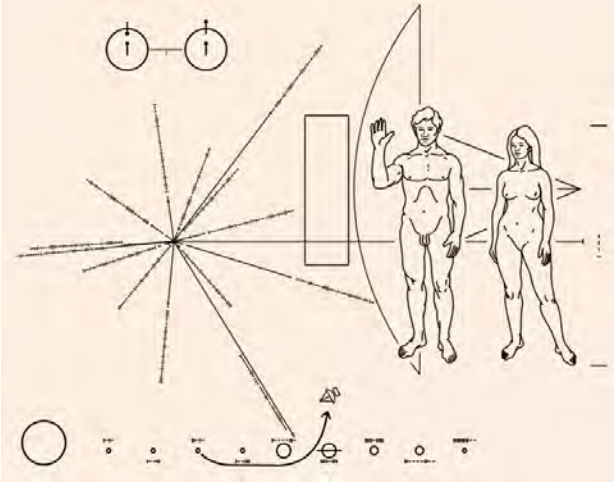

Figure 6.7 Pioneer Plaque

In order to be able to encode information using the more complex modulation techniques, and have it be decoded and understood, the message would probably need to be sent containing a key in the preamble. For example, in using a modulation technique wherein one symbol represents 4 bits the preamble would have to contain the numbers 0 to 15 encoded in binary immediately followed by the 16 symbols, representing 4 bits each, which would re-create the 64 bits sent beforehand. This would probably have to be repeated a few times before beginning the transmission of the message with the more complex modulation scheme. An example of the requisite preamble for more complex modulation schemes is shown in Figure 6.8.

0	0	0	0	0	0	0	1	0	0	1	0	0	0	1	1
0	1	0	0	0	1	0	1	0	1	1	0	0	1	1	1
1	0	0	0	1	0	0	1	1	0	1	0	1	0	1	1
1	1	0	0	1	1	0	1	1	1	1	0	1	1	1	1
0000				0001				0010				0011			
0100				0101				0110				0111			
1000				1001				1010				1011			
1100				1101				1110				1111			

Figure 6.8 Example of a Preamble Key for Complex Modulation Schemes

VIII. ORBITAL DEBRIS REMOVAL AND TRACKING

A. ORBITAL DEBRIS AND THE PROBLEM IT POSES

Orbital debris is defined by NASA as "man-made objects in orbit around the Earth which no longer serve a useful purpose." These man-made objects include everything from whole, intact rocket bodies and "dead" satellites to nearly spherical chucks of aluminum approximately one centimeter in radius [28]. This debris can be generated either intentionally, as part of normal operations via payload separation from the upper-stage of the launch vehicle; or unintentionally through collisions with micro-meteoroids, other debris, or worse, other spacecraft.

Figure 7.1 below is an image from returned shuttle mission STS-94 showing the damage a micro-meteorite (less than 1 mm in diameter) is capable of causing to a spacecraft in low-earth orbit (LEO) [29].

Figure 7.1 STS-94 Window Damage. From [29]

The object that impacted this window left an approximately 1 mm crater in the window and was estimated to be approximately 100 microns in size and traveling around 10 km/s. This micro-meteoroid was not among the nearly 20,000 objects that are tracked

by NASA and the U.S. Space Surveillance Network (SSN) for the protection of U.S. satellites. The SSN only routinely tracks objects greater than 10 cm by 10 cm [28].

Figures 7.2 and 7.3 are computer generated models of the orbital debris present at various altitudes as seen from geosynchronous orbit (GEO) and low-earth orbit (LEO).

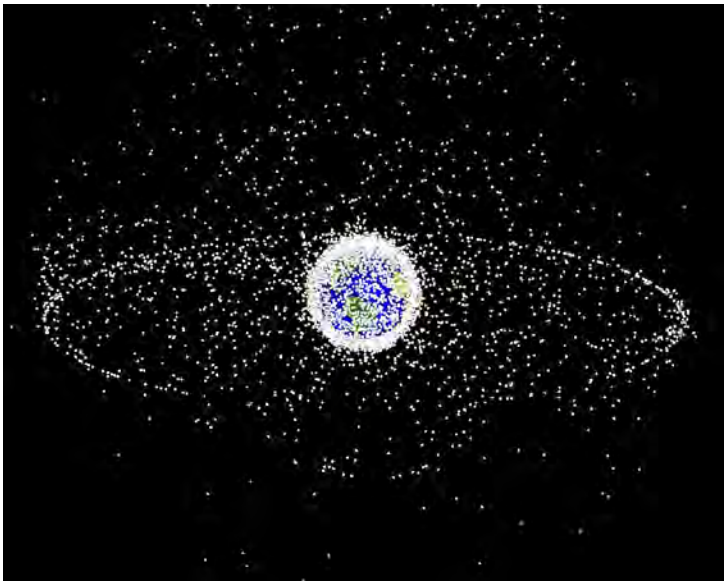

Figure 7.2 Computer Model of Debris as seen from GEO. From [30]

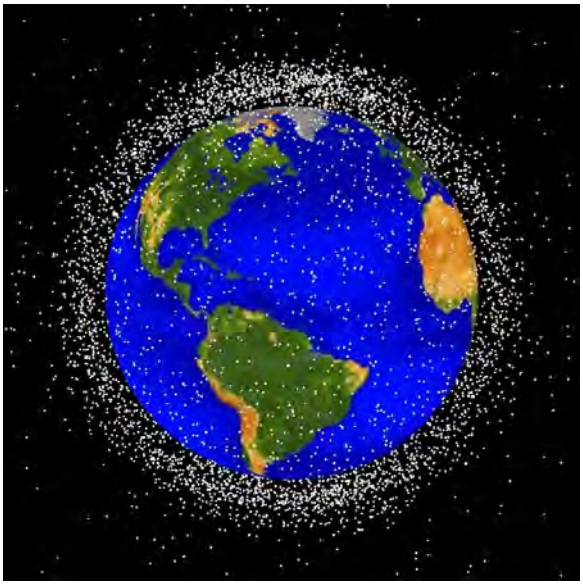

Figure 7.3 Computer Model of Debris as seen from LEO. From [30]

These two figures highlight the fact the largest orbital debris concentration is located in LEO, between 350 km and 1000 km. However, these figures only provide the information recorded for objects that are regularly tracked by the SSN, and thus any objects that are less than 10 cm on a side are not included in the figures.

Given the large number of debris objects that are below the tracking threshold of the SSN and in light of the damage seen in Figure 7.1 objects as small as 1 cm on a side are of significant concern to NASA. Figure 7.4 illustrates the necessity of increased shielding from debris impact on certain faces of the International Space Station (ISS) [29].

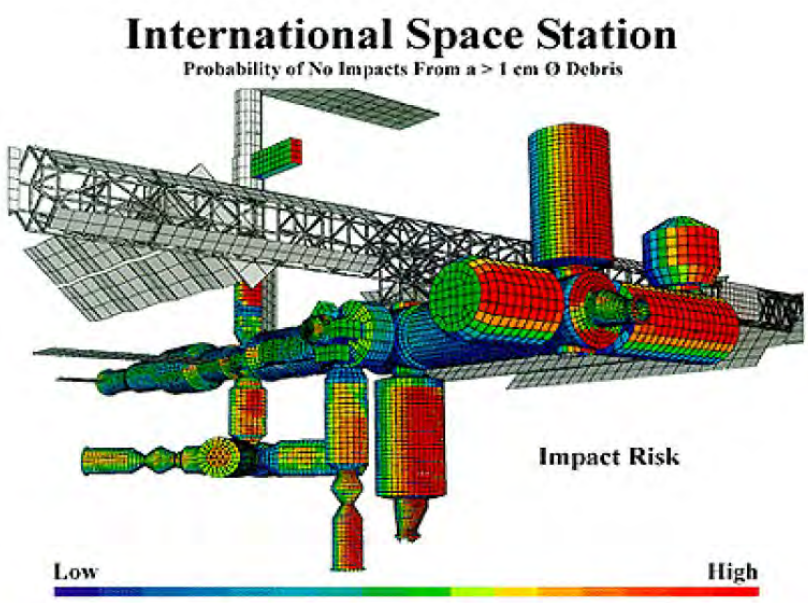

Figure 7.4 Probability of No Impact. From [29]

Figure 7.4 also shows the probability of the ISS not being struck on a side by objects of greater than 1 cm is very low. The viewgraph highlighted, for the engineers designing the ISS, the locations where more shielding would be required. This shielding is provided in the form of additional layers of material between the interior of the spacecraft and the impact point for the purposes of absorbing the kinetic energy of the debris on impact.

The kinetic energy of a piece of aluminum the size of that shown in Figure 7.5 can be very large. To evaluate the speed of impact, we first calculate how fast an object in LEO is traveling [30].

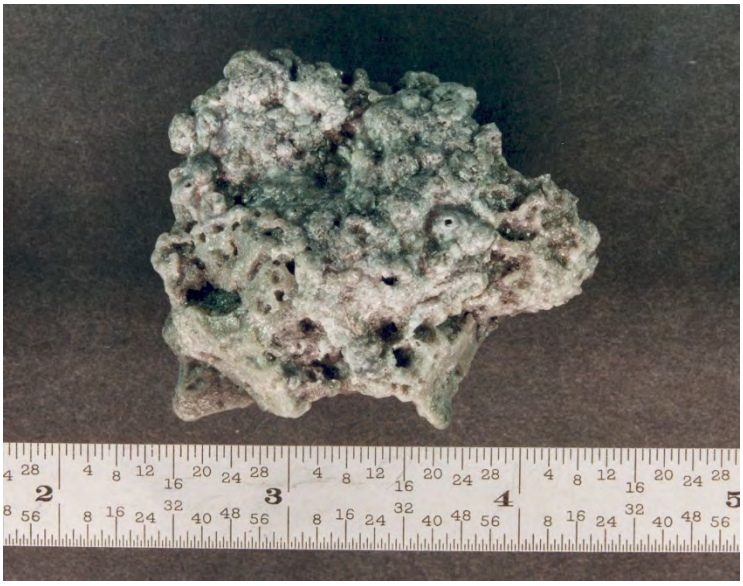

Figure 7.5 Aluminum Debris from a Rocket Motor. From [30]

The NASA Orbital Debris Program Office considers an object to be in Low-Earth Orbit if it resides between the altitudes of 160 and 2000 km [31]. If we assume the object is in a perfectly circular orbit, then the velocity is calculated from Equation 7.1

Eq. 7.1 $$v_{circ} = \sqrt{\frac{G * M_{Earth}}{(R_e + z)}}$$

where G is Newton's Gravitational Constant, 6.67e-11 $m^3/kg\text{-}s^2$; M_{Earth} is the mass of the Earth, 5.97e24 kg; R_e is the radius of the Earth, 6378 km; and z is the altitude of the orbit [32].

Varying the altitude between 160 and 2000 km yields a range in possible velocities of 7.8 km/s and 6.9 km/s. Thus, most collisions will occur with a relative velocity between 10 km/s and 15 km/s, dependent upon whether or not the collision is head-on. In the case of the ISS, with an average altitude of 350 km, a head-on collision with a piece of debris would have a total velocity, relative to the ISS, of approximately 15

km/s. If it was assumed the object was a solid, 1 cm cube of aluminum with mass = 2.7 x 10^{-3} kg, the energy transferred from the object to the ISS upon impact would be nearly 320 kJ. For purposes of comparison, this is the same amount of energy as a 2012 Ford Escape with mass = 1500 kg hitting a wall travelling at 47 mph (21 m/s) or a 12-pound bowling ball with mass = 5.5 kg hitting a wall travelling at 770 mph (340 m/s).

The threat to U.S. interests in LEO is serious. The following sections will consider two potential roles the FEL might fulfill. The first role would be to use the FEL as a means of active debris removal (ADR). The second role, and probably the one which would be realized first, is to utilize the FEL as a supplement to the current X-band Radar tracking system used by the SSN. The high-power FEL will be evaluated as a tool in obtaining a greater resolution than the current tracking system.

B. ESTIMATION OF ACCESS TIMES

Utilizing the Analytical Graphics Inc (AGI) Satellite Tool Kit (STK) a set of orbits was created for hypothetical pieces of debris to determine the range of access times the FEL a laser would have when illuminating targets at altitudes ranging between 350 km and 1000 km. Assuming the laser illuminates a single target for the entire duration of an overhead pass, the target would potentially be illuminated for as little as half a minute up to as long as 15 minutes. For the purposes being explored in the subsequent sections, the laser will not be required to illuminate a target for the entire overhead pass. Table 7.1 provides minimum, maximum, and mean access times for various altitudes using the Air Force Maui Optical and Supercomputing (AMOS) observatory as the location of the FEL.

Altitude (km)	Minimum (min)	Maximum (min)	Mean (min)
350	2.6	7.1	4.3
500	2.9	9.7	5.6
625	0.7	11.6	5.0
750	3.3	12.5	6.3
875	3.5	12.6	6.1
1000	3.6	14.9	7.3

Table 7.1 Access Times at Various Altitudes from AMOS

The mean access times, as provided in Table 7.1, are used in all calculations for the following sections.

C. ACTIVE DEBRIS REMOVAL (ADR)

Active Debris Removal (ADR) is the act of using an outside force to cause a piece of debris to be removed from its current orbit. This could be accomplished in a couple of ways using lasers: ablating, or melting/vaporizing, the debris with lasers and causing a change in orbital velocity via the resultant out-gassing; or using the laser light's radiation pressure to "push" the debris causing a change in orbital velocity. In an earlier thesis, using the FEL to ablate the surface of small, thin pieces of orbital debris was examined and found to be infeasible with the proposed technology [33]. Here the feasibility of the second approach, radiation pressure, is examined.

1. Radiation Pressure

Radiation pressure is the resultant force upon an object being bombarded by incident photons [15]. The hypothesis was that the FEL's beam would essentially push the object in the direction opposite to that of its tangential velocity causing it to experience a cumulative reduction in its velocity and thus reducing the altitude of the orbit 180˚ away from the laser-debris interaction. This is analogous to the change in altitude that occurs 180˚ away from an impulsive maneuver's burn, wherein a rocket is fired to either increase or decrease the tangential velocity of the orbiting body [32]. The

laser is believed to not have enough force in a single shot to cause the object to de-orbit on the following pass, but over successive shots, it may be possible to de-orbit an object in LEO [16].

For the purposes explored here, it was decided that an object would be considered de-orbited when its perigee, or the point in the orbit where the object is at its lowest altitude, had been reduced to an altitude of 200 km. At that time, atmospheric drag would be assumed to become the dominant force in causing the object to completely de-orbit. Another assumption that was made was that all objects being examined would be initially in a circular orbit. This assumption was made to simplify the calculations while still preserving the overall intention of the analysis. Figure 7.6 gives the overview of the laser-debris interaction and the basic free-body diagram, centered about a piece of debris, as a result of the laser illuminating the target.

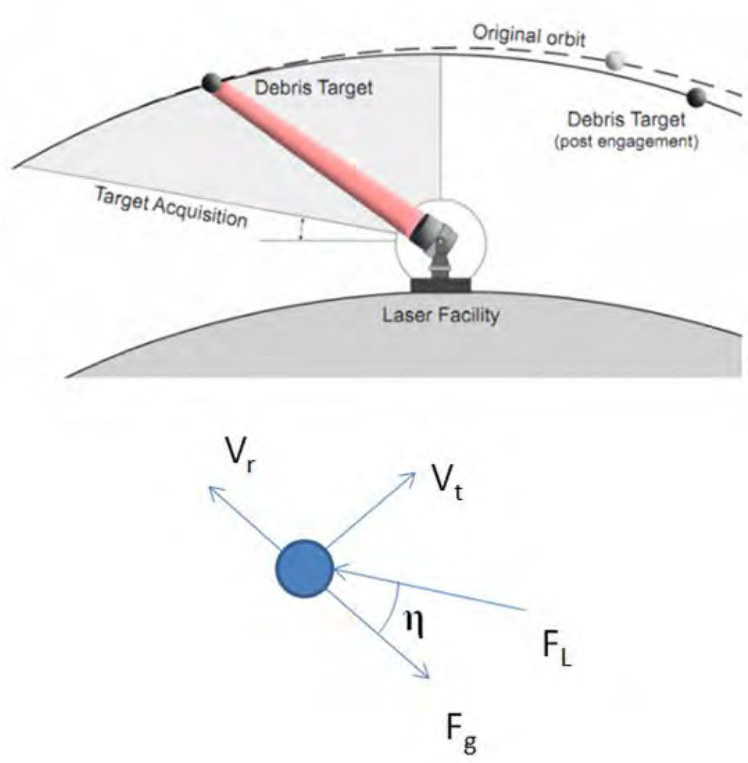

Figure 7.6 Free-body Diagram for Laser-Debris Interaction. From [34]

In Figure 7.6, F_L is the force generated from the radiation pressure provided by the laser; F_g is the force of gravity on the object, with the vector oriented from the center

of mass of the debris to the center of the Earth; and V_t is the vector representing the tangential velocity of the piece of debris. Also, V_t serves as the vector pointing along the positive direction of the fixed-body frame x-axis, while V_r serves as the vector pointing along the positive direction of the fixed-body frame y-axis. The angle between F_L and F_g is designated η and its definition can be derived from Figure 7.7, provided by [35].

The angular relationships depicted in Figure 7.7 are geometrically defined in [35], and can be manipulated to provide the value for the angle η between F_L and F_g. For the instance of using the FEL to target a piece of debris, the target and satellite in Figure 7.7 would be replaced with the FEL and the debris respectively.

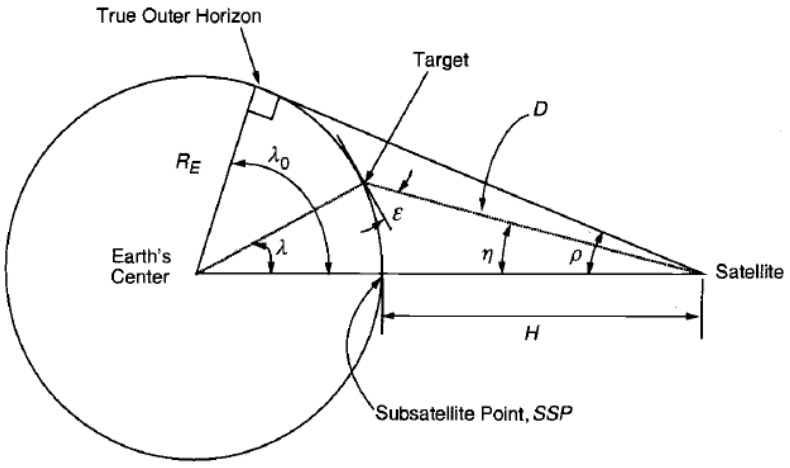

Figure 7.7 Angular Relationships Between Satellite, Target, and Earth's Center. From [35]

With regard to the remaining angles of importance, ρ is the angle between the true horizon and the direction of the vector resultant from the force of gravity; and ε is the elevation angle and is determined through measurements taken by the beam director while it tracks the target.

Using Equations 7.2 and 7.3, the angles necessary in determining the amount of energy imparted to the piece of debris and the magnitude of the change in velocity along the tangential velocity vector can be calculated.

Eq. 7.2 $$\rho = sin^{-1}\left(\frac{R_E}{R_E+H}\right)$$

Eq. 7.3 $$\eta = sin^{-1}(\cos(\varepsilon) * \sin(\rho))$$

In order to calculate the change in velocity in the x- and y- directions, the free-body diagram in Figure 7.6 must be broken into its components along the tangential (x-) and radial (y-) velocity vectors. Breaking the force from the FEL into its individual components yields Equations 7.4 and 7.5.

Eq. 7.4 $$F_{Lx} = -F_L \cos\left(\frac{\pi}{2} - \eta\right)$$

Eq. 7.5 $$F_{Ly} = F_L \sin\left(\frac{\pi}{2} - \eta\right)$$

There are no forces opposing the laser along the tangential velocity component and the only force opposing the laser along the radial velocity component is gravity. In order to calculate the force from the laser, F_L, the radiation pressure from the laser is needed. This is determined using Equation 7.6

Eq. 7.6 $$RP_L = \frac{I_L}{c}$$

where RP_L is the radiation pressure from the laser in N/m^2; I_L is the laser's intensity in W/m^2; and c is the speed of light at approximately 3 x 10^8 m/s [15]. The force of the radiation pressure on the debris is then given by Equation 7.7

Eq. 7.7 $$F_L = RP_L * SA_{Target}$$

where SA_{Target} is the surface area of the surface being illuminated by the laser on the target [15].

Table 7.2 provides the magnitudes of the three forces acting on a 1 cm^3 piece of aluminum debris (1 cm on a side) assuming a circular orbit; altitude of 500 km; elevation angle of 15°; laser power of 1 MW; laser wavelength of 1600 nm; beam director 1 meter in diameter; and interaction duration of 1 second. From these parameters, the resultant spot beam diameter is 1.4 m, which has an area of 1.6 m^2. This means the 1 cm^3 piece of aluminum receives an intensity of laser light of 0.6 MW/m^2. The decision for comparing the forces from a 1 second shot was to make the shot have a nearly immediate impact on the orbit, similar to an impulsive maneuver for a Hohmann-type transfer orbit.

	Force (N)
F_{Lx}	1.9×10^{-7}
F_{Ly}	9.3×10^{-8}
F_g	-22.7×10^{-3}

Table 7.2 Force Comparison

It can be seen in the table that the force of the laser acting in the y-direction is negligible when compared to the force on the object from gravity. The force in the x-direction, acting opposite the tangential velocity of the debris object, provides a change in velocity of -6.9 x 10–^{5} m/s. If this were the only shot on the object, the perigee would be reduced by less than 1 meter.

For further comparison, the change in velocity required to transition the debris into an orbit with a perigee below the altitude NASA considers as the de-orbiting threshold of 200 km, one can use Equation 7.8

Eq. 7.8 $$\Delta V_{impulse} = \sqrt{\frac{\mu_{Earth}}{R_1}} * \left(\sqrt{\frac{2R_2}{R_1+R_2}} - 1\right)$$

wherein R_1 is the altitude of the original circular orbit (500 km) and R_2 is the desired altitude at perigee (200 km) [32]. The ΔV required was calculated as -85.3 m/s. This confirms the hypothesis that the FEL does not provide enough force in a single, one second shot to provide the ΔV necessary to de-orbit an object on the subsequent pass.

Fortunately, the mean access time for an object at 500 km is just over 5.5 minutes, which means there is plenty of time available to take multiple shots at the piece of debris. If it is assumed that the laser-debris interaction will only take place during the first half of the overhead pass, as shown early in Figure 7.6, then that reduces the amount of interaction time to roughly 3 minutes. If it is also assumed that there may be obstructions that interfere or intercept some of the laser light, for example lower orbiting pieces of debris, then the interaction time could be feasibly reduced further. Another consideration is the fact that there exists an ideal cutoff elevation angle at which point the user is not

getting as much change in velocity per individual 1 second shot. Figure 7.8 illustrates the total change in altitude of the perigee of the debris o

rbit per single pass dependent upon the variation of maximum cutoff elevation angle.

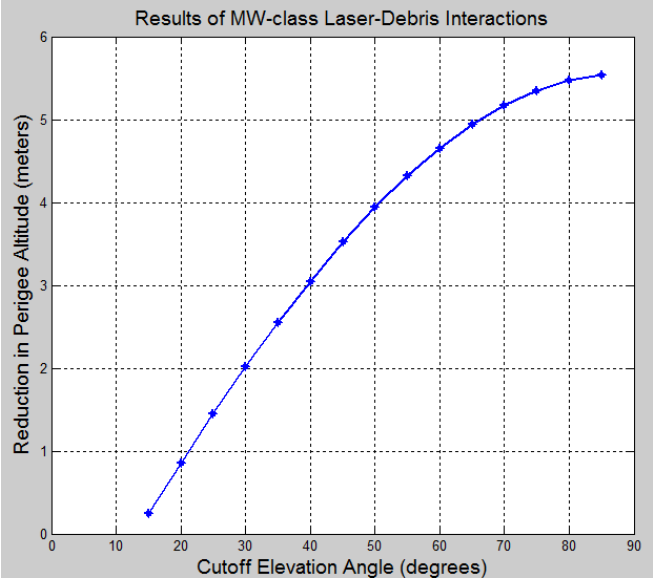

Figure 7.8 Results of MW-class Laser-Debris Interactions

Judging from the results in Figure 7.8, which highlights the fact that one pass only provides a total change in the altitude of the perigee on the order of a few meters, it does not seem feasible that even multiple shots from a FEL could achieve the end-state objective of de-orbiting a piece of orbital debris via radiation pressure. Extrapolating through multiple passes over the FEL facility leads to the realization that the altitude remains fairly constant over the location of the interaction as the velocity is steadily decreased with each set of pulses. From this, it was found that approximately the same amount of tangential velocity is removed from the piece of debris each interaction. Thus, if the orbit's perigee is reduced roughly 5.5 m each interaction, then nearly 55000 laser-debris interactions would be required to de-orbit the 1 cm^3 object. With the assumption of an average of 9 interactions per day, it would take around 15–17 years to de-orbit a single piece of debris.

2. Improvements Using Adaptive Optics

The next question to answer then becomes, is it possible to improve upon this? To which the answer is a resounding yes. In the previous example, the spot beam area was 1.6 m^2. In contrast, the target's single-side, surface area was 1 cm^2. A majority of the energy was being wasted in the previous example, as it did not even impact the debris. Figure 7.9 shows the linear relationship between the change in altitude at the orbit's perigee each pass and the surface-area-to-mass ratio.

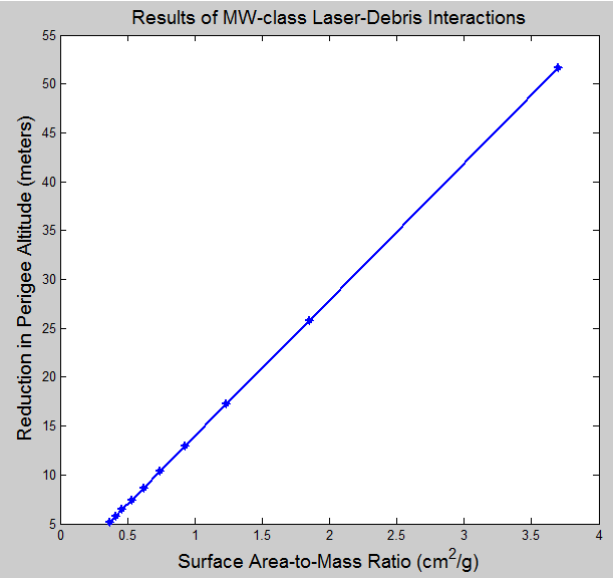

Figure 7.9 Surface Area-to-Mass Ratio versus Change in Perigee per Pass

For this data set, the mass of the object was held constant (2.7 grams) while the surface area was increased. This led to the conclusion that the primary factor in determining the rate objects of similar masses can be de-orbited via radiation pressure is the surface-area-to-mass ratio of the objects. In Figure 7.9, even the greater surface-area-to-mass ratios depicted do not de-orbit fast enough for the FEL to be a viable solution to the problem. The reason for this is the total incident power on the debris is still significantly lower than it needs to be to achieve the goal with any sort of timeliness. Two solutions presented themselves then: increase the laser's power; or reduce the spot

beam area to match the target and thus ensure all the energy is impacting upon the target. The laser being designed already has an output power of 1 MW, as such, attempting to increase the power further may be requesting too much. Now, if it were possible to match the spot beam area to the largest available surface area on a particular piece of debris, then significant improvements to the force upon the debris should be observed. The beam area adjustment could presumably be accomplished through use of an adaptive optics system at the beam director [1], [16]. Reducing the spot beam size provides laser intensities on the order of 10^{10} W/m^2 when interacting with a target with a single-side surface area of 1 cm^2. Using this method of beam shaping, where A_{beam} is equal to SA_{Target}, the primary factors driving the rate an object can be de-orbited is the total incident power from the FEL on the object and the object's total mass. This is shown through manipulation of Equation 7.7 to arrive at Equation 7.9.

Eq. 7.9
$$F_L = RP_L * SA_{Target} = \left(\frac{I_L}{c}\right) * SA_{Target}$$
$$= \left(\frac{P_L}{A_{beam}}\right)\frac{1}{c} * SA_{Target} = \frac{P_L}{c}$$
$$F_L = \frac{P_L}{c}$$

The resultant forces experienced by the piece of debris are listed in Table 7.3.

	Force (N)
F_{Lx}	1.1×10^{-3}
F_{Ly}	3.2×10^{-3}
F_g	-22.7×10^{-3}

Table 7.3 Force Comparison, Adaptive Optics

The force experienced in the x-direction would be increased by a factor of 10^4 through the use of adaptive optic technology. For a 1 cm^3 piece of aluminum this resulted in a change in velocity per overhead pass of -45.4 m/s. This means a 1 cm^3 piece of aluminum would have its orbit reduced to 200 km during the fourth overhead pass.

Based upon the assumptions that have been made to this point, the FEL coupled with adaptive optics would be able to de-orbit an object with a mass around 1 kg in less than 6 months.

There is, however, a downside that derails this entire theoretical exercise. In order to be able to successfully utilize this technique with the adaptive optics, the exact location of the target debris needs to be known. Unfortunately, the ability to track an object in orbit with precision accuracy currently is limited. The Space Surveillance Network (SSN) is generally able to predict the location of an object within a Circle Error Probable (CEP) of 1 km [36]. This means the object is located somewhere within the volume of a sphere with a 1 km radius. So, while numerically feasible to use a FEL that is transmitting from a beam director equipped with adaptive optics for the purposes of active debris removal, the realistic constraints brought on by short-falls in current tracking capabilities and techniques prevents this from being a viable solution to the orbital debris problem.

D. DEBRIS TRACK REFINEMENT

As described in the previous section, orbital debris tracking using the X-band radars of the SSN does not provide sufficient resolution to be able to use the FEL for active debris removal. A possible alternative to using the FEL for removing the debris in LEO was to then use the FEL to supplement the SSN and refine the ephemeris (track data) of the debris instead. One major reason for attempting to reduce the CEP for the pieces of debris is the direct impact on the longevity and service-life extension programs in effect for both military and commercial satellite assets. For example, given the current upper bound to a typical CEP is approximately 1 km in radius, a reduction of that radius by as little as a factor of two would be have significant implications. The resultant sphere would have a radius of 0.5 km and cover 25% the volume of the current sphere generated from the 1 km CEP. This ultimately equates to fewer false alarms for potential collisions with other objects in orbit, which means less unnecessary maneuvering of a satellite, which directly correlates with overall fuel savings and helps to extend the satellite's mission lifetime.

To successfully employ the FEL as a means of tracking orbital debris, the track data from the SSN would be a good starting point for initially gaining the track of the piece of debris being targeted. The data from the SSN serves to give the predicted orbital location and probable trajectory to search along using the FEL. The FEL's beam would have to be spread by design, through the use of an adaptive optics mirror.

Next, an automated search plan would be necessary to sweep the FEL's beam through the majority of the CEP provided by the SSN and to progress the beam along the track as the data from the SSN is propagated forward in time. Finally, for the orbit refinement, the principles of geometry incorporated into Gibbs method of orbit determination [32] would provide the core for the target tracking algorithm.

If the adaptive optics mirror was designed such that it could vary the radius of the spot-beam at various LEO altitudes between approximately 500 m (half the radius of the SSN CEP) and 10 cm, then the intensity incident upon an object from a MW-class FEL would vary from just over 1 W/m^2 to 1 MW/m^2. The initial track would be accomplished using the 500 m spot-beam. If the first sub-set of debris objects the FEL is used to assist the SSN in tracking are the objects at the lower limits of the SSN (which are 10 cm on a side, surface area of 100 cm^2), then the total power reflected from the object in the large spot-beam would be just over 1 W. As the track was refined, the adaptive optics mirror could reduce the spot-beam size until the exact orbital track was known to within a few meters.

At the ground receive station, the collected laser pulses will have significantly less power in them. This is attributed to the realization that surface of the piece of debris may not be smooth, and the laser light reflected off of that rough surface is scattered in a multitude of directions. I made the assumption that the laser light would be reflected and scattered in roughly a cone with an interior angle of 1 rad. This dispersion resulted in the intensity of the returned laser light being on the order of 10^{-13} W/m^2. As for the receiving APD, it was assumed to have a gain of 50 (made from InGaAs) and a radius of 1 meter. With this receiver, the detected power was 10^{-10} W (-100 dBW), which is more than enough power to register as a detection, considering the threshold for registering a detection was around -160 dBW in the previous chapter on communications. Figure 7.10

shows the received power of objects less than 10 cm on a side should be detectable, and most importantly, objects as small as 1 cm can be detected as well.

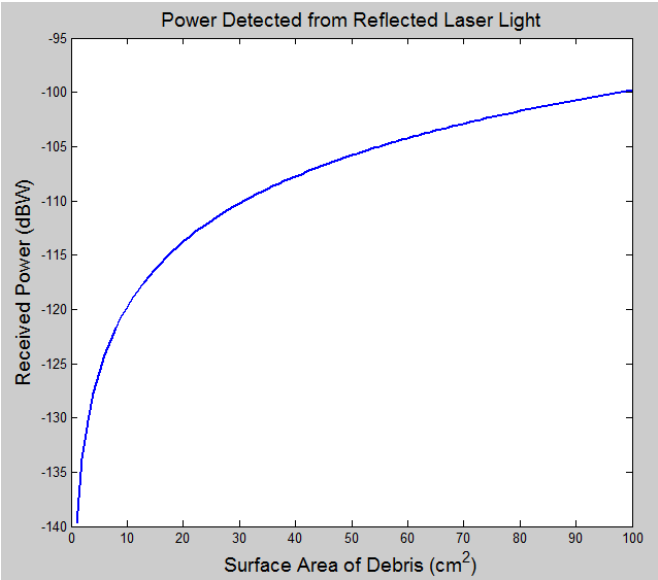

Figure 7.10 Detectability of Reflected Light from an FEL

1. Initial Search Pattern

The end-state goal of using the FEL in orbital debris tracking is to refine the ephemeris. The whole rationale for selecting a spot-beam radius that was half the CEP provided by the SSN was to significantly reduce the uncertainty of the location of the piece of debris. Having a spot-beam radius of this size ensured that any registered detection of the object within the FEL spot-beam would have the immediate effect of shrinking the instantaneous CEP from the 1 km per the SSN to the 500 m illuminated by the FEL. The downside to this is the fact the object could be anywhere within that 1 km CEP and so determining where within the CEP to illuminate becomes the tricky part of the problem.

The easiest search method would be a generic raster scan. This means the bore sight of the beam director would trace out a simple square wave along the SSN's predicted track for the target piece of debris. The angular velocity of the object can be

calculated from its predicted altitude and then translated to a local angular rate for the beam director as it scans across the sky. Figure 7.11 illustrates the manner in which this particular search would appear over several seconds. The large black circles represent the CEP cross-sectional area through the middle of the sphere; the red circles represent the FEL spot-beam area; and the blue line denotes the actual search pattern.

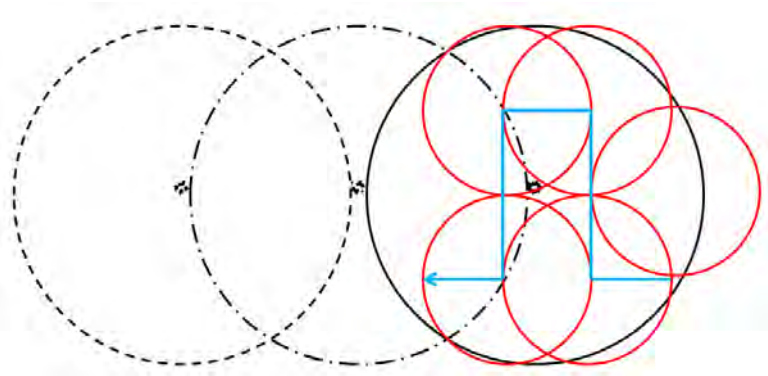

Figure 7.11 First-Pass Square Wave Search Pattern

After this initial pass was completed, the track for the piece of debris would be known down to a 500 meter CEP. On subsequent tracks, the spot-beam radius could be reduced further and the same search pattern conducted within the new CEP. This process could be continuously iterated until the orbital track is known exactly.

2. Gibbs Method of Orbit Determination

Gibbs method of orbit determination is intended to be the core of the algorithm, which may be eventually improved upon to refine the trajectory of a particular orbiting body. The rigorous derivation of the Gibbs method is provided in [32]. This method requires three different geocentric vectors and their associated elevation angles with respect to the laser bore sight. Figure 7.12 is an illustrative reference of the method simulated, created in STK, as it would be used in practice.

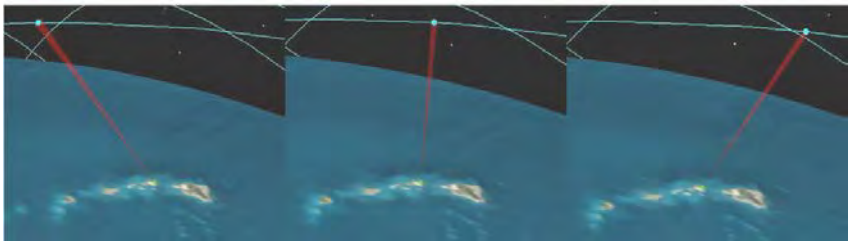

Figure 7.12 FEL at AMOS, Gibbs Method of Orbit Determination

Figure 7.12 presents an over-head fly-by of a piece of debris at the Air Force Maui Optical and Supercomputing (AMOS) facility. Each of the individual frames show the FEL engaged with the target at different ranges from the transmitter as well as different elevation angles above the beam director. The AMOS facility is located at such a high elevation above sea-level, the beam power losses due to atmospheric scattering are minimized.

The receiving station will complete all of the trajectory determination for the target object. Upon receiving detectable energy, the detector will calculate the range to that target as well as the elevation angle of the beam director at the time of the FEL's transmission. In order to distinguish the reflected light from sunlight, a filter would be required for the receiving APD to remove all light energy that is not at the FEL operating wavelength. To further distinguish the received light as light that was transmitted by the FEL would be to ensure the computational aspect of the receiver was capable of discerning the internal micro-pulse structure of the received light. This would serve to filter out the remaining sunlight at the operating wavelength, leaving only the light that had been transmitted from the FEL. Also, the fact there are three frames in Figure 7.12 is not coincidental. This depicts the primary geometric principle requirement of the Gibbs method: three, time-separated vectors are required to be able to obtain a meaningful result from the Gibbs method.

3. Limitations of the Gibbs Method

The primary concern with using Gibbs method for the purpose of orbital track refinement has to do with the errors in the accuracy of the calculations as dependent upon the time between vector measurements. Using the Satellite Tool Kit (STK) I designed and simulated a number of different orbits that were meant to represent orbits of various pieces of debris. The FEL was set to be located at the AMOS facility in Maui and limited the detection elevation to greater than 15 degrees. Then I incrementally stepped the simulation forward through time and recorded three position vectors with which to test the limitations of the algorithm used in Gibbs method. The time intervals between position measurements were 1, 5, 10, 30, 45, 60, 90, 120, and 180 seconds.

Two conclusions were drawn with regard to the limitations of the Gibbs method from these simulations. The first conclusion was that the "magic number" seems to be around 30 seconds. Any measurement separation less than 30 seconds and the calculated COE results would vary by a few percent or more from the actual COE's that were being propagated forward in STK. The greatest errors due to having too small of a separation interval appeared in the semi-major axis and eccentricity calculations. The second conclusion was that the Gibbs method appeared to have some difficulty handling calculations for the orbits that were very nearly circular. The noticeable errors that occurred when these types of orbits were tracked were the switching of the values calculated for the argument of perigee and the true anomaly. Granted, the angular sum of the argument of perigee and the true anomaly gave the exact angular location along the orbit of the target with respect to the node line in all cases. Thus, of my two conclusions about the Gibbs method, only the first one is of any real concern and that limitation is easily corrected by ensuring a 30 second or greater separation time between measurements.

THIS PAGE INTENTIONALLY LEFT BLANK

IX. CONCLUSIONS

In conclusion, the potential exists for using the FEL for applications beyond serving as a next-generation ship-defense weapon system. The FEL is extremely flexible and is capable of providing whatever operating wavelength is most advantageous for the completing the task at hand.

That said, without proper pointing control, the most advanced laser-based weapon system would be completely useless. Advancements in automated pointing control will be absolutely necessary to ensure the future of any laser-based weapon system. With this in mind, it has been shown here, through the SIMULINK modeling simulations conducted, that it may be possible to control the laser and align a beam director to the microradian accuracy necessary for damaging an anti-ship cruise missile (ASCM) target at distances in excess of 5 km. There is obviously more work that can be done in this field of study ranging from making the SIMULINK model more representative to attempting to apply the SIMULINK model to a physical testbed.

With regard to using the FEL for communications, it has been illustrated that this can be accomplished using an FEL that uses various modulation schemes and may be capable of attaining data rates on the order of 10's of Mbits/sec. The high-power levels provided by the FEL and its inherent flexibility make it a suitable candidate if ever an Earth-based laser communications facility is built. Unfortunately, Man's current technology requirement for communications beyond Mars is minimal.

As far as orbital debris is concerned, the primary advantage the FEL provides in solving that problem is related directly to its flexibility. The FEL is capable of adjusting its operating wavelength, as necessary, to find the wavelength that will propagate best in various environmental/atmospheric conditions. It was shown that it may be feasible to use the FEL in removing the orbital debris via radiation pressure, but the intensity of the laser light upon the target would have to be enough to generate a few milli-Newtons of force on the object, and the object would need to have a large surface-area-to-mass ratio, a value greater than 10. The complication that arose from the exploration of the FEL as a

means to eliminate orbital debris was the Space Surveillance Network (SSN) may not have a measured and predicted trajectory of any one particular piece of debris to an accuracy better than a 1000 m circle error probable (CEP). From this, using the FEL as a means of refining the orbital debris trajectories measured by the SSN was explored, and found to be promising. The only real limitation that existed was the closeness, in time, between subsequent range measurements. So long as there was a noticeable separation (approximately 30 seconds) between measurements of the geo-centric radial vector from the FEL ground facility to the piece of debris, the orbital trajectory could be calculated with some confidence.

X. FUTURE WORK AND POTENTIAL APPLICATIONS

A. POINTING ACCURACY MODEL ENHANCEMENT

Future work can still be done on line-of-sight stabilization. Jitter control due to platform jitter is not explicitly addressed in this thesis, and will need to be examined in the future. The impact of high-frequency, low amplitude disturbances on the final angular position of the laser bore sight must be realistically modeled to ensure the resultant disturbances can be corrected and thus further enhance the end-state pointing angle of the NFOV tracking loop. This research is on-going at NPS for integration into various currently operational combat vehicles.

B. ADAPTIVE OPTICS

Any beam propagation application at long ranges (beyond a few meters) requires consideration of the current atmospheric conditions when determining the amount the beam quality will be degraded before reaching the target. Adaptive optics technology provides a means of removing a portion of the degradation effects experienced by a laser as it propagates through the atmosphere. For the utilization of high-average power lasers as ship-defense weapon systems, or any other military capacity, this initial adjustment, or correction, of the beam quality is an absolute must.

C. ASTEROID DETECTION AND SPECTROSCOPY

The FEL has already been considered in use for refining orbital debris tracks, the next logical extrapolation of that application is to use the FEL to detect and track objects at much larger distances, such as close-approach asteroids or meteors. Also, if the return is found to be suitably strong, then there is a potential for using the returned light for spectroscopy of the asteroid or meteor surface.

D. SPACECRAFT POWER BEAMING TO HEO AND GEO

Recent thesis work at NPS has examined the possibility of using a high-energy laser for energy transfer form an Earth ground station to an orbiting satellite.

Considering the fact that most low-earth orbit (LEO) satellites pass overhead in less than 10 minutes, they were deemed an infeasible candidate for this technology. There is still the possibility that objects in high-elliptical orbits (HEO) or geosynchronous orbits (GEO) may benefit from this technology. Also, with the FEL's inherent flexibility, it could be a viable option for implementation at the ground station.

E. USE OF FEL FOR SOLAR CELL ANNEALING

While the FEL may be impractical for use at power beaming to LEO satellites, it may prove beneficial as a means of annealing solar cells that are at the end of their service life. In the simplest terms, annealing is the method by which a high-energy laser is directed at a solar cell resulting in the renewal of that solar cell and thus an increase in the solar cell's longevity. If proven, this technology could become part of the service life extension program (SLEP) for on-orbit LEO satellites.

F. POWER-BEAMING TO UNMANNED AERIAL VEHICLES (UAV)

The FEL can be run for prolonged durations (in excess of 30 days continuously) and as such could be used in an energy beaming capacity to unmanned aerial vehicles (UAV), which are strictly purposed with the surveillance operations around a particular friendly facility. The beam director could be elevator on a tower, the UAV could transmit that it requires energy, and then the FEL could be used to recharge the UAV's batteries, allowing it to remain in flight and operational for days at a time, barring any mechanical failures.

From an optimization problem stand-point, this research offers the opportunity to optimize re-charging timing for all the UAV's "on duty" as well as to determine the best patrol routes for the UAV's to cover in order to increase revisit time over the maximum area possible.

LIST OF REFERENCES

[1] "Free-Electron Laser," class notes for PH4055, Department of Physics, Naval Postgraduate School,

[2] W.B. Colson, C. Pellegrini, and A. Renieri, *Free-Electron Laser Handbook*. Amsterdam, The Netherlands: Elsevier Science Publishing Company, 1990.

[3] J. N. Corlett, et al., "A Next Generation Light Source at LBNL," in *2011 Particle Accelerator Conference*, 2011.

[4] C. R. Nave, HyperPhysics, "Rayleigh and mie scattering," 2000, http://hyperphysics.phy-astr.gsu.edu/hbase/atmos/blusky.html.

[5] R. A. Rohde, "Global Warming Art Project," June 2007, http://hyperphysics.phy-astr.gsu.edu/hbase/atmos/blusky.html.

[6] C. C. Chen, "Method for estimating the thermal blooming effect," Rand Corporation, Tech. Rep. R-1726-PR, April 1975

[7] T. Perez and M. Blanke, "Simulation of ship motion in seaway," Department of Electrical and Computer Engineering, The University of Newcastle, Australia, Tech. Rep. EE02037.

[8] C. T. Chen, *Analog and Digital Control System Design*. Oxford, NY: Oxford University Press, 1993.

[9] J. J. Kim (private communication), 2011.

[10] D. Kim, D. Frist, J. J. Kim, and B. Agrawal, "A HEL testbed for high accuracy beam pointing and control," Naval Postgraduate School, Monterey, California, Tech. Rep. NPS-MAE-09–001, 2009.

[11] EuroWEATHER, "Douglas Scale," December, 2011, http://www.eurometeo.com/english/read/doc_douglas.

[12] B. Sklar, *Digital Communications Fundamentals and Applications* (2nd ed.). Upper Saddle River, NJ: Prentice Hall, 2001.

[13] "Antenna Introduction / Basics," October 2011, http://www.kyes.com/antenna/navy/basics/antennas.htm.

[14] "National SIGINT systems," class notes for SATT-4265, short-course, Naval Postgraduate School, Winter 2010.

[15] Halliday, Resnick, and J. Walker, *Fundamentals of Physics, 8th ed., Extended.* Von Hoffman Press, 2008.

[16] W. B. Colson (private communication), 2010–2011

[17] Kirtland Air Force Base, "Factsheets: Starfire Optical Range at Kirtland Air Force Base, New Mexico," November 2009, http://www.kirtland.af.mil/library/factsheets/factsheet.asp?id=15868.

[18] W. Sheehan, *The Planet Mars: A History of Observation and Discovery*. Tucson: University of Arizona Press, 1993.

[19] S. G. Lambert and W. L. Casey, *Laser Communications in Space*. Norwood, MA: Artech House, Inc., 1995.

[20] *NAVSTAR GPS User Equipment Introduction*, September 1996.

[21] C. Wolff, "Radar Basics – Minimum Detectable Signal," December 2009, http://www.radartutorial.eu/18.explanations/ex29.en.html.

[22] National Aeronautics and Space Administration, National Space Science Data Center, "Spacecraft – Details – Pioneer 6," November 2011, http://nssdc.gsfc.nasa.gov/nmc/spacecraftDisplay.do?id=1965–105A.

[23] National Aeronautics and Space Administration, Solar System Exploration, "The Galileo spacecraft," July 2010, http://solarsystem.nasa.gov/galileo/images/mission-spacecraft-2.gif.

[24] Jet Propulsion Laboratory, "Mars Exploration Rovers," http://marsrovers.jpl.nasa.gov/mission/comm_size.html.

[25] A. Nordmann, "Arecibo Message," October 2005, http://en.wikipedia.org/wiki/File:Arecibo_message.svg.

[26] National Aeronautics and Space Administration and Michigan Tech University, "APOD: 2000 January 23 – A message from Earth," January 2000, http://apod.nasa.gov/apod/ap000123.html.

[27] "The Pioneer plaque," December 2006, http://en.wikipedia.org/wiki/File:Pioneer_plaque.svg.

[28] R. V. Carlone, "Space Program: Space debris a potential threat to space station and shuttle," U. S. General Accounting Office, Tech. Rep. GAO / IMTEC-90–18, 1990.

[29] National Aeronautics and Space Administration, "Orbital debris educational package," July 2009, orbitaldebris.jsc.nasa.gov/library/EducationPackage.pdf.

[30] National Aeronautics and Space Administration, Orbital Debris Program Office, "Photo gallery," http://www.orbitaldebris.jsc.nasa.gov/photogallery/photogallery.html.

[31] "NASA Safety Standards," National Aeronautics and Space Administration, NSS 1740.14, August 1995.

[32] H. D. Curtis, *Orbital Mechanics for Engineering Students, 2nd ed.* Elsevier: Butterworth-Heinemann, 2010.

[33] B. Wilder, "Power beaming, orbital debris removal, and other space applications of a ground based free electron laser," Naval Postgraduate School, Monterey, California, March 2010.

[34] "NASA might build laser cannons to shoot space junk," March 2011, http://armannd.com/nasa-might-shoot-lasers-at-space-junk-science.html/.

[35] J. R. Wertz and W. J Larson (editors), *Space Mission Analysis and Design, 3rd ed.* Hawthorne, CA: Microcosm Press, 1999.

[36] L. Simms, V. Riot, et al., "Optical payload for the STARE mission," Lawrence Livermore National Laboratory, Livermore, CA, Tech. Rep. LLNL-CONF-474234, 2011.

THIS PAGE INTENTIONALLY LEFT BLANK

INITIAL DISTRIBUTION LIST

1. Defense Technical Information Center
   Ft. Belvoir, Virginia

2. Dudley Knox Library
   Naval Postgraduate School
   Monterey, California

3. LCDR Henry Travis, USN
   Program Officer, 591 Curriculum
   Naval Postgraduate School
   Monterey, California

4. Professor Knox Millsaps
   Naval Postgraduate School
   Monterey, California

5. Professor Brij Agrawal
   Naval Postgraduate School
   Monterey, California

6. Professor William Colson
   Naval Postgraduate School
   Monterey, California

7. Professor Jae Jun Kim
   Naval Postgraduate School
   Monterey, California

8. Professor James Newman
   Naval Postgraduate School
   Monterey, California